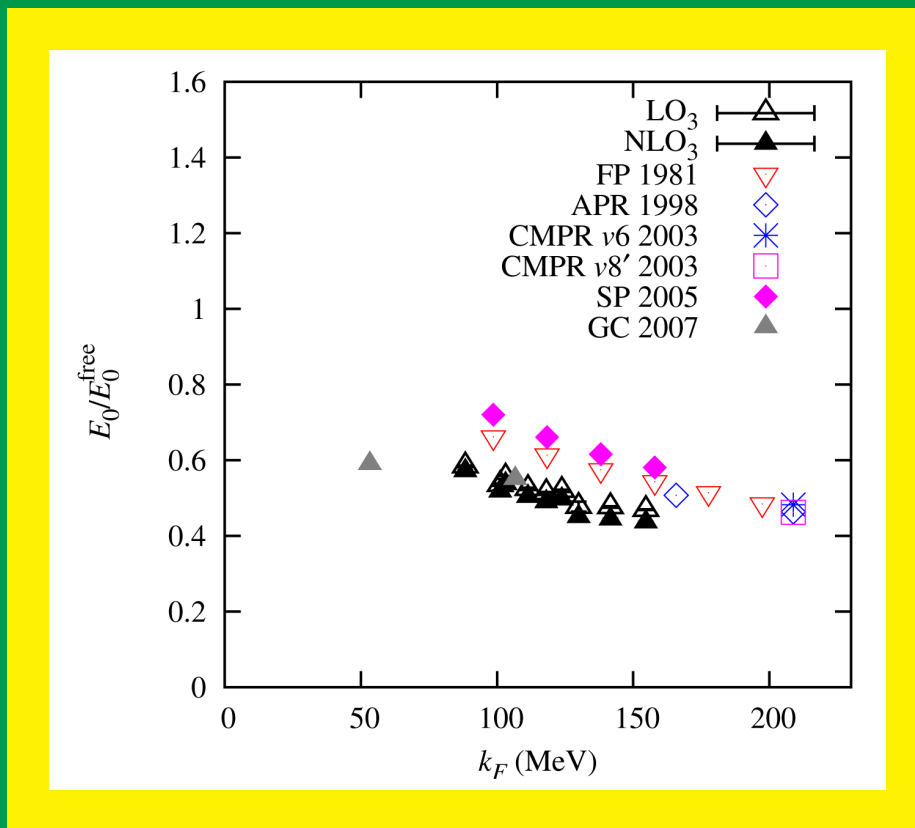


Jülich Center for Hadron Physics (JCHP)
 Institut für Kernphysik (IKP)
 COSY



ANNUAL REPORT 2009

Annual Report 2009

Institut für Kernphysik / COSY

DIRECTORS AT THE IKP:

Experimental Hadron Structure (IKP-1):

Experimental Hadron Dynamics (IKP-2):

Theoretical Nuclear Physics (IKP-3):

Large-Scale Nuclear Physics Equipment (IKP-4):

Prof. Dr. James Ritman

Prof. Dr. Hans Ströher

Prof. Dr. Ulf-G. Meißner

Prof. Dr. Rudolf Maier (managing director)

EDITORIAL BOARD:

Priv. Doz. Dr. Markus Büscher

Priv. Doz. Dr. Christoph Hanhart

Prof. Dr. Siegfried Krewald

Prof. Dr. Hartmut Machner

Prof. Dr. Rudolf Maier

Prof. Dr. Ulf-G. Meißner

Prof. Dr. James Ritman

Dr. Hans Stockhorst

Prof. Dr. Hans Ströher

Cover picture:

Ground state energy of neutron matter with Fermi momentum k_F in units of the energy E_0^{free} of the ground state of non-interacting neutrons, obtained in chiral lattice simulations in leading order LO_3 and next-to-leading order NLO_3 . In trapped cold atoms (${}^6\text{Li}$, ${}^{40}\text{K}$) experiments, a change of an external magnetic field can tune the atom-atom scattering length to infinity, thus realizing the so-called *unitarity limit* of a many-body system and finding $(\xi = E_0/E_0^{\text{free}})_{\text{atom}}$ in the range from 0.32 to 0.5. In neutron matter, the *unitarity limit* is approximately realized because the S-wave scattering length of neutrons is -18.5 fm, while the S-wave effective range is $r_0 = 2.7$ fm. Corrections due to r_0 lead to $(E_0/E_0^{\text{free}})_{\text{neutron matter}} = f(k_F a_0) + c_1 k_F r_0$. The present lattice simulations suggest c_1 to range between 0.14 and 0.27 and the universal constant $\xi = 0.31(1)$. For comparison, traditional many-body predictions for $(E_0/E_0^{\text{free}})_{\text{neutron matter}}$ are shown.

Preface

The IKP has achieved a strategic success in 2009: the proposal of the IKP for funding in the Research Program **Physics of Hadrons and Nuclei**, defined in the framework of the **Program Oriented Funding** of the Helmholtz centers, has been evaluated in February with great success. This decision guarantees the funding of IKP as well as those parts of ZAT and ZEL participating in the proposal for the time period from 2010 till 2014.

The following outstanding experimental results have been obtained:

- The WASA at COSY collaboration has used the $pd \rightarrow {}^3\text{He} \eta$ reaction to accumulate 30 million η -meson decays, obtaining clear signatures of 300 events of the type $\eta \rightarrow \pi^+ \pi^- e^+ e^-$. These data are relevant for tests of the chiral anomaly. Moreover, 22 events candidates for the rare decay $\eta \rightarrow e^+ e^- e^+ e^-$, so far never seen, have been obtained.
- Both the ANKE and the WASA collaborations have investigated two-pion production via the reactions $pp \rightarrow pp\pi^0\pi^0$ and $pn \rightarrow d\pi^0\pi^0$ to shed light on the nature of the enhancement of the invariant two-pion mass spectrum in hadronic reactions first observed by Abashian, Booth, and Crowe (ABC effect) in 1961, but still defying an explanation. A resonant structure at $\sqrt{s} = 2.38$ GeV, *i.e.* 80 MeV below the $\Delta\Delta$ mass, with a width of only 50 MeV is seen in the isoscalar reaction $pn \rightarrow d\pi^0\pi^0$ and confirmed in the fusion process $dd \rightarrow {}^4\text{He}\pi^0\pi^0$.
- The ANKE collaboration has studied the modification of the Φ -meson width in nuclear matter using C, Cu, Ag, and Au targets. Preliminary analysis suggests a width of $\Gamma_\phi^* = 65_{-13}^{+17}$ MeV.

Striking results of theoretical investigations are:

- The forward-backward asymmetry of the reaction $pn \rightarrow d\pi^0$ near threshold is directly proportional to the difference of the up- and down-quark mass. The experimental asymmetry then determines the strong contribution of the proton-neutron mass difference to be $(m_n - m_p)^{\text{QCD}} = (1.5 \pm 0.9)$ MeV. This is a non-trivial test of the chiral structure of QCD.
- The heavy baryon formalism of chiral effective field theory has been used to determine the leading contributions of the one- and two-pion exchange currents, paving the way for systematic analyses of electroweak reactions on light nuclei.
- First lattice simulations of light nuclei with isospin breaking interactions yield a mass difference of ${}^3\text{He}$ and ${}^3\text{H}$ of 0.78(5) MeV, in excellent agreement with the experimental value, 0.76 MeV.
- The meson $Y(4660)$ has been identified as a candidate for a $f_0(980)\psi'$ bound state; the Jülich model of meson-baryon reactions has characterized the nucleon resonances below 2 GeV by their complex poles and residues, and the Primakoff effect has been suggested as an experimental tool to determine the decay width of the neutral pion with increased precision.

A central mission of the IKP is the design and preparation of the high energy storage ring (HESR) within FAIR. IKP has developed a chromaticity correction scheme for the HESR to minimize the emittance growth caused by betatron resonances. In line with the recent

decision for a modular realization of the FAIR project, development of a new injection and accumulation scheme for HESR has started. Magnet design of dipole, quadrupole, sextupole, and correction dipole magnets has been finalized. A detailed concept of the vacuum system of HESR has been worked out.

For the PANDA detector, large progress has been made in optimizing the design of the microvertex detector, a central element of PANDA which will allow to detect D -mesons by measuring their decay length with a precision better than $100 \mu\text{m}$. Furthermore, the technique developed for the COSY-TOF straw tracker has been adopted for the proposed PANDA Straw Tube Tracker (STT) and a first prototype has been assembled.

The following upgrades of the experimental facilities at COSY have been completed in 2009:

- The first double polarization experiments have been performed by the ANKE collaboration, using the Polarized Internal Target (PIT) to study the deuteron charge exchange break up $\vec{d}\vec{p} \rightarrow (pp)n$.
- First measurements with the upgrades COSY-TOF detector were performed which involve the COSY-TOF Straw Tube Tracker. An essential improvement of the vertex reconstruction has been achieved.
- The WASA detector has been upgraded by a new forward veto hodoscope and trigger system. Concepts for a DIRC counter (Detection of Internally Reflected Cherenkov Light) have been worked out, which provide input for the design studios of the PANDA DIRC detectors.
- The former HERMES polarized target was transferred to COSY and upgraded as a polarized internal gas target. This is an important step to provide polarized antiprotons for FAIR.
- A cooperation with the Budker Institute of Nuclear Physics (BINP, Novosibirsk) began to manufacture components of a 2 MeV Electron Cooler.
- The interaction of the antiproton beam of HESR with an internal pellet target leads to a mean energy loss which cannot be compensated by cooling. Therefore, a broadband barrier bucket cavity is required. The barrier bucket cavity at COSY was used to optimize the compensation of the mean energy loss induced by the WASA pellet target.

We congratulate Prof. H. Ströher for obtaining an advanced grant of the European Research Council, Prof. E. Epelbaum for having received calls from the universities of Basel, Bochum, and Bonn, as well as Prof. U.-G. Meißner for his joint appointment as director of the institutes IKP-3 and IAS-4 and his appointment as Fellow of the American Physical Society.

We thank Prof. W. van Oers for his outstanding service as chairman of the Program Advisory Committee.

At this prominent place, I want to thank all colleagues and collaborators for their effective commitments and contributions which made this success possible.

Jülich, March 2010

James Ritman

Contents

1	Physics at COSY.....	1
2	COSY Operation and Developments ...	17
3	Further Experimental Activities.....	23
4	Theoretical Investigations.....	27
5	Preparation of the HESR.....	33
6	The PANDA Experiment.....	35
 Appendix		
A	Councils.....	39
B	Publications, Patents.....	40
C	Talks and Colloquia.....	46
D	Diploma and Ph.D. Theses, Habilitation	54
E	Awards & Offers for Professorships ...	57
F	Funded Projects.....	58
G	COSY-FFE Projects.....	60
H	Conferences (co-)organized by the IKP	62
I	Teaching Positions.....	64
J	Beam Time at COSY.....	65
K	Personnel.....	66
L	Substantiating Contributions.....	69

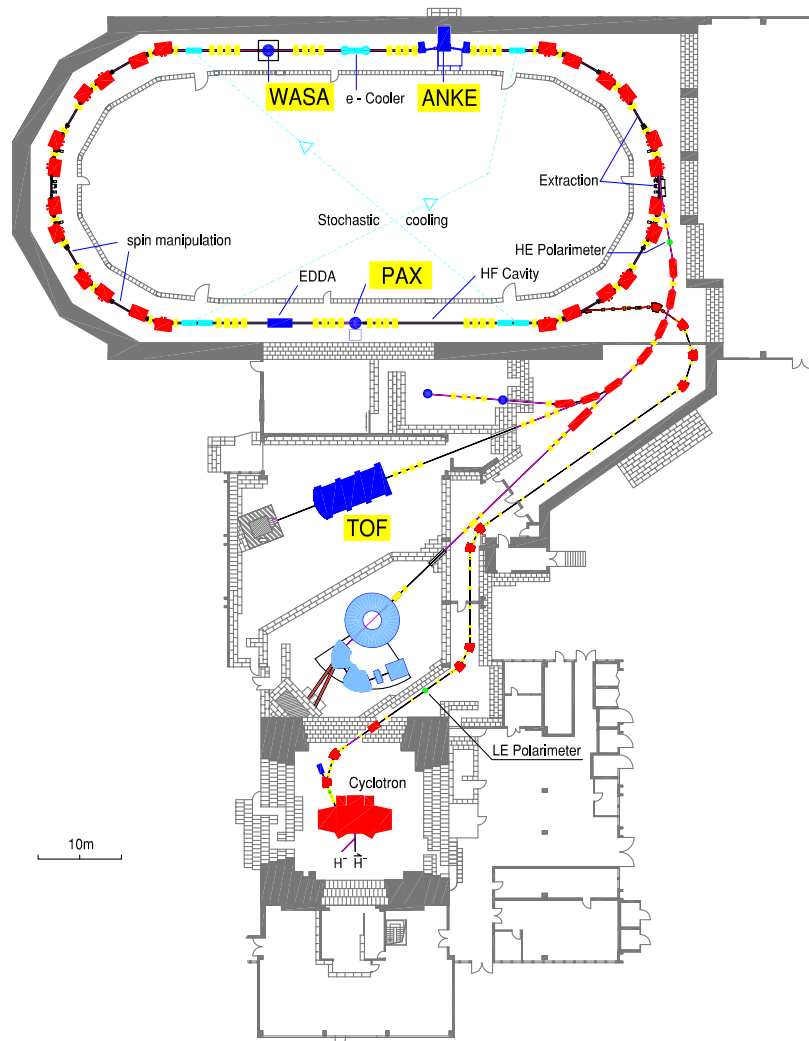
1 Physics at COSY

1.1 Overview

The cooler synchrotron and storage ring COSY delivers unpolarized and polarized beams of protons and deuterons with momenta up to 3.7 GeV/c for two internal experiments — ANKE and WASA — and one experiment — TOF — at an external target position. All three detection systems are operated by large international collaborations.

- **ANKE** (Apparatus for Studies of Nucleon and Kaon Ejectiles) is a large acceptance forward magnetic spectrometer at an internal target station in the COSY ring. The central dipole is movable to adjust the momenta of the detected particles independent of the beam momentum. Using deuterium cluster targets, reactions on the neutron are tagged by detecting the low-energy recoil proton in silicon strip detectors in vacuum next to the target. In addition, a polarized internal target with a storage cell can be used.
- **TOF** (Time Of Flight) is a non-magnetic spectrometer combining excellent tracking capabilities with large acceptance and full azimuthal symmetry allowing to measure complete Dalitz plots. TOF is optimized for final states with strangeness. With the new straw tube tracking system (STT), TOF will have a significantly improved mass resolution and reconstruction efficiency.
- **WASA** (Wide Angle Shower Apparatus), an internal 4π spectrometer for neutral and charged particles, is operated at the internal COSY beam. WASA comprises an electro-magnetic calorimeter, a very thin superconducting solenoid, inner and forward trigger and tracking detectors, and a frozen-pellet target.

In addition, the unique COSY capabilities are used by the SPIN@COSY-, dEDM- and PAX-collaborations to investigate spin-manipulations, to build a dedicated EDM-storage ring experiment, and to prepare experiments on polarization buildup in storage rings.



1.2 Major Physics Results at COSY

1.2.1 Decays of η Mesons

The key experiment for the WASA detector at COSY is the study of (rare) η meson decays. During the last two years data sets from pp and pd interactions have been collected. A very first production run in April 2007 yielded $8 \cdot 10^5$ events for the $pp \rightarrow pp(\eta \rightarrow 6\gamma)$ reaction. In the next four week run period in October 2008, η decays were studied using the $pd \rightarrow {}^3\text{He}\eta$ reaction at a beam energy of 1 GeV. An unbiased data sample of $1.1 \cdot 10^7$ η meson decays was collected. The data sample was increased to $3 \cdot 10^7$ η meson decays in an eight week continuation in August/September 2009. In addition, a few shorter runs aiming at the optimization of η meson production in pp interactions were also carried out. Here, the status of the analysis of selected decay channels is presented.

The cross section of the $pd \rightarrow {}^3\text{He}\eta$ reaction rises quickly and reaches a plateau value of 400 nb at 2 MeV above the production threshold. The requirement for a ${}^3\text{He}$ ion in the final state selects only a small fraction of about 0.1% of the total pd cross section. The discrimination of ${}^3\text{He}$ against protons and deuterons is reliable and can easily be implemented on the trigger level. Trigger rates at high luminosities are well within the data acquisition capabilities without imposing additional conditions on the η decay system. The $pd \rightarrow {}^3\text{He}\eta$ reaction is used at beam energy of 1.0 GeV where the ${}^3\text{He}$ ions can be measured in the forward detector which covers scattering angles from 3° to 18° . Figure 1 shows the missing mass of the reconstructed ${}^3\text{He}$ for all data samples collected in the 2008 pd run period. In the right panel, only events correlated with a reconstructed $\eta \rightarrow \gamma\gamma$ decay are shown.

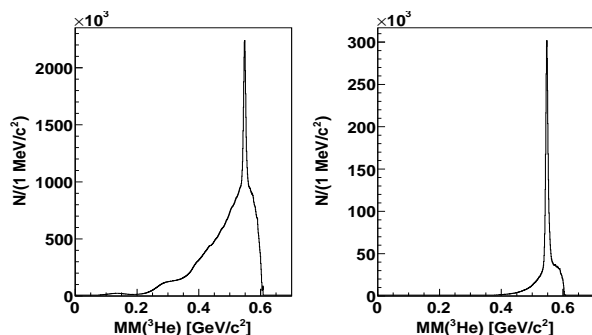


Fig. 1: ${}^3\text{He}$ missing mass distribution for the $pd \rightarrow {}^3\text{He}\eta$ reaction at 1.0 GeV. The trigger was based on a ${}^3\text{He}$ signature in the forward detector without bias on the meson decay system. The plot in the left panel shows all data collected in the 2008 run period with about $11 \cdot 10^6$ events in the peak. In the right panel, only events correlated with a reconstructed $\eta \rightarrow \gamma\gamma$ decay are shown.

Due to flux limitations from the calorimeter and mini-drift chambers, the acceptable rate of η mesons from the $pd \rightarrow {}^3\text{He}\eta$ reaction is about 10 η events/s. This rate is sufficient for studies of not-so-rare η decays. Further

progress towards rare η decays is being made by focusing on the $pp \rightarrow pp\eta$ production reaction. The reaction has a 10–20 times larger cross section ($10 \mu\text{b}$ at 1.4 GeV) and the inclusive pp cross section is two times lower than for pd interactions. The η meson yield is higher for a given luminosity plus a higher luminosity of up to two times can be used. Meanwhile, the tagging the $pp \rightarrow pp\eta$ reaction poses a challenge. This is illustrated in figure 2 showing missing mass distributions for two reconstructed protons in the forward detector in a run at a beam energy of 1.4 GeV.

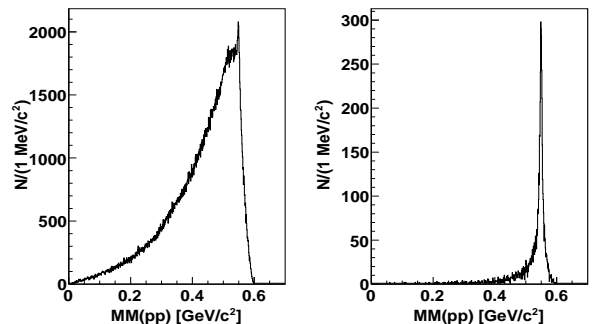


Fig. 2: Proton-proton missing mass distributions from the $pp \rightarrow ppX$ reaction at 1.4 GeV beam energy with a trigger requiring two tracks from charged particles in the forward detector and at least two clusters from neutral particles in the calorimeter. For the left panel, the data analysis is based on the forward detector tracks. For the right panel events with an invariant mass of the two photons ≥ 300 MeV/c^2 are selected.

The trigger condition in this case included the requirement for at least two tracks in the forward detector and at least two clusters from neutral particles in the calorimeter. The missing mass plot on the left hand side was obtained based on the events selected by the trigger. The right figure shows the pp missing mass after selection of the $\eta \rightarrow \gamma\gamma$ decay channel via the analysis. With the presently limited trigger selectivity, a production rate of about 100 η events/s has been achieved. Preparations for the improved trigger system are now underway.

The decay channel $\eta \rightarrow \pi^+\pi^-\gamma$ aims at the study of the box anomaly in QCD. The goal is to extract the shape of the photon energy spectrum which should allow to differentiate between the simplest gauge invariant matrix element and chiral perturbation theory calculations. The missing mass distribution for the identified $\eta \rightarrow \pi^+\pi^-\gamma$ channel is shown in figure 3.

A first step before constructing the photon energy distribution is a consistency check of the data by inspecting the second kinematic variable in the decay: the distribution of the π^+ direction in the pion-pion center of mass θ_π . The pions are expected to be in relative p wave. Figure 3 shows the experimental points from the preliminary analysis of the pd data from 2008 along with a p wave distribution. Background due to the $pd \rightarrow {}^3\text{He}\pi^+\pi^-$ reaction has been subtracted.

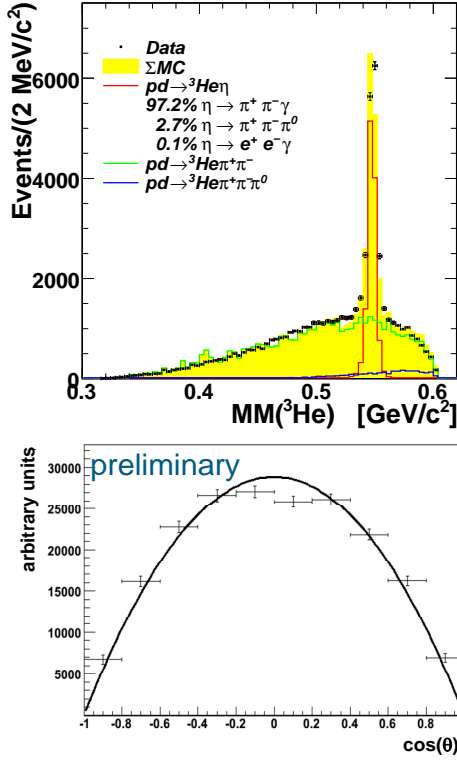


Fig. 3: Upper panel: ${}^3\text{He}$ missing mass spectrum for $\eta \rightarrow \pi^+\pi^-\gamma$ event candidates compared with simulated signal and background contributions. Lower panel: Preliminary experimental $d\Gamma/d\cos\theta_\pi$ distribution, acceptance corrected. The line is the expectation for the pions to be in relative p wave.

From the analysis of the 2008 data set, about 12000 $\eta \rightarrow \pi^+\pi^-\gamma$ events are expected, with an overall reconstruction efficiency of 3-5 %. The photon energy resolution is better than 10 MeV.

The decay $\eta \rightarrow \pi^+\pi^-e^+e^-$, related to $\eta \rightarrow \pi^+\pi^-\gamma$, provides precise tests of the chiral anomaly by comparison with existing chiral perturbation theory calculations. A high statistics measurement of $\eta \rightarrow \pi^+\pi^-e^+e^-$ will allow to provide constraints for a new kind of flavor conserving CP violation by measuring the asymmetry of the dihedral angle between the pion- and electron planes. The present Particle Data Group value for the branching ratio of the $\eta \rightarrow \pi^+\pi^-e^+e^-$ decay is $4.2 \cdot 10^{-4}$.

The status of the analysis of the $\eta \rightarrow \pi^+\pi^-e^+e^-$ decay is shown in Figure 4. A clear signature of the $\eta \rightarrow \pi^+\pi^-e^+e^-$ decay is seen in the ${}^3\text{He}$ missing mass, corresponding to about 300 events. The line represents a polynomial fit to the direct pion production reactions. According to the Monte Carlo simulations, 50% of the events in the η mass peak are from $\eta \rightarrow \pi^+\pi^-e^+e^-$.

Major background contributions come from the $\eta \rightarrow \pi^+\pi^-\gamma$ decay, with external γ conversion in the beam tube. Additional background stems from $\eta \rightarrow \pi^+\pi^-\pi^0$, due to internal (Dalitz decay of the π^0) and external conversion of one of the photons from $\pi^0 \rightarrow \gamma\gamma$ decays.

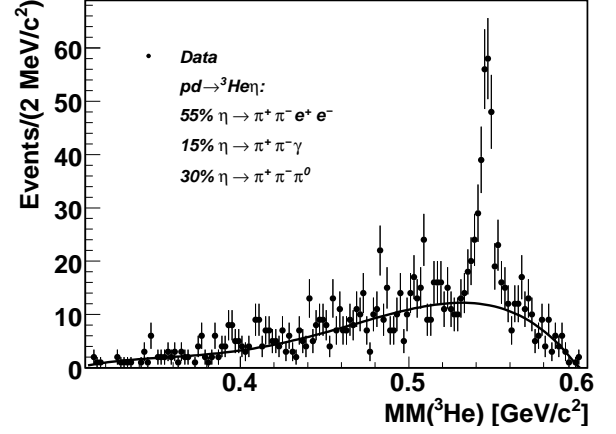


Fig. 4: Missing mass of ${}^3\text{He}$ for events compatible with $\eta \rightarrow \pi^+\pi^-e^+e^-$. The line is a polynomial fit to the background.

At present, the analysis does not include any vertex reconstruction which will help to suppress the background from external conversion. The remaining background will be dominated by $\eta \rightarrow \pi^+\pi^-\pi^0_{\text{Dalitz}}$ and can be further reduced by improving the detection sensitivity for the additional photon. The overall reconstruction efficiency is limited by requesting the suppression of the background and is 5–10 %.

The observation of the double Dalitz decay $\eta \rightarrow e^+e^-e^+e^-$ enables the study of the η meson form factor for two time-like virtual photons. Figure 5 demonstrates the status of the analysis of data collected in 2008. Presently, the selection cuts for obtaining the event sample are being optimized. The data distribution shown here contains 22 event $\eta \rightarrow e^+e^-e^+e^-$ candidates.

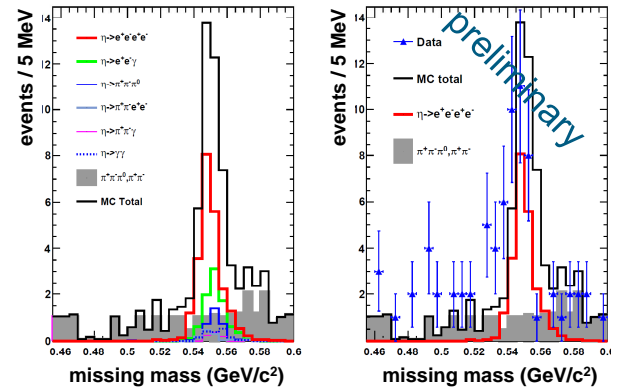


Fig. 5: The figure shows the missing mass distributions for the $\eta \rightarrow e^+e^-e^+e^-$ decay. The left panel is the simulated decomposition into signal and background channels. The right panel demonstrates the agreement between simulated and data signal.

It is concluded that the signal/background ratio is better than 2:1 which is encouraging. Further improvements are expected from a kinematic fit and possibly a vertex fit. This decay channel has not previously been studied.

1.2.2 ABC-Effect in pp, pn, pd and dd Reactions

In an continuing effort to understand the nature of the ABC effect and its possible origin in a baryon-baryon resonance two-pion production reactions have been investigated with a variety of initial collision partners.

The acronym ABC stands for an unexpected enhancement at low masses in the invariant $\pi\pi$ mass spectrum $M_{\pi\pi}$ first observed by Abashian, Booth and Crowe in the double pionic fusion of deuterons and protons to ${}^3\text{He}$. Follow-up experiments revealed this effect to be of isoscalar nature and to show up in cases, when the two-pion production process leads to a bound nuclear system. Initially the low-mass enhancement had been interpreted as an unusually large $\pi\pi$ scattering length and evidence for the σ meson, respectively. Since the effect showed up at beam energies corresponding to the excitation of two Δ resonances in the nuclear system, the ABC effect was interpreted later on by a t -channel $\Delta\Delta$ excitation in the course of the reaction process leading to both a low-mass and a high-mass enhancement in isoscalar $M_{\pi\pi}$ spectra. Together with previous results from CELSIUS the new data obtained at WASA for the $pp \rightarrow pp\pi^0\pi^0$ reaction at $T_p = 1.4$ GeV (cf. contribution by T. Tolba in Sect. L) are in support of the t -channel $\Delta\Delta$ process - although no significant low-mass enhancement is observed in the $M_{\pi\pi}$ spectrum. However, this is not unexpected, since the two final nucleons are not bound and hence are allowed to have large relative momenta. If this freedom is suppressed by a severe cut on the M_{pp} spectrum, then the ABC effect should show up also in this reaction. In fact, ANKE measurements of the $pp \rightarrow ppX$ reaction with the constraint $M_{pp} < 2m_p + 3 \text{ MeV}/c^2$, *i.e.* leading to the fusion of a quasi-bound ${}^2\text{He}$ exhibit a $M_{\pi\pi}$ spectrum moderately enhanced at low-masses in agreement with the t -channel $\Delta\Delta$ process.

From this we conclude that the pp induced two-pion production, which originates from the *isovector* NN channel behaves regularly, *i.e.* as expected from the conventional t -channel process. This is also true for the total cross section, which follows the expected smooth energy dependence.

The situation changes profoundly, if the double-pionic fusion starts from the *isoscalar* pn channel. The most basic fusion reaction $pn \rightarrow d\pi^0\pi^0$ measured via the quasifree process in $pd \rightarrow p_{\text{spectator}}d\pi^0\pi^0$ at WASA exhibits a very pronounced narrow resonance structure at $\sqrt{s} = 2.38$ GeV, *i.e.* 80 MeV below the $\Delta\Delta$ mass. The width of this structure is only 50 MeV, *i.e.* five times smaller than expected from the conventional t -channel $\Delta\Delta$ excitation — see Annual Report 2008. The low-mass enhancement in the $M_{\pi\pi}$ differential distribution is much stronger than observed in the case of pp induced two-pion production. Moreover, this huge low-mass enhancement is only observed in the energy region, where the resonance structure shows up in the total cross section.

Complementary to the WASA measurements the ANKE collaboration has investigated the two-pion production in pd collisions for the non-quasifree process, *i.e.* the co-

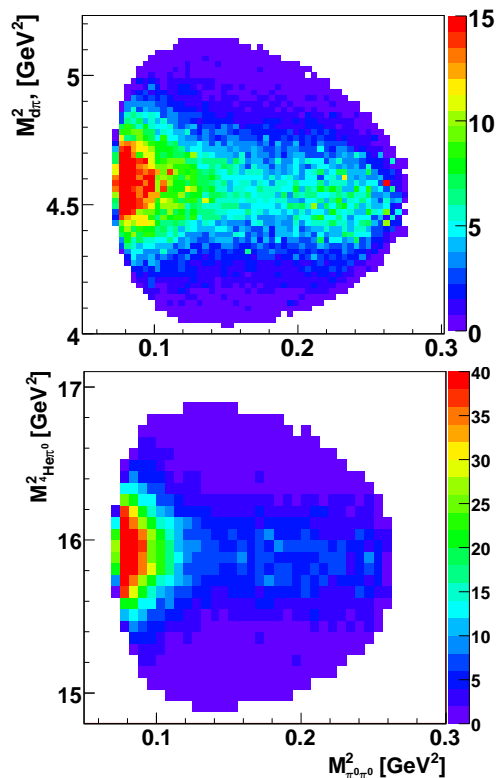


Fig. 6: Top: Dalitz plot of $M_{\pi^0\pi^0}^2$ versus $M_{d\pi^0}^2$ at $\sqrt{s} = 2.38$ GeV, the maximum total cross section of the reaction $pn \rightarrow d\pi^0\pi^0$. Bottom: The same but for the reaction $dd \rightarrow {}^4\text{He}\pi^0\pi^0$ at $\sqrt{s} = 4.24$ GeV.

herent two-pion production as measured in the reaction $pd \rightarrow pdX$ with the mass of X corresponding to the $\pi\pi$ region. The missing mass of the observed proton, which corresponds to the invariant mass of the $d\pi\pi$ system, exhibits an energy dependence compatible with that observed for the total cross section of the quasifree reaction, *i.e.* exhibits also this narrow resonance-like structure. The cross section of this coherent process is found to be three orders of magnitude smaller than the quasifree process.

In order to see, whether the ABC effect and its associated resonance structure in the total cross section survives also in the *isoscalar* double-pionic fusion to nuclei heavier than the deuteron, the fusion process $dd \rightarrow {}^4\text{He}\pi^0\pi^0$ has been investigated at WASA. The analysis of the data is still in progress, but first results show again some resonance-like structure in the total cross section.

The Dalitz plot of $M_{\pi^0\pi^0}^2$ versus $M_{{}^4\text{He}\pi^0}^2$ for the fusion process to ${}^4\text{He}$ is compared in Fig. 1 to that for basic fusion process to D . In both cases the Dalitz plots are shown for the beam energy, where the total cross section is at maximum. Both plots exhibit the same characteristics: an extreme $\pi\pi$ low-mass enhancement combined with the signature of a mutual excitation of two nucleons into the Δ state each.

1.2.3 The Energy Dependence of the $pp \rightarrow K^+ n \Sigma^+$ Reaction Close to Threshold

The energy dependence of the total cross section for associated strangeness production in the $pp \rightarrow K^+ p \Lambda$ reaction near threshold has been extensively investigated at COSY-11 by detecting the K^+ and proton and identifying the Λ as a missing-mass peak. More exclusive measurements at COSY-TOF led to the extraction of many differential observables. The excitation function for $pp \rightarrow K^+ p \Sigma^0$ measured using the same system at COSY-11 showed that Σ^0 production was much weaker than that of Λ at the same value of the excitation energy ε . Furthermore, the dependence on ε was different for the two hyperons, with the Λ rate being enhanced significantly near threshold by the Λp final state interaction.

Any measurement of $pp \rightarrow K^+ n \Sigma^+$ is much more challenging since it requires the detection of either the neutron or the Σ^+ decay products in coincidence with the kaon. Very large values of the total cross section near threshold were found at COSY-11 by studying $K^+ n$ correlations. An initial study at ANKE looked rather at the π^+ coming from the Σ^+ decay in coincidence with the K^+ and found instead a cross section for Σ^+ production that was of the same order of magnitude as for the Σ^0 . Since this experiment was carried out at a somewhat higher ε , it could not rule out an anomalous near-threshold behaviour of the production process.

Below the threshold for $pp \rightarrow K^+ n \Lambda \pi^+$ at 1.975 GeV, the only source of genuine $K^+ \pi^+$ coincidences is the $pp \rightarrow K^+ n \Sigma^+$ reaction. Since ANKE can reliably identify the kaon using the delayed-veto telescopes, the only drawback in this approach is the small π^+ acceptance, which yields only low statistics.

The new ANKE experiment was carried out at four energies above the Σ^+ threshold ($\varepsilon \leq 82$ MeV). After subtracting a random background, estimated from below-threshold data, and correcting for acceptances and efficiencies, the resulting cross sections are shown in the figure, along with the first ANKE result, as a function of ε . These data show production cross sections for the Σ^+ which are slightly less than those for the Σ^0 at the same values of excess energy. They are over two orders of magnitude smaller than the COSY-11 values obtained on the basis of $K^+ n$ coincidences.

The dominant features in the $K^+ p$ missing-mass spectrum are the Λ and Σ^0 peaks associated with directly produced protons. These allow estimates to be made of the $pp \rightarrow K^+ p \Lambda$ and $pp \rightarrow K^+ p \Sigma^0$ total cross sections, though with significant model dependence in the Λ case. Nevertheless, with plausible assumptions, the data lead to total cross sections that are consistent with results in the literature. The comparison of the ANKE experimental points on the total cross section for Σ^0 production with the world data (parameterised by the dotted line) is also shown in the figure.

The $pp \rightarrow K^+ n \Sigma^+$ reaction also contributes to the $K^+ p$ coincidences through the decay $\Sigma^+ \rightarrow p \pi^0$. The effect shows up best at maximum missing masses, where there

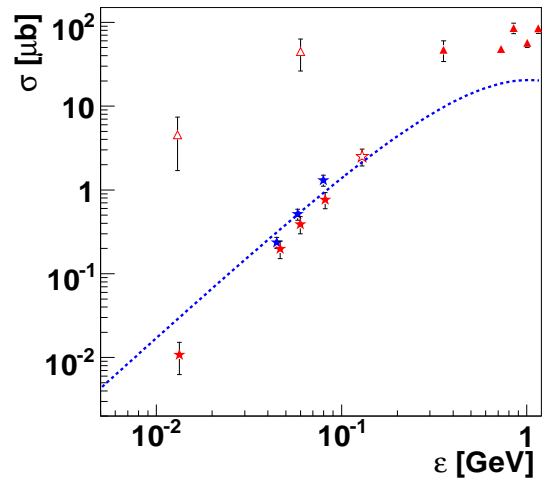


Fig. 7: Total cross section for the $pp \rightarrow K^+ n \Sigma^+$ reaction, shown in red. Closed stars represent the new ANKE data while the open one corresponds to their previous measurement. The COSY-11 results are shown by open triangles while the closed ones are taken from a compilation of higher energy data. Blue stars show values obtained for the $pp \rightarrow K^+ p \Sigma^0$ total cross section in the ANKE experiment. The line represents a phase-space fit to world data for this reaction.

can be no contribution from Λ production. Values of the $pp \rightarrow K^+ n \Sigma^+$ cross section extracted from these data are in complete agreement with the $K^+ \pi^+$ measurements. They have smaller statistical error bars, though it is harder to estimate the associated systematic uncertainties.

Information was also derived from the simultaneous measurement at ANKE of the inclusive K^+ cross section. Above the Σ thresholds, this has contributions from Λ , Σ^0 , and Σ^+ production and one has to subtract the dominant Λ cross section in order to get estimates for the Σ contributions. This is very model-dependent because of the small angular acceptance for the $K^+ p \Lambda$ channel well away from threshold and because the K^+ spectrum could change near the ΣN threshold. Nevertheless, by comparing the ANKE K^+ inclusive counting rates just above and below the Σ thresholds, it was possible to find an upper limit which showed that the cross section for Σ^+ production should be less than about twice that for Σ^0 . Even this weak limit is around two orders of magnitude below the COSY-11 results.

The ANKE data shown in the figure seem to rise steeper than phase space, especially if the bubble chamber results at higher energies are taken into account. Such a dependence, which is in complete contrast to the Λ case, might be associated with the strong coupling between the $\Sigma^+ n$ and Λp channels close to the Σ thresholds.

Hyperon production studies will continue at ANKE with the measurement of the $pn \rightarrow K^+ p \Sigma^-$ reaction. This is possible through the use of a deuterium target and the detection of the ‘‘spectator’’ proton in dedicated solid state telescopes that have been developed at IKP.

1.2.4 ϕ -Meson Width in Nuclear Matter

One of the goals of the experiment on ϕ meson production in pA collisions is to study the ϕ properties in nuclear matter at normal density. According to theoretical predictions the ϕ meson modification in mass is small and the main medium effect is a significant increase of its width up to an order of magnitude compared to the free (vacuum) value.

The experiment was carried out at an incident proton energy of 2.83 GeV with the ANKE spectrometer in 2007. The measurements were performed with four thin strip targets made from C, Cu, Ag and Au. About 5000–6000 ϕ -mesons via the K^+K^- decay were detected per nucleus at ANKE.

During its propagation out of nucleus the ϕ meson acquires an additional width connected to the imaginary part of the meson-nuclear potential which is responsible for the meson absorption in nuclear matter. Thus, the information about a modification of the ϕ width can be obtained from the A -dependence of the cross sections for ϕ production off nuclei with different atomic mass number A .

to be 21^{+5}_{-4} mb. This preliminary value exceeds that in vacuum (10 mb) by a factor of about 2. As a next steps we intend to study the momentum dependence of the ϕ meson width in the nuclear medium as well as determine the absolute values of the cross sections for ϕ meson production on C, Cu, Ag and Au nuclei.

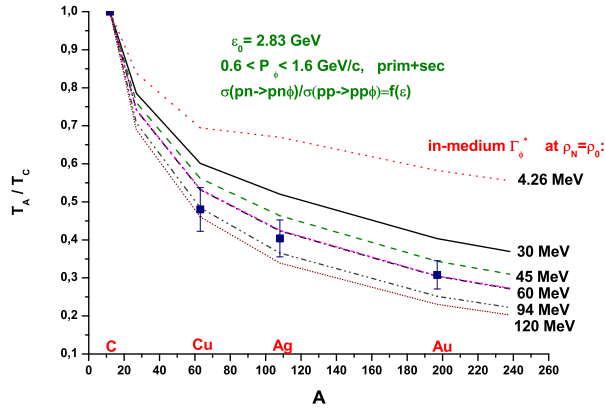


Fig. 8: Comparison of the measured transparency ratios R (preliminary) with theoretical folding model calculations.

In Fig. 8 the measured cross sections per nucleon for ϕ production on nucleus A normalized to the corresponding cross section on carbon $R = (12/A)(\sigma^A)/(\sigma^C)$, which is usually termed as a transparency ratio T_A/T_C , are presented together with theoretical calculations. The quantity $\Gamma_\phi^* = \Gamma_{\text{dec}}^* + \Gamma_{\text{coll}}^*$ stands for the total width in the ϕ rest frame and includes both decay and collisional parts. To determine the ϕ width in nuclear medium the set of the theoretical curves as well as experimental ratios were approximated by the function $(A/12)^{\alpha-1}$. The comparison of the experimental value of α with theoretical dependence of α on Γ_ϕ^* yields magnitude of $\Gamma_\phi^* = 65^{+17}_{-13}$ MeV taking into account the uncertainties of the performed fits. Under the assumption that the decay width is not modified in nuclear matter (keeps its vacuum value 4.26 MeV) the effective ϕN cross section in nuclear matter is found

1.2.5 Comparison of pd-Breakup and Backward Elastic Scattering

The deuteron breakup reaction $pd \rightarrow \{pp\}_s n$, where the diproton $\{pp\}_s$ is a fast proton pair emitted in forward direction with small excitation energy $E_{pp} < 3$ MeV, has been studied at proton beam energies of 0.5 – 2.0 GeV using the ANKE spectrometer at COSY-Jülich (S. Dymov *et al.*, “Deuteron breakup $pd \rightarrow \{pp\}_s n$ with forward emission of a fast 1S_0 diproton”, submitted to Phys. Rev. C). The reaction kinematics was similar to that of pd backward elastic scattering thus theoretical models previously developed for the $pd \rightarrow dp$ process and modified for the diproton channel were used for analysis of the data. In addition to the previously reported results (V.I. Komarov *et al.*, Phys. Lett. B **553**, 179 (2003)), the high statistics obtained at beam energies of 0.5, 0.8, 1.1, 1.4, and 1.97 GeV allowed us to determine the dependence of the differential cross section on the excitation energy E_{pp} of the proton pair, on the proton emission angle in the rest frame of the proton pair θ_k , and on the neutron emission angle θ_n . For E_{pp} less than 3 MeV the distributions of E_{pp} (see Fig. 9) and θ_k are caused by the final-state interaction between the protons, and are used here to validate the dominance of the 1S_0 pp state.

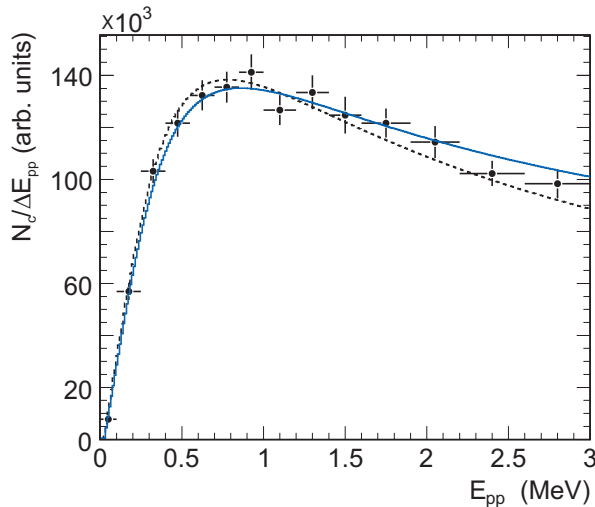


Fig. 9: Excitation energy E_{pp} of proton pairs from the $pd \rightarrow \{pp\}_s n$ reaction. The data were summed in the beam energy interval of 0.5 – 1.4 GeV. The curves show fits with the ONE + SS + Δ approximation (full line) and the Migdal-Watson (dashed).

The shape of the energy dependence of the measured differential cross section of the $pd \rightarrow \{pp\}_s n$ reaction obtained at $\theta_n = 180^\circ$ is similar to the one of pd backward elastic scattering (see Fig. 10), the cross section of the deuteron breakup reaction being about two orders of magnitude smaller. Interestingly both reactions exhibit an s^{-n} behavior with $n \sim 12$. The fits in the range 0.95 – 2.0 GeV for pd backward elastic scattering and $pd \rightarrow \{pp\}_s n$

yield exponents of $n = 11.70 \pm 0.32$ and $n = 11.88 \pm 0.53$, respectively. In the angular range from 168° to 180° the differential cross sections of the $pd \rightarrow \{pp\}_s n$ process change smoothly with θ_n and exhibit only a small variation of the slope near $\theta_n = 180^\circ$ as function of energy.

In view of high internal momenta $q \sim 0.5 - 0.6$ GeV/c probed by the ONE mechanism in this energy region, it is important to gain more insight into the ONE contribution by independent measurements. The planned measurements of the tensor analyzing power T_{20} and spin correlation $C_{y,y}$ of the $\vec{p}\vec{d} \rightarrow \{pp\}_s n$ reaction could clarify further the underlying dynamics of this process and shed light on the role of the ONE mechanism.

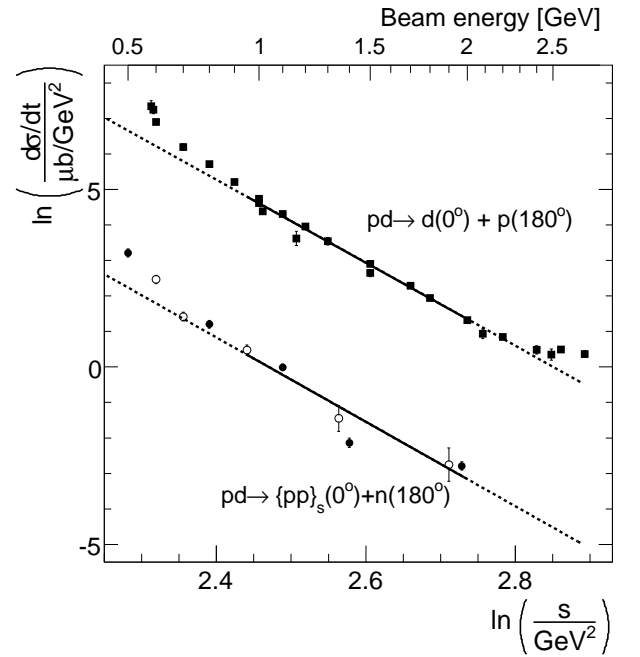


Fig. 10: Differential cross section $\ln\left(\frac{d\sigma}{dt}\right)$ as function of $\ln(s)$ for pd backward elastic scattering and the $pd \rightarrow \{pp\}_s n$ reaction. The previously obtained data are shown by open circles, the new data by bullets. The upper scale indicates the incident proton beam energy.

1.2.6 Investigations of the Deuteron-Proton System

Cross sections and vector analyzing powers of the ${}^1\text{H}(\vec{d},pp)n$ breakup reaction in the domain of very forward polar angles of the two breakup protons were determined in a dedicated experiment with the **GeWall** detector. They extend the available data base at 130 MeV and allow one to test several aspects of the $3N$ -system dynamics. Especially, the Coulomb interaction which strongly influences observables in this region of phase space, as it was hinted by previous experiments at KVI, was worth investigating.

One of the most important outcomes of the preliminary data analysis are arbitrary normalized breakup cross section distributions. Particular kinematical configurations of the breakup channel were selected by identifying the outgoing protons and integrating the events within the angular ranges of $\Delta\theta = \pm 1^\circ$ and $\Delta\varphi = \pm 5^\circ$. Those events were finally projected onto central kinematics and the intensity distributions along its length, parametrized with the variable S , were obtained. Figure 11 presents examples of such cross section distributions for a few kinematical configurations. The normalization is still arbitrary, thus only the shapes can be compared. The dips at the centers of the experimental distributions are quite characteristic and clearly illustrate sensitivity to the effect of Coulomb interaction in very forward polar angles and small relative azimuthal angles φ_{12} of the two protons, what is in very good agreement with theoretical expectations. Final absolute normalization of the data will allow to conclude about the overall ability of the theory to predict the breakup cross sections in the phase space region strongly affected by the long-range electromagnetic interaction.

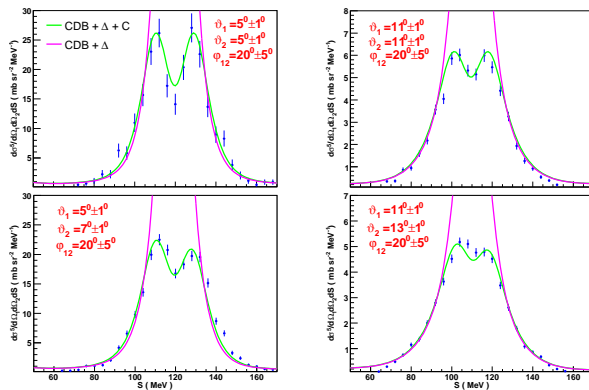


Fig. 11: Arbitrary normalized breakup cross sections for four sample angular configurations of the two breakup protons. The lines represent the results of the theoretical calculations within the Coupled Channel formalism with the CDBonn + Δ potential, with (green) and without (magenta) Coulomb interaction included.

In the next stage of the analysis breakup vector analyzing powers for selected kinematical configurations were evaluated. To achieve this goal, first the values of the vector

polarization of the deuteron beam was determined by using the elastic scattering events. In the experiment purely vector polarized beam ($P_z = -\frac{2}{3}$, $P_{zz} = 0$) and an unpolarized beam were used. After normalization, the numbers of the elastic scattering events for the vector polarization state $N_{\text{pol}}^{\theta_p}$ and for unpolarized state $N_0^{\theta_p}$, for a given polar angle θ were obtained, a ratio $f^{\theta_p}(\varphi)$ was constructed

$$f^{\theta_p}(\varphi) = \frac{N_{\text{pol}}^{\theta_p}(\varphi) - N_0^{\theta_p}(\varphi)}{N_0^{\theta_p}(\varphi)} \quad (1)$$

and plotted as a function of the azimuthal angle φ . This function depends on the polarization value P_z in a following way:

$$f^{\theta_p}(\varphi) = P_z i T_{11} \sqrt{3} \cos \varphi. \quad (2)$$

Applying the experimental values of $i T_{11}$ at $\theta^{\text{LAB}} = 13^\circ$ for the elastically scattered particles (KVI experiment), allows to obtain the beam polarization P_z from a fit of the $f^{\theta_p}(\varphi)$ distribution. On the other hand, using the P_z value evaluated at one angular point, one can use the above outlined procedure to calculate the elastic scattering analyzing powers $i T_{11}$ at other experimentally covered angles. This forms a valuable extension in the angular range of data for this observable to the area not covered by other experiments. The results, together with other data sets, are presented in Fig. 12.

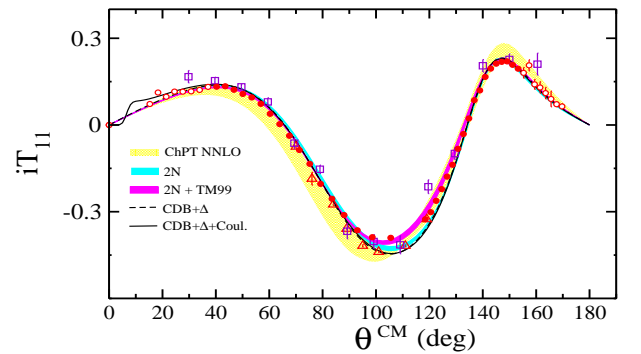


Fig. 12: Vector analyzing power $i T_{11}$ for dp elastic scattering: present experiment (red circles), KVI data (full red dots) and earlier data sets (triangles and squares). Theoretical predictions of different approaches (specified by the legend) are also shown.

In case of the breakup process, analogous function $f^\xi(\varphi_1)$ for a given kinematical point $\xi = (\theta_1, \theta_2, \varphi_1, \varphi_{12}, S)$ is defined and can be used to extract vector breakup analyzing powers A_x and A_y , by employing symmetry features which allow to simplify the calculations and reduce the systematic uncertainties. In the data sample processed until now one observes that none of the two observables reveals any significant sensitivity to the dynamical effects and that they are rather correctly reproduced by the state-of-the-art calculations. These conclusions shall be verified by the proceeding analysis of the whole data set.

1.3 Developments for the Experimental Facilities

1.3.1 First Double-Polarized Neutron-Proton Scattering Experiment at ANKE

In order to extract the basic spin-dependent two-body scattering information from the study of $\vec{d}\vec{p} \rightarrow (pp)n$, the deuteron charge-exchange break-up reaction, the ANKE collaboration together with the COSY crew have conducted successfully the first very complex double-polarized measurements. A key feature of the experiment was the use of a Polarized Internal Target (PIT) located between the dipole magnets D1 and D2 at the ANKE position (see Fig. 13).

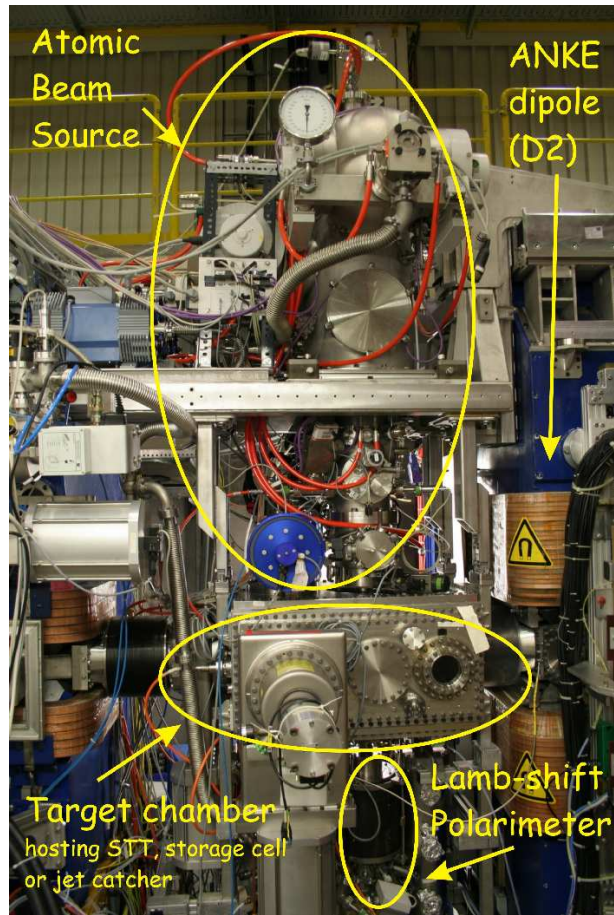


Fig. 13: Photo of ANKE with the Polarized Internal Target (PIT) in front of the spectrometer dipole D2. The main components of the PIT system: Atomic Beam Source (ABS), Lamb-shift Polarimeter (LSP), and the target chamber hosting the Storage Cell (SC) together with the Silicon Tracking Telescope (STT) system are indicated.

During the five weeks duration beamtime (in October/November 2009) the following achievements have been made:

- For the first time, studies with the COSY polarized deuteron beam were performed using a stor-

age cell (25 μm aluminium foil, with the inner surface covered by Teflon, of $20 \times 15 \text{ mm}^2$ cross section and 370 mm length). For this purpose the machine group furnished a special super cycle (including two or three flat-tops) with a polarized deuteron beam, electron cooled, stacked at injection and accelerated to $T_d = 1.2$ and $T_d = 2.27 \text{ GeV}$. The achieved beam quality generally allowed the deuterons to pass through the cell without touching the walls;

- To improve the COSY beam intensity, a longer stacking injection was implemented. In double-polarized measurements we worked with a super cycle of 15 and 45 minutes duration for two different flat-tops. Under these conditions about 4 to $6 \cdot 10^9$ polarized deuterons were accelerated to the flat-top energies;
- The expected density for the polarized hydrogen (\bar{H} gas) storage cell target of $d_t \leq 10^{13} \text{ cm}^{-2}$ was achieved. This value, together with the beam intensity of $6 \cdot 10^9$ stored polarized deuterons, led to a luminosity of $L \simeq 7 \sim 8 \cdot 10^{28} \text{ s}^{-1} \text{ cm}^{-2}$;
- The clean identification of events for the $\vec{d}\vec{p}$ -induced reactions when using a long cell target has been demonstrated. This was done on the basis of experimental information obtained from the \bar{H} gas target and on the known shape of the background from the cell walls, which is imitated through the use of N_2 gas in the cell. The exact shape of the background under the missing-mass peak from the cell-wall events has been determined under real experimental conditions and was under control during on-line measurements;
- Using the missing-mass technique for the measured single- and double-track events in ANKE, it has been shown that a very clean identification of the following reactions is possible: $\vec{d}\vec{p} \rightarrow dp_{\text{sp}}\pi^0$ (both branches of quasi-free $\bar{n}\vec{p} \rightarrow d\pi^0$), $\vec{d}\vec{p} \rightarrow (pp)n$, and $\vec{d}\vec{p} \rightarrow dp$. The last channel was identified unambiguously with very little background by using the silicon detectors, placed close to the storage cell in the vacuum target chamber (see Fig. 14), in coincidence with the forward detector system;
- In parallel to the data-taking, the ABS source has been tuned with Lamb-shift Polarimeter (LSP) measurements. The goal was to determine the target polarization (Q_y) from the quasi-free $n\vec{p} \rightarrow d\pi^0$ reaction. At this time the achieved value of average target polarization from the on-line analysis was around $\langle Q_y \rangle \sim 75\%$, which is quite close to the value obtained in the first measurements in 2007;
- We have extracted the value of the deuteron beam vector polarization P_z from the same quasi-free $\bar{n}p \rightarrow d\pi^0$ reaction using the angular dependence

of the analysing power of the $\vec{p}p \rightarrow d\pi^+$ reaction, which was also used to determine the target polarization. The result, $\langle P_z^{\text{ANKE}} \rangle = 0.660 \pm 0.09$, is consistent with the value of $\langle P_z^{\text{LEP}} \rangle = 0.646 \pm 0.008$, obtained from the Low Energy Polarimetry (LEP) measurements.

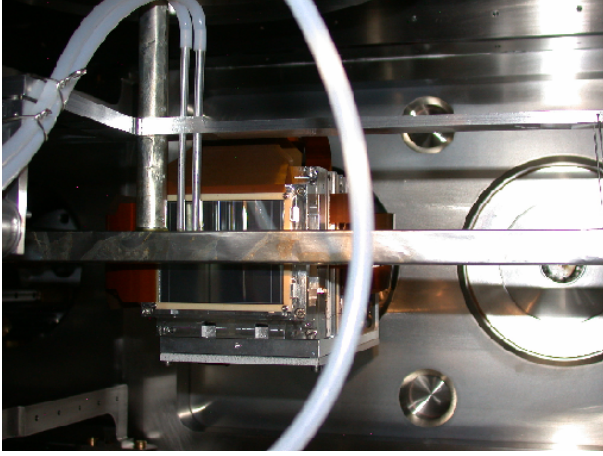


Fig. 14: Photo of the extended storage cell target position in the ANKE vacuum chamber together with the very closely located Silicon Tracking Telescope system.

Given the above successes in collecting a large amount of data from the $\vec{d}\vec{p} \rightarrow (pp)n$ deuteron charge-exchange break-up reaction, the main focus now is to extract the energy dependence of the spin-dependent np elastic amplitudes. We have recently published an extended paper on this issue (*c.f. D. Chiladze et al., Eur. Phys. J. A 40, 23 (2009)*). In order to show that one can extract information about neutron-proton amplitudes and not merely ratios, one has to describe absolute cross sections as well as analysing powers. The agreement of our experimental data at around $T_n = 600$ MeV/nucleon and calculations in impulse approximation using the SAID input np amplitudes is very encouraging. The ANKE data at $T_d = 2.27$ GeV ($T_n \approx 1.15$ GeV) are currently being analysed and the first preliminary results are shown in Fig. 15. Here the neutron-proton amplitudes are not well known and the deviations from the curves predicted on the basis of the current SAID analysis strongly suggest that these data can contribute to the establishment of reliable np amplitudes. The absolute normalisation will be achieved here on the basis of the fast spectator protons since the $pn \rightarrow d\pi^0$ cross section is too low at high energies. Now, the most important issue is to extract the spin correlation parameters to determine the relative phases of these amplitudes in addition of their overall magnitudes. This work is in progress.

It was already shown at Saclay many years ago that at $T_d = 2$ GeV one can also excite the $\Delta(1232)$ isobar in the charge-exchange reaction $\vec{d}\vec{p} \rightarrow (pp)n$ and substantial tensor analysing powers were measured. In impulse approximation, these are also sensitive to a spin-transfer

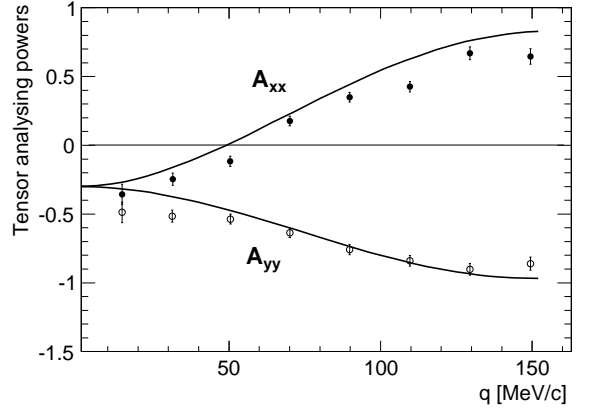


Fig. 15: Cartesian tensor analysing powers A_{yy} (open symbols) and A_{xx} (closed) of the $dp \rightarrow (pp)n$ reaction at beam energy of $T_d = 2.27$ GeV for $E_{pp} < 3$ MeV. The solid curves are the results of the impulse approximation program, for which the 1150 MeV input amplitudes were taken from the SAID database.

from the neutron to the proton in $np \rightarrow p\Delta^0$, which is very hard to measure directly. The Saclay spectrometer SPESIV had a very small acceptance and the experiments are now being repeated at ANKE. It is far too early to quote results but it is seen from Fig. 16 that the $\Delta(1232)$ is seen very clearly in the raw data.

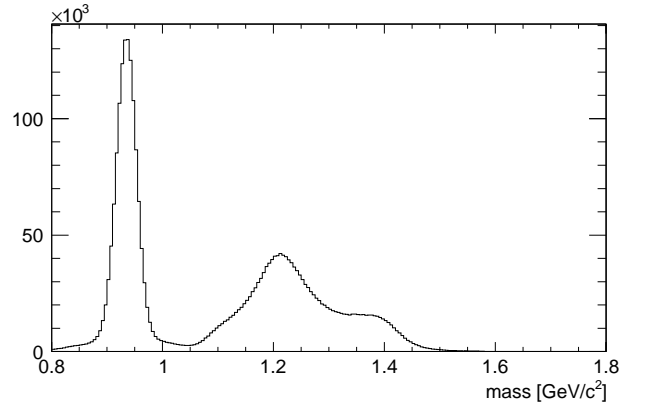


Fig. 16: Numbers of events from the unpolarised $dp \rightarrow \{pp\}_S X$ at $T_d = 2.27$ GeV as a function of the missing mass m_X . In addition to the neutron peak, one sees clear evidence for the excitation of the Δ^0 isobar.

Hence it seems that ANKE will also provide useful information on the spin structure of Δ excitation in neutron-proton collisions. This field will expand tremendously when the beam and target are interchanged and ANKE measures $pd \rightarrow \{pp\}\Delta$ with both slow protons in the Silicon Tracking Telescope system and the products of the $\Delta^0 \rightarrow p\pi^-$ in the ANKE magnetic spectrometer.

1.3.2 First Measurements with the Upgraded COSY-TOF Detector

A first measurement with the upgraded COSY-TOF Detector was performed in 2009 with a polarized proton beam at a momentum of 2.95 GeV/c. The COSY-TOF Straw Tube Tracker (13 double layers with in total 2704 tubes) and the Quirl Micro Strip Detector (2 double sided layers with in total 512 channels) provide an essential improvement of the tracking and vertex reconstruction of the COSY TOF detector.

The beam polarization was determined by measuring the asymmetry of elastic scattered protons by detecting both protons. In Fig. 17 the longitudinal versus the transversal momentum component of all measured particles of two prong events are plotted. A sharp band of the elastic scattering is seen over the background of events with mostly multi-pion production.

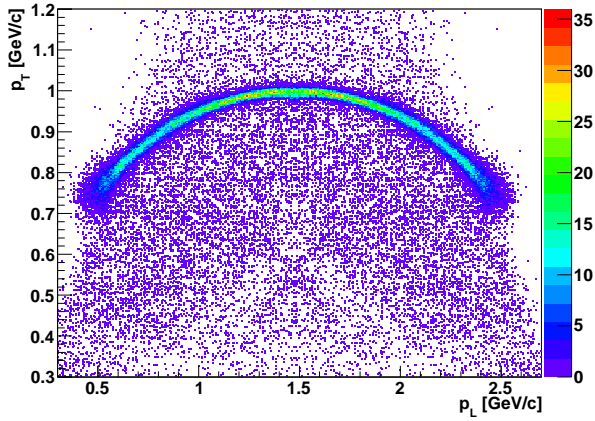


Fig. 17: Longitudinal versus transversal momentum of tracks of two prong events, which are coplanar in the limit of $\pm 2.5^\circ$.

Taking the sample of elastic events, which corresponds to $\vartheta^{\text{cm}} = 40^\circ - 70^\circ$ the asymmetry is measured to $(7.3 \pm 0.1)\%$ (see Fig. 18). The mean analyzing power in this angular range is 0.15 ± 0.02 . The resulting beam polarization is $(50 \pm 7)\%$.

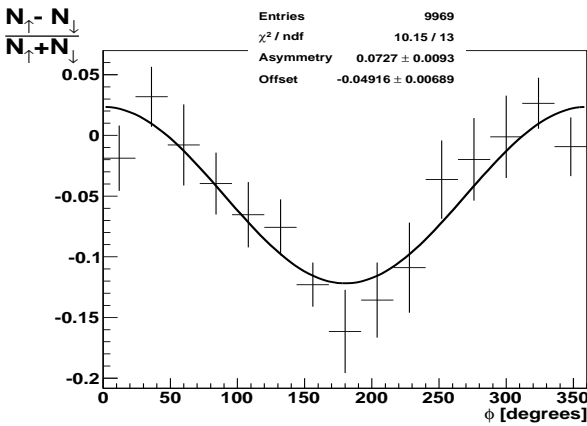


Fig. 18: Measured asymmetry for $\bar{p}p \rightarrow pp$ in the range of $\vartheta^{\text{cm}} = 40^\circ - 70^\circ$.

The efficiency and the resolution of the track finding algorithm for the straw tube tracker has been improved. In Fig. 19 one of the three orientations of the chamber stack is shown with a possible candidate for a $\bar{p}p \rightarrow pK^+\Lambda$ event. Two tracks are pointing to $x = 0$ cm at $z = 0$ cm, which is the target position, while the other two tracks stem from a secondary vertex around $z = 15$ cm, which may be the decay point of a Λ particle.

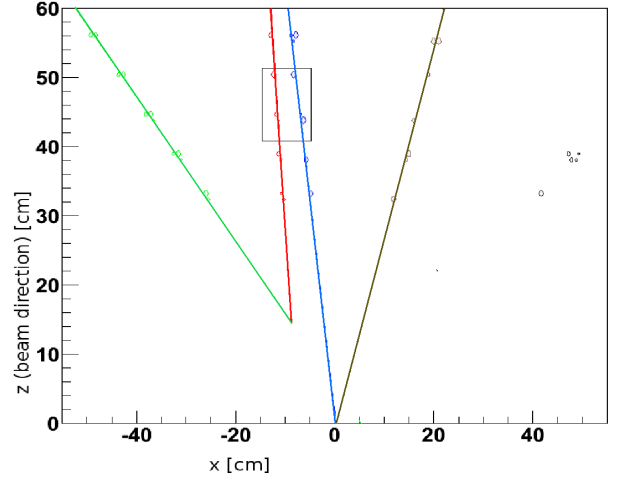


Fig. 19: For one event all tubes of planes with horizontal orientation, which have a hit, are marked with their isochrone circles. The lines represent the calculated tracks. z is the beam axis, x is the axis perpendicular to the beam and to the wires.

In Fig. 20 an enlarged view is shown. Each circle represents the isochrone of a tube wire, which was hit. The radius of the isochrones is determined from the measured drift time with a calibration function. In the ideal case a track should be a tangent to each of the isochrones.

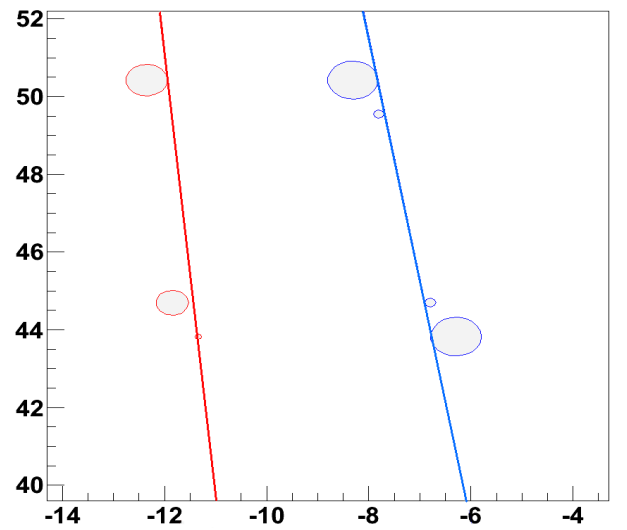


Fig. 20: Enlarged view of two of the tracks with isochrones. The displayed area is indicated by the rectangle in Fig. 19.

1.3.3 Achievements with the WASA Detector

In 2009, with the emphasis on η -decay studies the physics programme of WASA-at-COSY was successfully continued taking 8 weeks of data in Aug/Sep for the reaction $pd \rightarrow {}^3\text{He}\eta$ at proton energy of 1000 MeV. The data were collected at luminosities of up to few times $10^{31}\text{cm}^{-2}\text{s}^{-1}$ and typical trigger rates of 1–2 kHz. Together with the η sample of a 4 weeks run taken in Sep2008, more than 30 mio η -decays are currently available. During the long campaigns in 2009, WASA-at-COSY was operating very stable for all components and as a consequence of modifications to the gas system, the deuterium pellet target performance has shown duty factors larger than 80% throughout the 8 weeks $pd \rightarrow {}^3\text{He}\eta$ production run. That beam time represented the longest continuous operation of the WASA-at-COSY detector so far. In summary the technical improvements done in 2009 comprise first successful prototype testing of a new trigger board, which will be employed to compute basic kinematic variables online on the trigger level using an FPGA chip. New photomultiplier tubes were installed in the forward range hodoscope to improve the linearity of the signal response. A new high voltage system for the forward scintillator detectors was installed, which provides better stability and replaced the old LeCroy HV-system increasingly exhibiting problems due to aging.

In the following the developments on the new forward veto hodoscope, the new trigger system and the options on the anticipated DIRC concept for WASA-at-COSY are discussed in more detail.

New Forward Veto Hodoscope for WASA-at-COSY

In order to match the increased luminosity of the WASA detector at the COSY ring the Forward Detector has been upgraded. In addition to the new two-layer Forward Window Hodoscope (FWC) a new Forward Veto Hodoscope (FVH) has been built and installed by the Tübingen group. Since the Forward Range Hodoscope (FRH) has been extended by two new layers in 2007, the old FVH no longer covers the full angular range. The new FVH as shown in Fig. 21 is higher segmented and has been

- placed at maximum distance from the target spot, *i.e.* just in front of the COSY quadrupoles downstream the beamline, in order to have a 2.5 m flight path between the FWC as start detector and the new FVH as stop detector for TOF measurements,
- mounted as vertical bars, so that together with the horizontally mounted bars of the updated old FVH we get a pixel structure, which can be used for trigger purposes and position measurements,
- equipped with two horizontal bars at the upstream side to allow a convenient timing calibration of the full layer.

The construction phase started 2008. In order to get maximum light output for an optimal performance — in particular with regard to timing — adiabatic lightguides as

shown in Fig. 21 were built. The installation was completed in August 2009. The commissioning during the subsequent beam time showed that all detector parts work as designed.

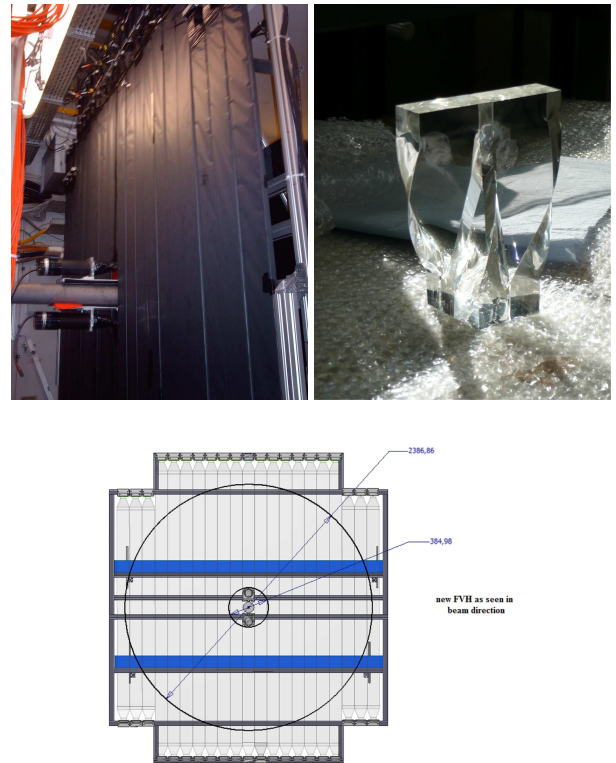


Fig. 21: New forward veto hodoscope at WASA-at-COSY. Upper left: Front view of the new FVH layer. Upper right: Adiabatic lightguide for an optimum performance of light collection. Lower: Design of the new FVH layer, which consists of 22 vertical and 2 horizontal bars. The latter as well the vertical bars touching the beampipe are read out by 90° deflection via prisms.

The new trigger system The new trigger system will take advantage of the newly developed continuous-sampling front-end QDC modules. The QDCs are equipped with 12-bit ADC converters running at 160 Msamples/s. The modules contain programmable logic (FPGA), which are used to extract times and integrals of the detector signals. The trigger uses an extraction algorithm which runs in parallel to the normal data acquisition branch. The data for the trigger are transmitted by high speed serial optical links from the QDC to the trigger unit, which in turn evaluates complex physical quantities like invariant and missing masses, using the QCD information from the detector.

The main component of the system is the trigger board equipped with 16 SFP optical links and a set of I/O connectors. The trigger system receives signals from the 120 sector elements of the Forward Range Hodoscope (FRH)

and angular information ' θ ' for each sector, evaluated from the Forward Trigger Hodoscope (FTH).

The new trigger setup was installed and tested in a WASA-at-COSY test in December 2009. A user interface was implemented, which will allow to readout, data quality monitoring, loading of the setup data, trigger diagnostic and control. The trigger board shown in Fig. 22 based on the Virtex 5 FXT FPGA chip was successfully integrated into the WASA DAQ-system.

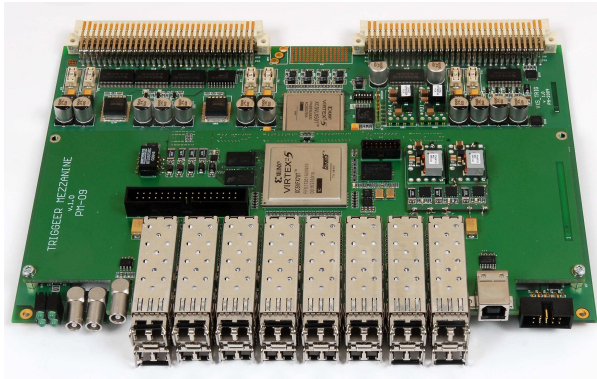


Fig. 22: Trigger board with Virtex 5 FXT FPGA chip.

The future plans include the commissioning and subsequent use of the new trigger system during the runs in February 2010. By using the online calculated kinematical quantities in the trigger process it will be possible to significantly enhance the trigger selectivity. This will be the crucial step in increasing the luminosities in upcoming $pp \rightarrow pp\eta$ runs. Later also additional information of the calorimeter and the MDC will be included.

DIRC Detector

The WASA-at-COSY collaboration plans to build a focussing disc DIRC counter (DIRC=Detection of Internally Reflected Cherenkov light). Usually such a RICH-type Cherenkov counter which measures the velocity is used for particle identification, but in the case of WASA the focus is on kinetic energy measurement. The planned DIRC will improve the kinetic energy measurement for protons in the forward direction from ~ 400 MeV to ~ 800 MeV, measuring their velocity at the few % c -level.

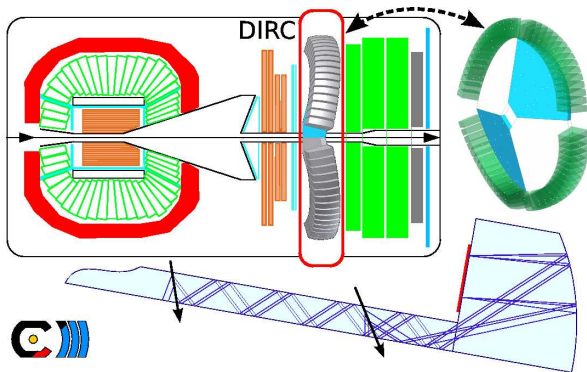


Fig. 23: DIRC concept for WASA-at-COSY.

In the DIRC radiator discs, about one half of the Cherenkov photons are contained by total internal reflection and travel along a zigzag line through the plate. The parallel surfaces preserve the Cherenkov angle until the photons reach the focussing light guides circling the disc rim. These convert angle into position information as they image the Cherenkov light onto a focal plane covered with photon sensors.

The version of the CEARA (Cherenkov-Emissions-Analysierender Ringscheiben-Apparat) design proposed to suit WASA uses four quarter-circle acrylic glass radiator plates tilted 20° from perpendicular orientation to beam. Each of the 64 focussing light guides (16 per quarter disc) covering an angular range of 20° to 50° are instrumented with two multi-pixel-PMTs and read out as 16 pixels of $6 \times 48 \text{ mm}^2$.

Such a disc type DIRC is planned to be placed between the FTH and the three largest FRH layers as is shown in Fig. 23. Via $\Delta E - E$ correlations, the FRH-elements continue to provide particle identification. The segmentation into four quarter-discs allows to incline the radiator relative to the incoming particles and thus lower the threshold velocity for light propagation inside the DIRC radiator.

When measuring η' rare decays where most final state protons punch through we expect a considerably improved missing mass resolution with the DIRC upgrading of the WASA-at-COSY detector.

Outlook

It is anticipated to enlarge the statistics of η -decays produced in the reaction $pp \rightarrow pp\eta$ in an eight weeks run granted by the PAC in spring 2010. The study of η -production/decay via the pp -reaction becomes feasible with selective trigger conditions and the commissioning of the new trigger concept. WASA-at-COSY will also embark on η' production in $pp \rightarrow pp\eta'$ reactions for 1 week in autumn 2010.

Employing the Glasgow photon tagging spectrometer at the Mainz Mikrotron (MAMI) tagged photons in the energy range of ~ 40 -1400 MeV will be used for measuring the response functions of the sodium doped CsI-crystals as they are used in the WASA-at-COSY calorimeter in spring 2010.

Work on pellet detection with optical position measurements using lasers and fast line-scan (linear CCD) cameras was continued at TSL and at FZJ. The plan for 2010 is to get a 'toy' system in operation at UPTS and to start to prepare a simple tracking system based on 3-4 line-scan cameras for WASA-at-COSY.

In order to further improve the velocity resolution for high energy protons better than 1% and therefore significantly improve the missing mass resolution and signal-to-background ratio for the tagging of heavier mesons, studies to complement the forward detector with a DIRC type Cherenkov detector are continued in 2010. The current R&D work for the DIRC realization at WASA-at-COSY, its prototyping and future operation at COSY will provide at the same time valuable input for the conceptional design studies of the PANDA DIRC-detector at HESR.

1.3.4 Status of the PAX Experiment

Decisive steps have been accomplished by the PAX Collaboration in 2009. Two Proposals, to the COSY PAC and to the CERN SPS-Committee, have been submitted to perform spin-filtering studies with protons at COSY and with antiprotons at the AD ring at CERN.

The submissions came as natural consequence of two fundamental achievements:

- the result of the depolarization studies performed at COSY in 2008 that demonstrated the impossibility of polarizing a stored beam of protons (antiproton) by spin-flip exploiting the electromagnetic interaction and confirmed that spin-filtering by hadronic interaction with a polarized internal target, is the only viable method to polarize a stored beam;
- the introduction of a new solution for the realization of the low-beta section employing only warm magnets, that allowed the development of a staged approach for the PAX installation at AD entirely compatible with the existing users community.

Coming to the aim of the proposals, the scientific objectives of the experiments at COSY are twofold. Despite the fact that a proof of the spin-filtering principle has already been produced by the FILTEX experiment at the TSR-ring, a measurement of the polarisation build-up at COSY will yield values for the proton-proton spin-dependent total cross sections at different energies, allowing to match these cross sections to the spin-filtering process involving machine related issues. Therefore, spin-filtering experiments at COSY would provide the necessary data to test and improve our present understanding of spin-filtering processes in storage rings. Secondly, we would like to commission the setup, which will be used for the experiments with antiprotons at AD.

The aim of the experiments at CERN is to determine for the first time total spin-dependent $\bar{p}p$ cross section at antiproton beam energies in the range from 50 to 450 MeV. The data obtained are of interest by themselves for the general theory of $\bar{p}p$ interactions since they will provide a first experimental constraint of the spin-spin dependence of the nucleon-antinucleon potential. In addition, measurements of the antiproton polarization buildup are required to define the optimum parameters of a future, dedicated Antiproton Polarizer Ring (APR), intended to feed a double-polarized asymmetric $\bar{p}p$ collider with polarized antiprotons.

The COSY-PAC recognized that two experiments PAX and WASA will be the main users of COSY beam time in the future and “reiterated the importance of the proposed measurement of polarization build-up”. It additionally stated that: “A program of $\bar{p}p$ scattering at these facilities is of great current interest and should be developed with vigor”.

The CERN SPS-Committee acknowledged the effort of the Collaboration in the preparation of the proposal, but

before to proceed further it encouraged “the PAX Collaboration to first perform their spin filtering measurements at COSY”.

The explicit request from the CERN-SPSC puts the measurements at COSY into an optics of wider attention and importance as they become a necessary step for the following investigations with antiprotons at AD.

The first concrete step towards the experiments at COSY has been already performed in summer 2009 with the installation in COSY of four new quadrupoles at the new PAX interaction point for the implementation of the low beta-section.

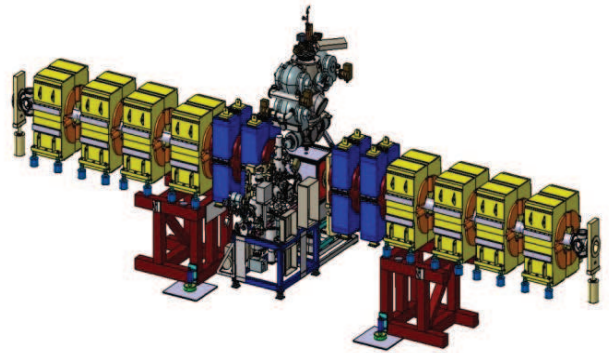


Fig. 24: New PAX interaction point, showing in yellow the existing COSY quadrupoles and in blue the new installed ones.

The magnets have been successfully operated at the required excitation at injection energy in January 2010. After readjustment of the regular COSY quads, no reduction of the performance of COSY was observed. Finally it is worth mentioning the prestigious and encouraging acknowledgment by from the European Research Council (ERC) that shortly before Christmas approved the Advanced Research Grant application entitled “Production of Polarized Antiprotons (POLPBAR)”. The Principal Investigator is Prof. Dr. H. Stricker, director of IKP2. The grant covers a 5 year period, including both the measurements at COSY and at AD.

1.3.5 A Polarized Internal Gas Target for Spin-Filtering Studies at COSY and AD

The high physics potential of experiments with stored high-energy polarized antiprotons led to the PAX proposal for the High Energy Storage Ring (HESR) of the FAIR facility (Facility for Antiproton and Ion Research) at GSI. It is proposed to polarize a stored antiproton beam by spin filtering with a polarized hydrogen (deuterium) gas target. In order to understand the underlying processes and find the best working conditions several experimental studies with protons (at COSY) as well as with antiprotons (at AD/CERN) have to be carried out. These investigations require an experimental set-up including a polarized internal gas target (PIT) and a system of Silicon detectors implemented in a large acceptance section of the storage ring.

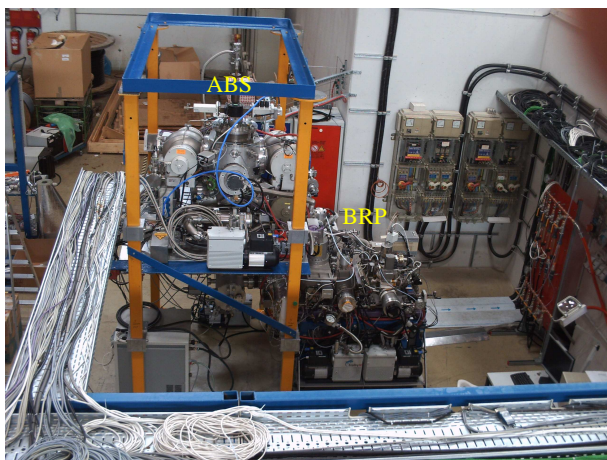


Fig. 25: The polarized internal target at the so-called LKW-Schleuse in the COSY hall.

The former HERMES polarized target was transported and put into operation at the IKP in the COSY accelerator hall with a modified vacuum system and a new support (Fig. 25). It was completely re-cabled to allow a fast assembly and disassembly at COSY and AD. The ABS produces a polarized atomic hydrogen or deuterium beam which is injected into a storage cell. The present cell design consists of $5\ \mu\text{m}$ Teflon walls supported by an aluminum frame. This solution allows to reach the necessary areal densities for spin filtering and to avoid depolarization and recombination. A small sample of the storage cell gas is extracted and analyzed in the so-called Breit-Rabi polarimeter (BRP). Different combinations of high frequency transitions (HFT's) together with a sextupole magnet system select distinct hydrogen hyperfine states. The occupation numbers of these states are measured in the BRP quadrupole analyzer.

In order to measure the polarization of the target gas the efficiencies of the high frequency transitions in the BRP have to be obtained. Several ABS injection modes together with different settings of BRP HFT's provide the necessary data to evaluate these efficiencies (Fig. 26).

First measurements with the BRP show high efficiencies

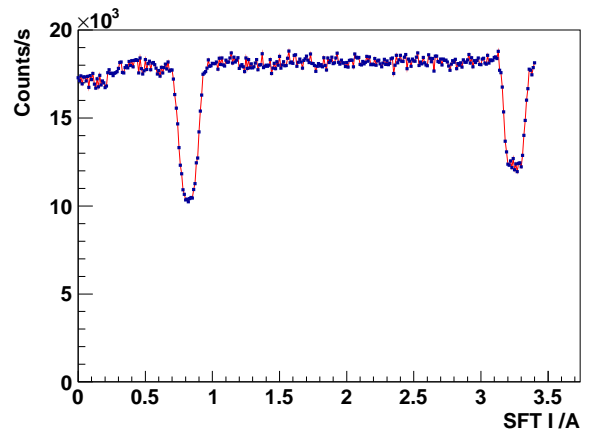


Fig. 26: Efficiency measurement of one BRP HFT. The ABS injects states $|1\rangle$ and $|2\rangle$. The dependence of the BRP counting rate on the current through the magnetic field coils of the strong field transition (SFT) is shown. At 0.8 A (3.2 A) state $|1\rangle$ ($|2\rangle$) is exchanged with state $|4\rangle$ and afterwards removed by the sextupole magnet system. Therefore the rate drops.

(Table 1) for the used high frequency transitions (HFT's) in the BRP for hydrogen.

Table 1: The efficiencies of the BRP HFT's.

transition		efficiency	ideal
SFT	ϵ_{14}	0.974 ± 0.008	1
	ϵ_{24}	1.008 ± 0.012	1
MFT	ϵ_{13r12}	1.023 ± 0.075	1
	ϵ_{13r23}	0.918 ± 0.059	1
	ϵ_{23r12}	0.082 ± 0.007	0
	ϵ_{23r23}	0.892 ± 0.012	1

Next steps are the preparation of the target gas analyzer to measure the relative fraction of hydrogen atoms and molecules in the target gas and the implementation of the operation with deuterium.

2 COSY Operation and Developments

2.1 Status of the 2 MeV Electron Cooler

The 2 MeV electron cooling system for COSY was proposed to further boost the luminosity even in presence of strong heating effects of high-density internal targets. The project is funded since mid 2009. Manufacturing of the cooler components has already begun. The space required for the 2 MeV cooler is being made available in the COSY ring. The design and construction of the cooler is accomplished in cooperation with the Budker Institute of Nuclear Physics (BINP) in Novosibirsk, Russia.

The 2 MeV cooler is also well suited in the start up phase of the High Energy Storage Ring (HESR) at FAIR in Darmstadt. It can be used for beam cooling at injection energy and is intended to test new features of the high energy electron cooler for HESR.

The basic parameters for the COSY cooler are listed in Table 2. The mechanical dimensions are given by the space available in the COSY ring. The height is limited to 7 m by the building. In Fig. 27 the layout of the 2 MeV cooler is shown. The high voltage (HV) terminal is installed inside the pressure vessel filled with SF₆ gas.

To preserve the low transverse temperature of electrons the accelerating structure inside the pressure vessel is surrounded by solenoid coils. A HV section is a module containing two coils, a HV power supply providing the voltage to the accelerating tubes, a low voltage power supply to power the coils, and the power generator. All components of any single HV section are at the same electrical

Table 2: Basic Parameters of the 2 MeV cooler.

Energy Range	0.025 – 2 MeV
High Voltage Stability	$< 10^{-4}$
Electron Current	0.1 – 3 A
Electron Beam Diameter	10 – 30 mm
Length of Cooling Section	2 – 3 m
Toroid Radius	1.00 m
Magnetic Field (cooling section)	0.5 – 2 kG
Vacuum at Cooler	$10^{-9} - 10^{-10}$ mbar
Available Overall Length	6 m
Maximum Height	7 m
COSY Beam Axis above Ground	1.8 m

potential. The HV system of the cooler consists of 33 identical HV sections.

The design of the cooling section solenoid is similar to the ones of CSR (IMP Lanzhou) and LEIR (CERN) designed by BINP. However, for the 2 MeV cooler the requirement on the straightness of magnetic field lines ($\Delta\theta < 10^{-5}$) is so high that a system for the control of magnetic field in vacuum becomes necessary.

For the last few years the COSY-BINP collaboration has developed prototype elements for the magnetized cooler. Two types of power generators for the HV sections, were studied, one utilizes a gas turbine the other is based on an inductance-coupled cascade generator.

The turbine electro generator driven by compressed gas was built and tested. The gas is used to produce power for individual sections and, at the same time, to cool the magnetic coils. In a test bench at BINP the prototype of the HV section was successfully tested under differ-

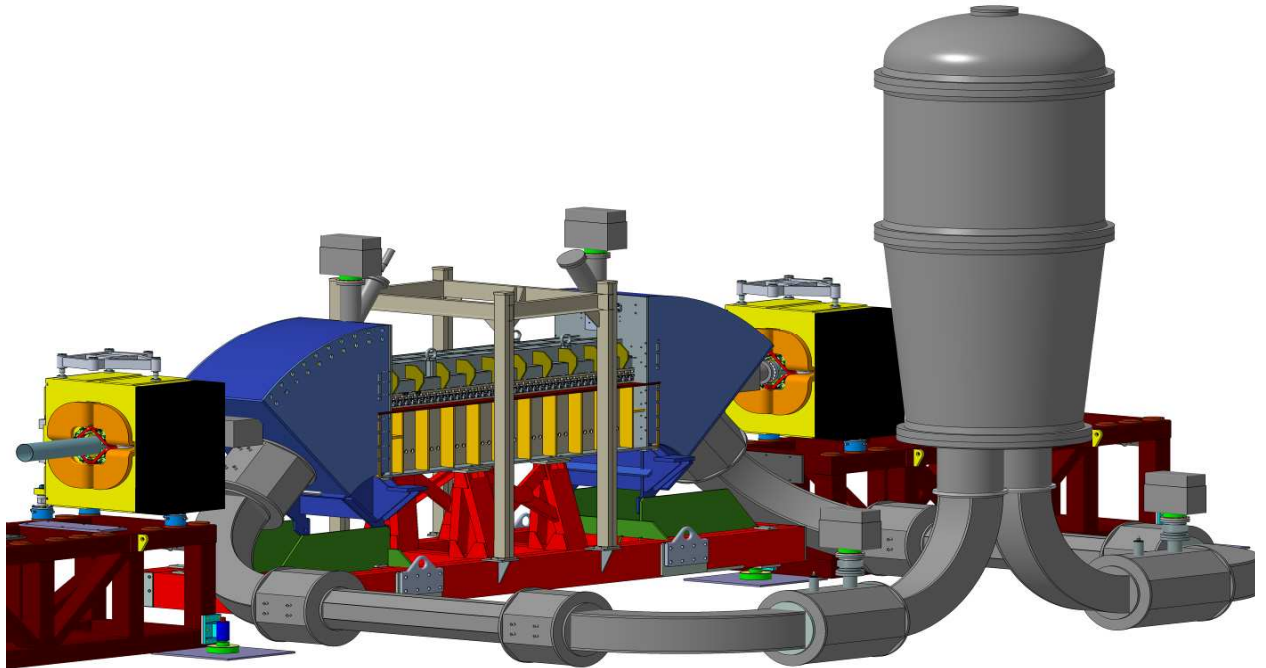


Fig. 27: Layout of the 2 MeV electron cooler.

ent gas mixtures and pressures. The specified voltage of 60 kV per section was demonstrated under an SF₆ pressure of 1.6 atm (c.f. *J. Dietrich et al., Status of the 2 MeV Electron Cooler for COSY Jülich, Proc. COOL 2009, Lanzhou, China*). A voltage stability of better than 10⁻⁴ was achieved. The required magnetic field of 500 G in the two coils of one HV section was obtained. For electron energies above 2 MeV the turbine generators are a good choice.

Now, a new power generator, which seems to be a more practical solution for up to 2 MeV electron energy, is being considered. The basic idea of the power generator is that the HV terminal and the collector represent a high frequency multiple-stage cascaded resonant rectifier system. AC power is inductively coupled in series from one transformer rectifier stage to the next. The system consists of 33 transformers with cascaded connection. From the ground energy is transferred from section to section toward the HV terminal. Along this way a fraction of the energy is consumed by the HV sections. The main issue with such a solution is the magnetic field leakage from the transformer that can be resolved by adding a compensating capacitance. The transformer column has a spark gap system for safety in case gas a breakdown occurs (c.f. *Conceptual Design Report, Novosibirsk 2009*).

The electron cooling system utilizes electron beam energy recuperation scheme. The beam coming from the electron gun is accelerated in the accelerating tube structure and decelerated in the collector.

The final energy of the electron beam to be dumped in the collector should be minimal.

For suppression of high energy electron beam losses at IMP and LEIR coolers electrostatic bending was used. The shape of the 2 MeV transport lines, however, dictates a different approach. The collector (inside the HV terminal) will be modified to suppress return flux.

A sketch of the collector is shown in Fig. 28. The top electron current is 3 A and the maximal voltage is 5 kV. The collector accepted power is 15 kW. A water or oil cooling system for the collector should be used. In the case of water cooling system a heat exchanger should be installed at the HV terminal. Removing the heat from the high-voltage terminal can be done with oil system only because of the presence of high voltage (2 MV). Special emphasis in designing the collector is placed on minimizing the number of reflected electrons.

The efficiency of the collector may be improved by installing a velocity filter. The region with crossed electric and magnetic fields lets the electrons moving in one direction pass and strongly deflects the electrons moving in the opposite direction ($E \times B$ Wien velocity filter). This approach is similar to using electrostatic bending but offers technological advantages.

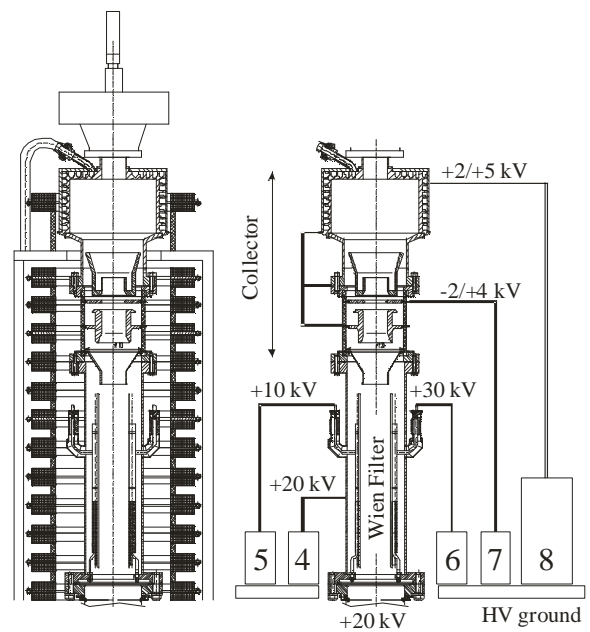


Fig. 28: Sketch of the collector subsystem. The power supplies for: 4 – drift tube of the Wien filter, 5 – negative electrostatic plate of Wien filter, 6 – positive electrostatic plate of Wien filter, 7 – suppressor electrode of the collector, 8 – collector.

2.2 Tests of Momentum Cooling Techniques with Internal Target and Barrier Cavity

Theoretical investigations of stochastic momentum cooling for the HESR clearly reveal that the strong mean energy loss induced by the interaction of the beam with an internal pellet target can not be compensated by cooling alone (*c.f.* H. Stockhorst *et al.*, *Compensation of Mean Energy Loss due to an Internal Target by Application of a Barrier Bucket and Stochastic Momentum Cooling at COSY*, Proc. COOL 2009, Lanzhou, China). A promising method to compensate the mean energy loss and thus to provide an antiproton beam with a significantly reduced momentum spread is the application of the broadband barrier bucket (BB) cavity in the HESR. Two stochastic cooling techniques are envisaged. In the filter cooling method a pickup in sum mode measures the beam current and the discrimination of particles with different momentum deviations is obtained by inserting a notch filter in the signal path before it drives a kicker in sum mode. The advantage of this method is that Schottky particle noise is substantially suppressed in the centre of the particle momentum distribution. A severe restriction in the practical cooling bandwidth comes from mixing between pickup and kicker. Large mixing from pickup to kicker will reduce the maximum momentum spread that can be cooled for a given upper cooling frequency without particle losses. Strong unwanted mixing from pickup to kicker prevents especially filter cooling below 3.8 GeV/c in the HL-mode. In the low momentum range 1.5 GeV/c up to 3.8 GeV/c TOF cooling is therefore envisaged. In this method the filter in the cooling chain is removed and the signal transit time from pickup to kicker is adjusted to the time-of-flight of a particle with nominal momentum. Mixing from pickup to kicker can now be used to discriminate between particles of different momenta. This method attains a larger cooling acceptance which is especially preferable for the HL-mode. Larger initial momenta can thus be cooled without particles losses. The main disadvantage of this method is however that due to the absence of the notch filter strong particle noise diffusion occurs in the distribution centre. The gain of the cooling system should be then reduced to avoid too much Schottky heating in the center of the distribution.

At COSY stochastic cooling and internal targets are available similar to those which will be operated at the HESR. A barrier bucket cavity is routinely in operation (*c.f.* R. Stassen *et al.*, *COSY as ideal Test Facility for HESR RF and stochastic cooling hardware*, Proc. PAC09, Vancouver, Canada). Thus, the machine is exquisitely suitable for beam dynamic experiments in view of the HESR. Important feasibility studies to compensate the large mean energy loss induced by an internal pellet target similar to that being used by the PANDA experiment at the HESR with a barrier bucket cavity (BB) have been carried out. Stochastic momentum cooling as well as transverse cooling can be applied. The system consists of

two bands. Band I covers the frequency range (1 – 1.8) GHz and band II the range (1.8 – 3) GHz. The pickup and kicker electrode bars are movable to achieve a maximum in sensitivity. In these experiments only momentum cooling in band II is considered. A remote 90° phase shifter was added in the cooling path which is necessary to switch between TOF and filter cooling. The proton beam was accelerated to 2.6 GeV/c. To avoid transition crossing during acceleration the optics in the arcs is manipulated so that the transition energy is shifted upwards. When the flat top momentum is reached the acceleration rf-cavity is switched off and the optics is changed again so that now the machine is operated above transition energy. By this both straight sections of COSY attain zero dispersion. The pellet target of the WASA installation is located at a dispersion free position in the target straight section. A flat top time of about 1000 was chosen and the particle number was about $(1 - 2) \cdot 10^9$.

In the experiments the beam was initially heated by applying band-limited white noise with $\Delta W = 700$ Hz at harmonic number one with a momentum kicker in order to show the larger cooling momentum acceptance of TOF cooling as compared to filter cooling. In Fig. 29 the result of only filter cooling is displayed. After 200 s the distribution is cooled but exhibit still tails towards lower and higher frequencies. This indicates that filter cooling is more effective in the center. Particles with lower or higher frequencies in the tails see a wrong sign in the cooling force and are driven further out of the center.

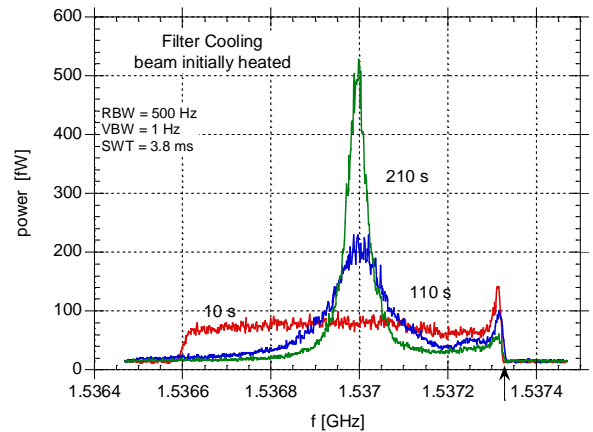


Fig. 29: Power spectra at harmonic number 1000 during filter cooling. The beam is initially heated.

As a result a fraction (28%) of the beam particles in the tails is heated by the cooling system and is lost at the momentum acceptance of the machine.

At 1.5374 GHz a small peak (see arrow in Fig. 29) is visible which is due to a vanishing local frequency slip factor. The available particle frequency attains here a maximum value. Particles which loose energy due to the heating can not have frequencies beyond that value. They enhance the density in the vicinity of this value leading to asymmetric distributions. As seen in Fig. 29 the tails are reduced by cooling and heating as time proceeds.

In order to avoid initial particles losses the beam was pre-cooled with the TOF method for 200 s. After pre-cooling the cooling system was switched to filter cooling: The filter part that contains the delay by one revolution was closed and the gain was inverted. The result is shown in Fig. 30 where one observes that the tails are reduced by cooling. Particles are moved to the center during pre-cooling ($t = 210$ s). Also the particle enhancement at the small peak is reduced by TOF cooling. In this case almost no particle losses were observed. The final relative momentum spread after 900 s of cooling was $1 \cdot 10^{-4}$ (FWHM).

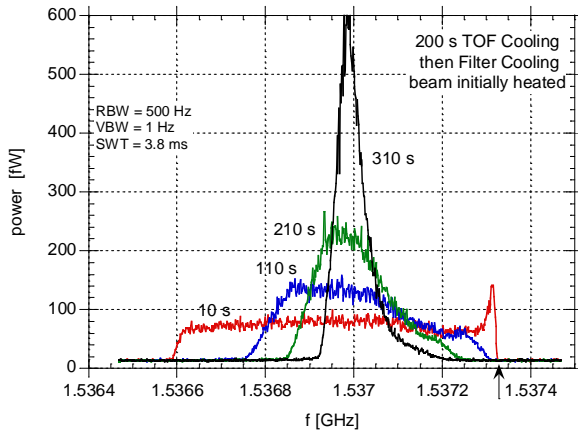


Fig. 30: Power spectra at $n = 1000$ during cooling. The beam is pre-cooled with TOF cooling for 200 s. The cooling system is then switched to the filter cooling method.

This experiment proved that the TOF cooling technique possesses the theoretically predicted behaviour and that one can switch from TOF to Filter cooling without particle losses. After this stochastic momentum cooling of protons subject to the synchrotron motion induced by a barrier bucket or $h = 1$ cavity was carried out.

Figure 31 compares from top to bottom filter cooling without synchrotron motion and cooling with a barrier bucket cavity and the $h = 1$ cavity operation. The maximum available barrier bucket peak voltage $U_0 = 175$ V was used. The $h = 1$ cavity was operated at a peak voltage $U_0 = 200$ V. The target was switched off for this study. Figure 31a shows filter cooling of the initially not heated beam. A significant cooling is visible after 310 s. The filter frequency is slightly above the initial center frequency. The influence of the synchrotron motion of the protons in a barrier potential becomes visible in Fig. 31b. After 310 s the beam width is reduced by cooling. The resulting width is however broader as compared to only filter cooling in Fig. 31a. While in Fig. 31a the filter determines the center of gravity of the distribution it is determined by the barrier frequency.

Momentum cooling becomes less effective with synchrotron motion induced by the $h = 1$ cavity. Particle losses occur and the momentum spread is only slightly reduced (Fig. 31c).

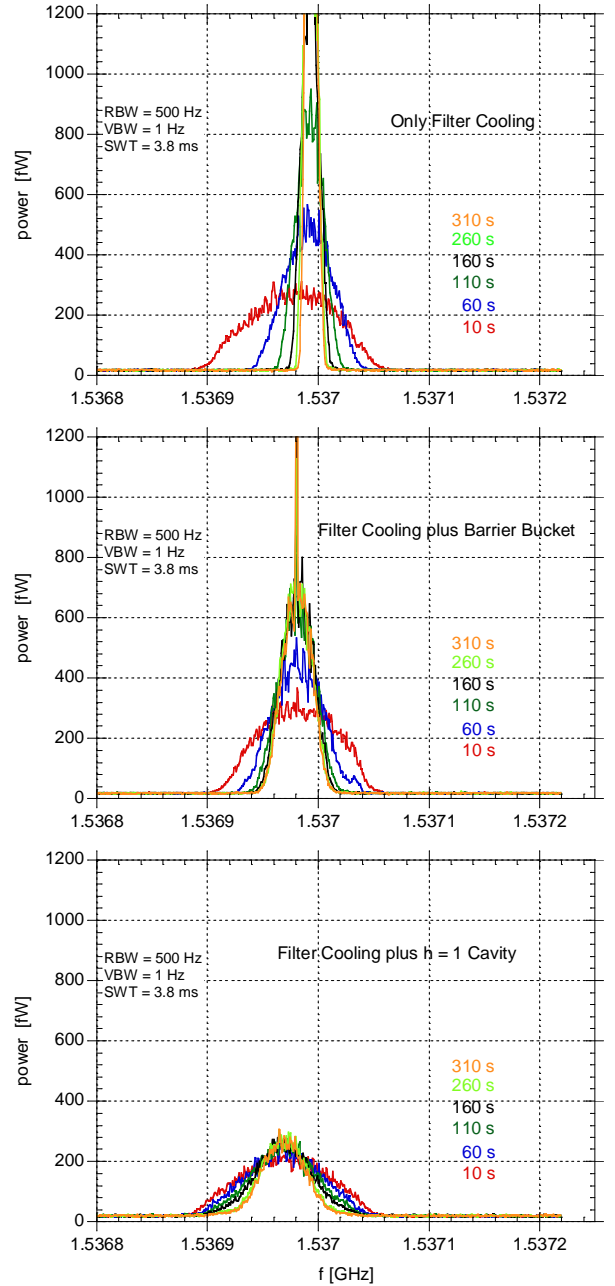


Fig. 31: Filter cooling without/with synchrotron motion

While in the barrier bucket case the bunch is nearly DC the beam is bunched when the $h = 1$ cavity is operated. The bunches become shorter during cooling (Fig. 32).

To investigate cooling with an internal target the mean energy loss in the pellet deuterium target of the WASA installation has been first deduced by measuring the linear time dependence of the frequency shift of the spectral Schottky line at harmonic number $n = 1000$. The mean energy loss (E) is determined from a measurement of the linear frequency shift per unit time and the frequency slip factor $\eta = 1/\gamma^2 - \alpha$: $\Delta E \approx -12$ meV/turn.

The effective target thickness is then calculated with the Bethe-Bloch formula yielding $N_T = 2 \cdot 10^{15}$ atoms/cm². The target thickness is thus comparable to that in the

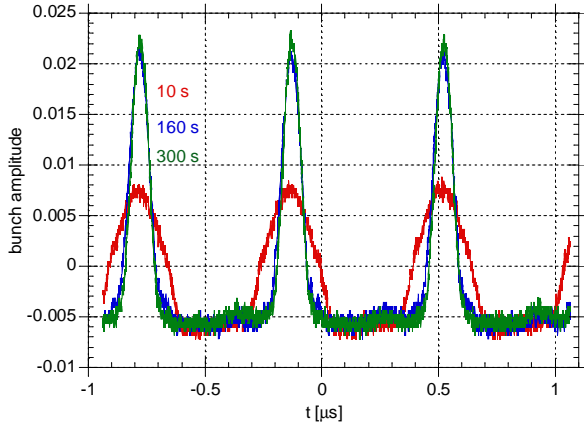


Fig. 32: Bunch evolution during filter cooling

PANDA experiment at the HESR. The cooling result is displayed in Fig. 33.

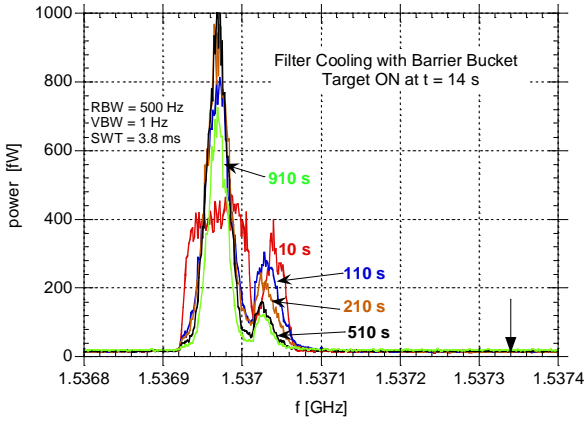


Fig. 33: Power spectra at $n = 1000$ during filter momentum cooling and barrier bucket operation. The pellet target is switched on at $t = 14$ s.

The target is switched on at $t = 14$ s. The barrier extends from 1.53692 GHz to 1.537015 GHz. It is seen that at $t = 10$ s 29% of the particles visible as a hump are outside the barrier. At $t = 110$ s this hump becomes smaller and is moved closer to the center due to cooling. At the same time the density in the barrier is increased (Fig. 34) and the width of the distribution is reduced by cooling. For $t > 300$ s the peak density attains a maximum for a while and then drops down. The maximum is reached when the particle losses start to become stronger than the increase in peak density due to cooling, see Fig. 34. Figure 33 shows that the particles losses can only be due to a transverse emittance increase caused by the beam-target interaction. Particle losses in the longitudinal phase space would be visible in a similar enhancement of particles as in Fig. 29 at a frequency of 1.5374 GHz, see arrow in Fig. 33. Note that the center of gravity of the distributions keeps the same which means that the mean energy loss is compensated.

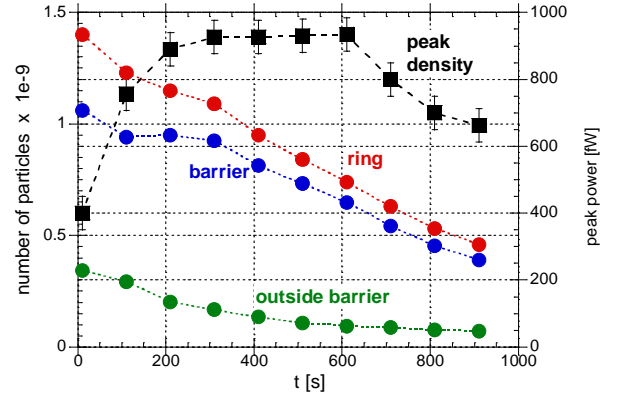


Fig. 34: Peak power of particles in the barrier, number of totally stored particles and stored particles in as well as outside the barrier region during cooling.

In summary, the experiments have verified that the TOF cooling method as theoretically predicted is feasible and can be successfully applied to reduce the initial momentum spread for filter cooling. The filter or TOF technique for a proton beam with synchrotron motion induced either by a barrier or a $h = 1$ cavity has been investigated experimentally. Cooling with a barrier bucket turned out to be more efficient since the beam is similar to a DC-beam. The barrier bucket cavity was applied to compensate the mean energy loss induced by the WASA pellet target with a thickness comparable to that in the PANDA experiment at the HESR. The beam momentum spread could be cooled but particle losses probably caused by a transverse emittance increase reduced the life time of the beam. Further experimental and theoretical investigations are necessary to gain in experience and to determine the optimal barrier voltage and cooling system quantities.

3 Further Experimental Activities

3.1 Pionic Deuterium

Negative pion absorption at rest in deuterium is dominated by true absorption $d\pi^- \rightarrow nn$, which is related to s-wave pion production $pp \rightarrow d\pi^+$ by charge symmetry and detailed balance. An unusual but effective way to determine the $d\pi \leftrightarrow NN$ transition strength α at threshold is to exploit the hadronic broadening Γ_{1s} of the pionic deuterium (πD) ground state accessible by means of X-ray spectroscopy. It circumvents the problem of Coulomb corrections to the cross section, which is necessary in pion-production experiments.

The hadronic part of the production cross section is usually parametrised by $\tilde{\sigma}_{pp \rightarrow \pi^+ d} = \alpha\eta + \beta\eta^3 + \dots$ with $\eta = p_\pi^*/m_\pi$ being the reduced momentum of the pion in the πd rest frame. For $\eta \rightarrow 0$, higher partial waves (β, \dots) vanish and only the threshold parameter α contributes owing to pure s-wave production. Detailed balance relates the reactions $\pi^+ d \rightarrow pp$ and $pp \rightarrow \pi^+ d$ and, neglecting a small phase space correction, charge symmetry requires $\tilde{\sigma}_{\pi^+ d \rightarrow pp} = \tilde{\sigma}_{\pi^- d \rightarrow nn}$. Applying the optical theorem, one obtains for the process $\pi^- d \rightarrow nn$ a relation between the imaginary part of the scattering length and the threshold parameter $\Im a_{\pi^- d \rightarrow nn} \propto \alpha$.

On the other hand, the complex pion-deuteron scattering length $a_{\pi D}$ is obtained by the Deser formula from the ground-state shift ε_{1s} and width Γ_{1s} in pionic deuterium where $\Im a_{\pi D} \propto \Gamma_{1s}$. $\Im a_{\pi D}$ is identical to $\Im a_{\pi^- d \rightarrow nn}$ after correcting for the branching ratio of final states other than nn , which is measured precisely to be $(26.6 \pm 0.4)\%$.

X-rays from the $\pi D(3p-1s)$ transition were measured at the high-intensity low-energy pion beam $\pi E5$ of the proton accelerator at the Paul Scherrer Institut using the cyclotron trap II and a double focusing crystal spectrometer equipped with an array of charge-coupled devices as position-sensitive X-ray detector.

Besides the experimental response and the natural line width given by the hadronic broadening Γ_{1s} , so called Coulomb transitions may contribute. They occur when excited exotic hydrogen atoms penetrate the electron cloud of target atoms and the energy release of the de-excitation step is converted into kinetic energy shared by the πD system and another D atom. Therefore, subsequent X-ray transitions may be Doppler broadened. The acceleration is counteracted by elastic and inelastic scattering during the life time of the πD atom.

Searches failed for any contributions to the line width induced by Coulomb transitions when fitting the data (Fig. 35) by means of a χ^2 analysis. This is remarkable because in the case of pionic hydrogen a Doppler broadening due to Coulomb de-excitation is clearly seen.

Detailed Monte-Carlo studies have been performed to quantify which amount of Doppler induced components may be missed for the statistics achieved in the experiment. It was found that a contribution of 25% can be excluded at the level of 99% for the strongest expected component around 80 eV kinetic energy corresponding to

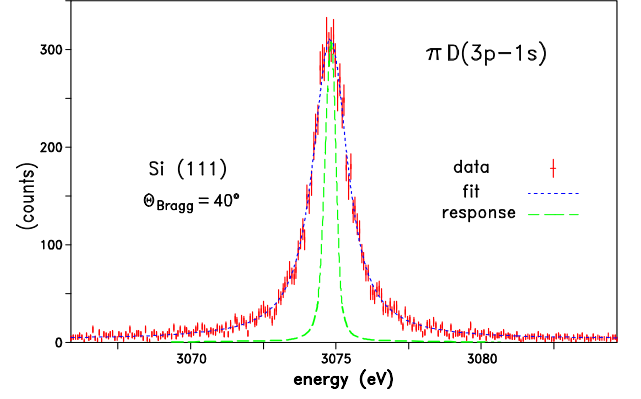


Fig. 35: $\pi D(3p-1s)$ transition as measured with a Si (111) Bragg crystal. The narrow line represents the resolution of the spectrometer determined to be 436 ± 3 meV (FWHM).

the $(4-3)$ Coulomb transition. The chance to identify a 10% contribution is still about $2/3$ corresponding to 1σ . Omitting any Coulomb contribution yields the upper limit for Γ_{1s} . Taking the limit of sensitivity of 10% — according to the above-mentioned 1σ criterion — results in a bound 43 meV lower than the upper limit.

The result for the hadronic broadening is including the statistical uncertainty

$$\Gamma_{1s} = (1171_{-49}^{+23}) \text{ meV} \quad (3)$$

in good agreement with previous X-ray measurements (Fig. 36). It yields for the threshold parameter

$$\alpha = (252_{-12}^{+5}) \mu\text{b}. \quad (4)$$

Results for α from pionic deuterium, pion-production data, and theoretical approaches are compared in Figure 36. The values derived from pion-production and absorption experiments scatter widely. However, sometimes only statistical errors are given. The fluctuations suggest significant systematic uncertainties possibly due to normalisation and/or Coulomb corrections. A recent calculation within χPT up to next-to-leading order (NLO) terms yields $\alpha^{NLO} = 220 \mu\text{b}$. The uncertainty of about $\pm 30\%$ is expected to decrease to below $\pm 10\%$ by next-to-next-to-leading order (NNLO) calculations.

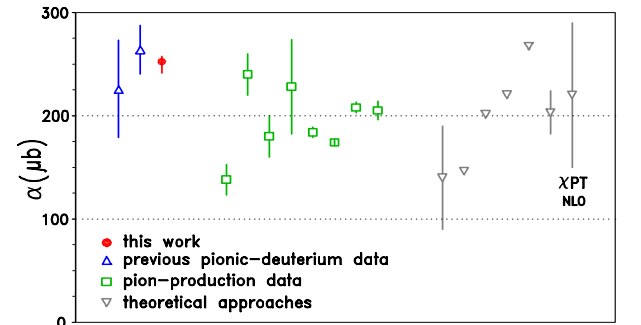


Fig. 36: Comparison of results for the threshold pion-production strength α from various sources.

3.2 A serendipitous effect — the production of a tensor-polarized deuteron beam in a carbon target

Nuclear spin dichroism leads to the appearance of tensor polarization p_{zz} in an initially unpolarized, forward transmitted beam of deuterons behind a spin zero target like carbon due to the difference of the total cross sections σ_0 and $\sigma_{\pm 1}$, describing the interaction of deuterons oriented perpendicular and parallel to the beam axis. Integration over the deuteron energies in the carbon target from E_{in} to E_{out} , the calculated cross-section differences of Fig. 37 yield $p_{zz} = +0.014$ for $E_{in} = 20$ MeV and $E_{out} = 11$ MeV and -0.0035 for $E_{in} = 11$ MeV and $E_{out} = 5.5$ MeV.

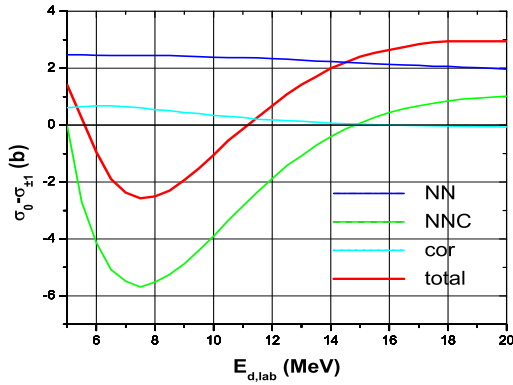


Fig. 37: Calculated total deuteron-carbon cross-section difference as function of the deuteron energy and the contributions by nuclear interaction (NN), nucleon-nucleon Coulomb interference (NNC) and a correction term.

The values, measured with unpolarized deuteron beams from the tandem accelerator of the Institut für Kernphysik, Universität zu Köln, behind seven 36 to 188 mg/cm² thick targets and the use of a polarimeter based on the reaction $\vec{d} + {}^3\text{He} \rightarrow p + {}^4\text{He}$, show a surprising energy dependence with an extreme value of $-(0.28 \pm 0.03)$ for $E_{in} = 14.8$ MeV and the 129 mg/cm² target (Fig. 38).

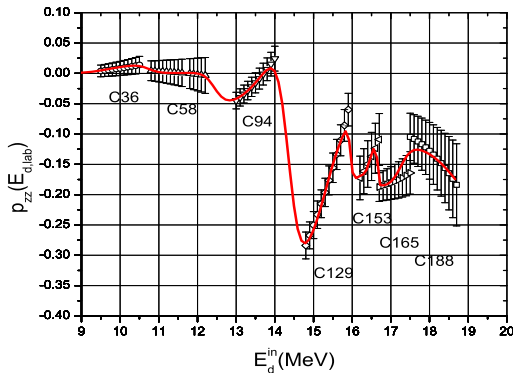


Fig. 38: Tensor polarization p_{zz} measured in the forward-transmitted deuteron beam behind the 36 to 188 mg/cm² carbon targets (labelled C36 to C188) as function of the primary beam energy and the fit by 12 Gaussian-shaped cross sections.

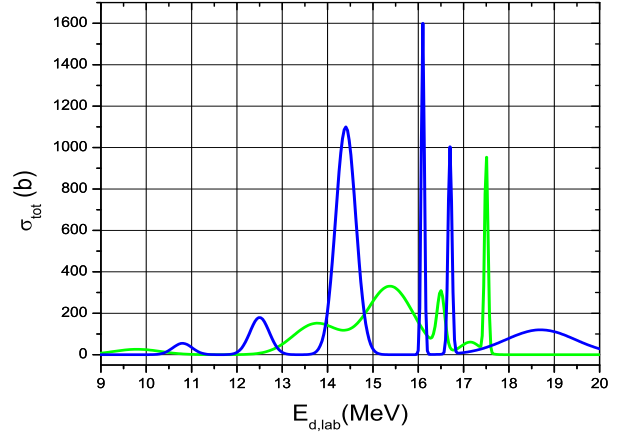


Fig. 39: The Gaussian-shaped cross-sections (blue: $\sigma_0 \neq 0$, $\sigma_{\pm 1} = 0$ leading to $p_{zz} > 0$, green: $\sigma_0 = 0$, $\sigma_{\pm 1} \neq 0$ leading to $p_{zz} < 0$, when crossed during deceleration of the deuterons in the target.

The measured distribution is fitted by 12 Gaussian-shaped cross sections (Fig. 39). Due to the narrow energy ranges, the required cross sections are appreciably higher than the calculated ones (Fig. 37).

Additional processes in the deuteron-carbon interaction have to be invoked. The cross-section distribution allows the production of tensor-polarized deuteron beams by carbon targets as is shown in Fig. 40.

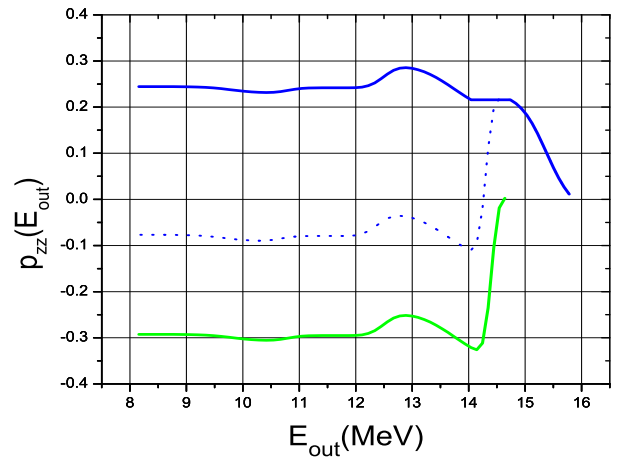


Fig. 40: Tensor polarization p_{zz} produced by graphite targets from unpolarized deuteron beams as function of the energy behind the target, E_{out} , depending on the target thickness (green: $E_{in} = 14.8$ MeV; blue ($E_{in} = 15.8$ MeV): the full line for a target with a different sandwiched material suppressing the negative polarization by carbon around 14.4 MeV, the dotted line below $E_{out} = 14.8$ MeV for a pure graphite target.

3.3 The Beauty of the ATRAP-Experiment and its Performance in 2009

The scientific goal of cold antihydrogen studies is a precise comparison of observables from antihydrogen and hydrogen atoms to check if their structure or gravitational interactions differ. CPT invariance implies that antihydrogen and hydrogen atoms have the same structure and interactions. Such invariance follows from axiomatic quantum field theories that are Lorentz invariant like the Standard model, and is thus a well established fundamental symmetry. Caution seems appropriate given that the physics community once incorrectly thought that reality was invariant under parity transformations, and later (also incorrectly) that reality was invariant under CP transformations. The precise comparison of the simplest atoms of antimatter and matter should produce the most stringent test of CPT symmetry with leptons and baryons. Highest precision CPT tests are of great interest and if CPT violation could be detected it may be the key to the explanation of the imbalance of matter and antimatter in the universe. The ATRAP apparatus, displayed in Figure 41, has a vertical magnetic field for its cryogenic Penning traps, and a positron accumulator ~ 10 meters apart. A pulse of antiprotons from the antiproton decelerator (AD) of CERN

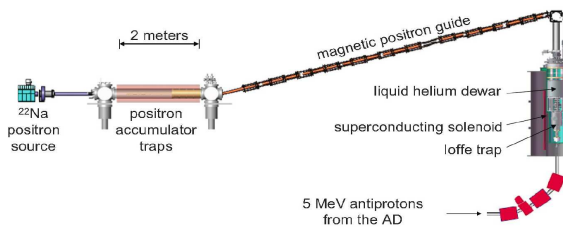


Fig. 41: Overview of the ATRAP antihydrogen apparatus.

is directed by bending magnets into the superconducting solenoid every ≈ 100 s. They are captured in the lower section of a series of Penning traps — shown in the right part of Figure 42 together with a photo of the apparatus — made by applying voltages to ring electrodes with a magnetic field (up to 3 Tesla) along their axis.

Antihydrogen atoms are normally produced within a nested Penning trap which includes a short inverted potential well filled with positrons within the \bar{p} potential well by reducing the potentials to mix the two particle species. Another, in view of very slow antihydrogen promising method, is the laser-controlled production via Cs Rydberg atoms which has also been demonstrated at ATRAP. Antihydrogen trapping requires magnetic field gradients contradicting to the constant field necessary for the stability of charged particles trapping. Recently ATRAP succeeded in producing antihydrogen atoms within a Ioffe trap field, but no trapped antihydrogen atoms could yet be reported. Better control of the antihydrogen formation seems crucial for their trapping. Therefore serious studies of temperatures and distributions of the cold antiproton and positron plasmas are demanded to better understand and control the formation of

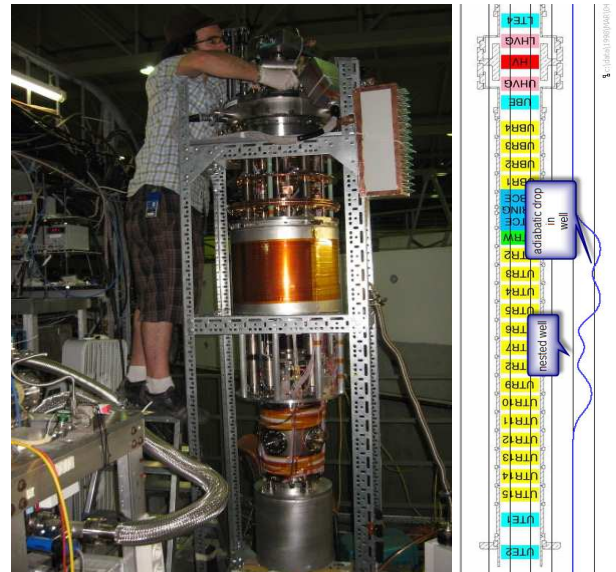


Fig. 42: The ATRAP antihydrogen apparatus and the Penning trap arrangement.

antihydrogen atoms.

After these general considerations the achievements of the ATRAP collaboration during the last year 2009 should briefly be summarized:

The main focus for 2009 was the search for signals of trapped antihydrogen. Three-body recombination experiments were used in attempts to trap antihydrogen. For these trials a heater was used to induce a quench in the superconducting Ioffe trap quadrupole which reliably quickly reduces the field and would release any trapped atoms. Experiments were done with up to 4 million antiprotons and 60 million positrons with the Penning trap at temperatures as low as 1.2 K.

Low temperatures are crucial for these experiments considering the Ioffe trap depth of about 400 mK. The reduction of the electrode temperature from the 4.2 K liquid Helium surrounding down to 1.2 K will increase the fraction of trappable \bar{H} atoms by a factor of about 7 if the low temperature can be transferred to the produced antihydrogen. Studies on electrons and positrons indicate plasma temperatures in the 1.2 K region but the reproducibility to prepare these low temperature plasmas need more basic studies and the cooling of the antiproton plasma down to 1.2 K has still to be shown.

Techniques for fast measurements of plasma modes and temperatures have been developed and are now integrated into the antihydrogen production experiments. Figure 43 shows the result of such a temperature measurement. Presently antiproton clouds as low as 30 K have occasionally been observed by this method. Further investigations are necessary here.

In order to reduce the radius of electrons, positrons, and antiprotons and thereby the particle loss, a split electrode with rotating electric field has been used. The compression of electron-antiproton plasmas by increasing the ro-

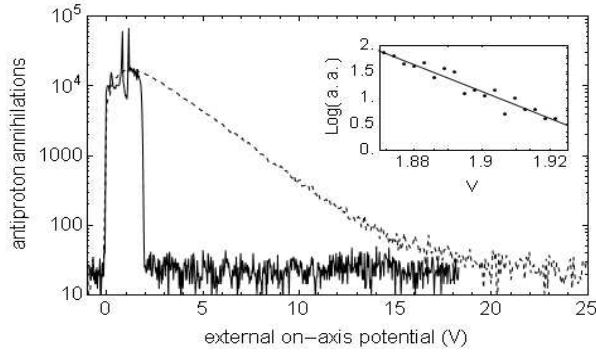


Fig. 43: Energy distribution of antiprotons, determined by measuring annihilation events while reducing the potential well height. The exponential distribution of the antiproton annihilations (straight line on the log plots) is due to the thermal axial energy distribution. The dashed-line distribution results when heating with a noise drive to 15,000 K. The solid-line distribution has been cooled to 100 K by adding electrons. The inset is a blowup of the start of the solid-line distribution fitted by an exponential.

tation frequency has allowed to stack 6 million antiprotons as is demonstrated in Figure 44 which is about 3 times more \bar{p} 's than last year. Without the rotating wall, when many \bar{p} 's are loaded the plasma expands and a high loss is observed when the \bar{p} solenoid, used to increase the magnetic field for an improved trapping efficiency, is ramped down after loading.

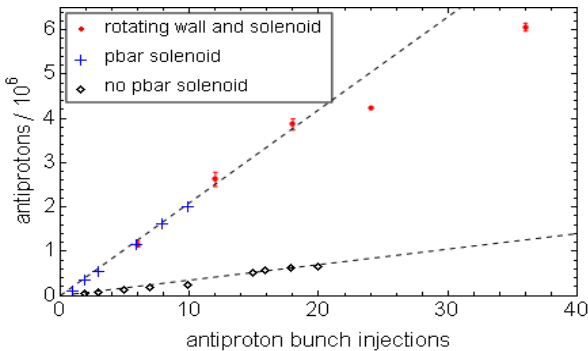


Fig. 44: An extension of ATRAP's stacking procedure up to nearly 6 million \bar{p} 's.

This previously limited the trapping of antiprotons to approximately 2 millions. The largest stacks achieved with increased plasma rotation of 4 and 6 million \bar{p} 's fall below the linear stacking line due to initial losses when applying the rotating wall drive. Developments will follow next year to remove these losses and possibly the stacking will continue to even larger numbers.

During 2009 ATRAP has started to study the antihydrogen production as a function of plasma shape and density. In studies with ≈ 2.5 million antiprotons more than

half of the antiprotons are lost if no rotating wall is used ($r = 8$ mm). If the cloud is compressed to $r = 2.5$ mm the loss is reduced to less than 5%.

The radius is determined in these measurements from the two mode frequencies for the center-of-mass and the quadrupole axial oscillations with the known particle number. The rotating wall technique appears to work similarly in the cases of only electrons using about 100 million e^- and electrons with antiprotons using about 100 million e^- and 2.5 million \bar{p} 's as demonstrated in Figure 45.

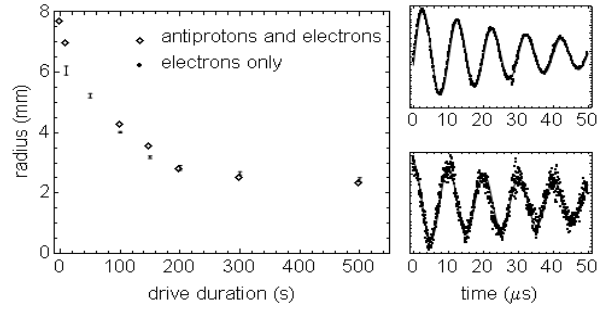


Fig. 45: Plasma radius that results from applying plasma rotation for a certain duration (left). Center-of-mass (top right) and quadrupole (bottom right) axial oscillations (plasma modes) used to determine the radius.

Besides the optimization of the three body recombination schemes a system for the alternative antihydrogen production technique via charge exchange using Rydberg Cs atoms has been commissioned in the second generation trap arrangement including the Ioffe-trap system during the last year, see Figure 46. The advantage of this technique is the low expected antihydrogen velocity given by the temperature of the \bar{p} plasma. Rydberg Cs atoms have been detected before and after they pass through the Penning trap within a 1 T magnetic field. Antihydrogen charge-exchange experiments have been started, but \bar{H} 's have not yet been observed.



Fig. 46: Cs apparatus mounted on a Ioffe trap with feed-throughs for photodiodes, Stark shifting plates, field ionization plates, getter current, and temperature sensor. The optical fiber at the top carries both excitation wavelengths.

4 Theoretical Investigations

Introduction

The IKP theory group studies the strong interactions in their various settings — spanning topics in hadron structure and dynamics, the nuclear many-body problem and high-energy Quantum Chromodynamics (QCD). The main focus is on the formulation and application of effective field theories for precision hadron and nuclear physics based on the symmetries of QCD. Within the virtual institute on “Spin and strong QCD” work focuses on applications for physics at COSY and FAIR. Some of the high-lights of these activities are discussed in the following.

4.1 Quark masses and the reaction $pn \rightarrow d\pi^0$

The strong contribution to the mass difference of the proton and the neutron is a fundamental quantity in the regime of non-perturbative QCD. It is directly related to the violation of isospin symmetry, which is a symmetry of pure QCD in the limit of equal light quark masses. On the level of the fundamental building blocks of the Standard Model, isospin is violated by two sources: electromagnetism and the up-down quark mass difference. Most isospin violating hadronic low-energy observables are dominated by the relatively large charged-to-neutral pion mass difference, which is almost exclusively of electromagnetic origin. However, there is a special kind of isospin violating interactions — those that are charge-symmetry-breaking (CSB) (charge symmetry is an isospin rotation by 180 degrees, which exchanges up and down quarks) — where the pion mass difference does not contribute and where, as a consequence, quark mass effects are expected to contribute as strongly as electromagnetic effects.

Extracting information about the quark mass difference induced CSB effects in hadronic low-energy observables provides direct access to the expectation value of the quark mass matrix in hadronic environments. Since the transition from the quark world to the hadronic one is highly non-perturbative, strongly influenced by the spontaneous chiral symmetry breaking, information on the above mentioned matrix elements therefore provides unique access to the chiral structure of the QCD Lagrangian. The first model independent extraction of Δm^{qm} goes back to Gasser and Leutwyler, who calculated its electromagnetic counter part from a dispersion integral (the so-called Cottingham sum rule), finding $\Delta m^{qm} = (2.05 \pm 0.30 \text{ MeV})$ — below we call this method the direct extraction. Recently the same quantity was extracted from a lattice QCD calculation with the result $\Delta m^{qm} = (2.26 \pm 0.57 \pm 0.43 \pm 0.10) \text{ MeV}$, where the first error is statistical, the second error is due to the uncertainty in the ratio of light quark masses, and the third

error is an estimate of the systematic due to chiral extrapolation.

It was first observed by Weinberg that, as a consequence of the abovementioned spontaneous chiral symmetry breaking, the quark mass term not only influences static observables like the neutron-proton mass difference but also dynamical observables like isospin violating pion-nucleon scattering — to leading order with the same strength parameters. To establish this link would provide a non-trivial test of our assumed chiral structure of QCD in the non-perturbative regime. The observable Weinberg suggested to get direct access to Δm^{qm} was the difference between the $\pi^0 p$ and the $\pi^0 n$ scattering lengths — where the small $\pi^0 p$ phase can in principle be measured in neutral pion photoproduction off the proton but the $\pi^0 n$ phase is very difficult if not impossible to measure. In our recent work we showed that also the measured CSB forward-backward asymmetry of $pn \rightarrow d\pi^0$ in the threshold region to leading order is directly proportional to Δm^{qm} , $A_{fb}^{L0} = (11.5 \pm 3.5) \cdot 10^{-4} (\Delta m^{qm} / \text{MeV})$. The theoretical analysis with controlled uncertainty of this kind of reaction became possible, since mainly by our group in recent years an appropriate power counting scheme was found and tested in a variety of pion production reactions in nucleon-nucleon collisions. The analysis revealed

$$\begin{aligned} \Delta m^{qm} &= (1.5 \pm 0.8(\text{exp}) \pm 0.5(\text{th})) \text{ MeV} \\ &= (1.5 \pm 0.9) \text{ MeV} , \end{aligned}$$

with the relatively large uncertainty dominated by the experimental uncertainty — the theoretical uncertainty is comparable to that of the direct determination. The values of Δm^{qm} extracted with very different methods are all consistent with each other, which is a great success of chiral perturbation theory, although a reduction in uncertainties especially of the $pn \rightarrow d\pi^0$ analysis (which would require a new measurement and also a refined analysis) would be very desirable.

4.2 Two-pion exchange currents in nuclear chiral Effective Field Theory

Probing nuclei with photons and electrons yields important information on the nucleon and nuclear structure and the underlying dynamics. Theoretical analyses of such reactions require the knowledge of the nuclear current operators which have to be employed consistently with the nuclear potentials used to describe the initial- and final-state interactions. Chiral effective field theory offers an appropriate theoretical framework to achieve this goal and has already been applied to carry out high-precision studies of nuclear forces and to explore the properties of light nuclei. For the limited kinematics with photon energy and momentum of the order $\omega \sim |\vec{q}| \sim M_\pi^2/m_N$, the exchange nuclear currents have already been worked out in chiral effective field theory up to leading one-loop order eQ^4 . Here, e and $Q \sim M_\pi$ refer to the electric charge and the soft scale of the chiral expansion. Clearly, this

kinematics offers only a very narrow window to study electron scattering off nuclei.

We applied the heavy-baryon formulation of chiral effective field theory to derive the leading two-pion exchange contributions to the nuclear electromagnetic current- and charge-density operators for the more general kinematics $\omega \sim M_\pi^2/m_N$, $|\vec{q}| \sim M_\pi$.

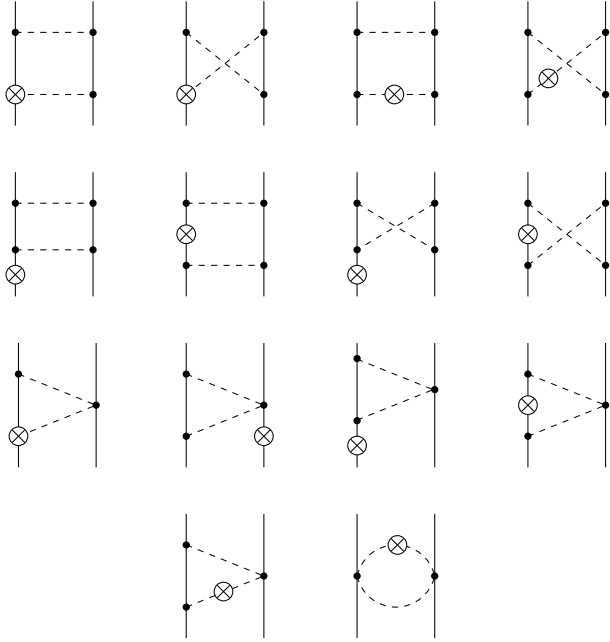


Fig. 47: Diagrams showing contributions to the leading two-pion exchange currents. Solid and dashed lines refer to nucleons and pions, respectively. Solid dots are the leading vertices from the effective chiral Lagrangian while the crosses represent external electromagnetic sources. Diagrams resulting from interchanging the nucleon lines and/or application of time reversal are not shown.

The corresponding diagrams are shown in Fig. 47 and have been evaluated using the method of unitary transformation. The results are given in coordinate as well as momentum space and do not involve any unknown parameters. The obtained exchange currents can be used in combination with modern chiral nuclear forces to study a wide range of processes with light nuclei reaching from radiative capture and breakup reactions to electron scattering with momentum transfer of the order of the pion mass. Derivation of the one-pion exchange and short-range terms to one loop which also contribute at order eQ^4 is in progress.

4.3 Nuclear lattice simulations with isospin-breaking forces and for light nuclei

Since a few years, we have started a systematic study of light nuclei and neutron matter combining methods from chiral effective field theory (EFT) and Monte Carlo simu-

lations to solve the nuclear few- and many-body problem. The main intention for these studies is to extend the systematic and precise framework of chiral nuclear EFT into a larger region of the nuclear chart. First results at next-to-next-to-leading order for light nuclei like the deuteron, Triton and Helium-4 as well as neutron-deuteron scattering look promising. These pioneering calculations were done under the assumption of isospin symmetry, *i.e.* equal forces between protons and neutrons. However, to achieve a truly quantitative description, isospin violation has to be included. We have thus performed the first lattice simulations ever that account for the various sources of isospin breaking that in the Standard Model are driven by the mass and charge differences of the light up and down quarks. In the two-nucleon system, we have included – in harmony with the power counting underlying the EFT – the following mechanism: i) the charged-to-neutral pion mass difference in the one-pion exchange potential, ii) the Coulomb interaction between protons and iii) the two leading isospin-asymmetric and momentum-independent four-nucleon contact interactions. The latter induce two unknown low-energy constants, that are determined from a fit to the pp , pn and nn scattering lengths. The other parameters that appear at our next-to-next-to-leading order calculation are fixed from a global fit to the np S- and P-waves and the deuteron quadrupole moment. The resulting neutron-proton and proton-proton 1S_0 phase shifts for nucleon three-momenta up to the pion mass are displayed in Fig. 48.

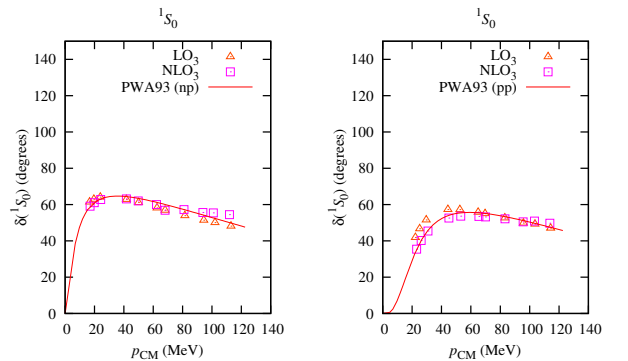


Fig. 48: Neutron-proton (left) and proton-proton (right) 1S_0 partial wave at LO (triangles) and NLO (squares) compared to the Nijmegen PWA (solid line).

One still needs two three-nucleon data to fix the two isospin-symmetric three-body LECs that appear at next-to-next-to-leading order. Using the Triton binding energy and the low-energy doublet nd scattering data to determine these, one can then predict the binding energy (BE) difference of the Triton and Helium-3, noting that the volume dependence of the three-particle ground state energy is given by $E(L) = BE - a \exp(-bL)$, for a cubic box with volume $L \times L \times L$. The resulting prediction for the binding energy difference is shown in Fig. 49. In the infinite volume limit, we obtain $E_{\text{Helium-3}} - E_{\text{Triton}} = 0.78 \text{ MeV}$,

which compares favourably with the empirical value of 0.76 MeV. This shows that precision calculations in such a framework are possible and we are presently simulating the ground states of the Lithium-6 and Carbon-12 nuclei.

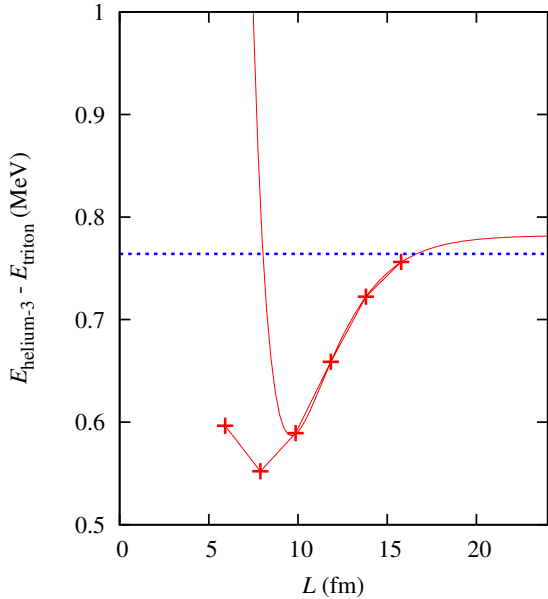


Fig. 49: Binding energy difference for Helium-3 and the Triton in the finite volume (crosses) as fitted through its volume dependence (solid line). The dotted line gives the empirical value.

4.4 Prediction of a new hadronic molecule $Y_\eta(4336)$

For a long time the non-relativistic quark model was believed to provide the correct effective description of charmed mesons. However, in recent years experimental evidence has accumulated for a sizable number of states that seem to not fit into a standard $\bar{q}q$ assignment. Not only deviate their masses significantly from the predictions, also their properties seem to be inconsistent with the expectations.

A common feature to all those states is that they are located close to a threshold for the production of a particle pair in an s -wave. Because of this many authors speculated that these states might well be born out of non-perturbative meson-meson interaction instead of interquark interactions. Those states were called hadronic molecules. It is important to note that these kinds of states can be identified directly from data, if the pole is sufficiently close to the corresponding threshold, via the absolute value of the effective coupling constant of this state to continuum state — this observation is based on an idea by Weinberg further developed by our group.

Using the technique described above it was possible to collect striking evidence that the $f_0(980)$ is predominantly a $\bar{K}K$ molecule. In addition, we demonstrated recently that the experimental information available for the

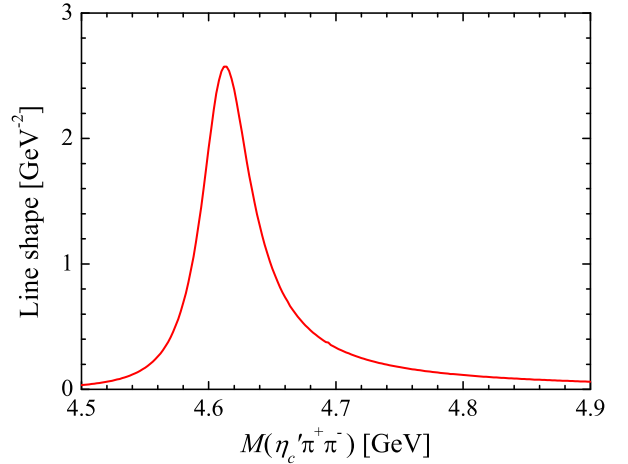


Fig. 50: Prediction for the lineshape of the $Y_\eta(4616)$ as a $f_0(980)\psi'$ bound state.

vector state $Y(4660)$ is fully consistent with its being an $f_0(980)\psi'$ bound state, with the ψ' being the first excited vector charmonium state. This observation is of particular interest, for, if confirmed, it would point at a mesonic nucleus, due to the mentioned composite nature of the $f_0(980)$. It is thus important to further study the implications of the mentioned conjecture about the nature of the $Y(4660)$.

In the heavy quark limit ($m_Q \rightarrow \infty$) the interactions of QCD are spin-independent. Thus, in that limit spin degenerate multiplets should emerge and indeed in the spectrum of mesons with charm or bottom quarks this symmetry becomes apparent through the proximity of states with pseudo-scalar and vector or scalar and axial-vector quantum numbers, respectively. The mass splittings within these multiplets can be systematically calculated as corrections of order Λ_{QCD}/m_Q within heavy quark effective field theory. It is this spin symmetry of QCD that allows us to derive a non-trivial prediction from the above mentioned possible structure assignment for the vector state $Y(4660)$: we predict the existence of a $\eta'_c f_0(980)$ bound state with pseudo-scalar quantum numbers at

$$M_{Y_\eta} = M_{Y(4660)} + M_{\eta'_c} - M_{\psi'} = 4616 \pm 6 \text{ GeV},$$

with properties very similar to those of the $Y(4660)$. Especially we can predict its width to be $\Gamma_{Y_\eta} = (60 \pm 30)$ MeV and even the corresponding, visibly asymmetric line shape in the $\eta'_c \pi \pi$ channel, see Fig. 50.

The asymmetry is a consequence of the large coupling to the f_0 together with the quickly growing $f_0 \eta'_c$ phase space above the resonance position. In addition, the mass relation given should be quite accurate given that corrections to it should be suppressed by $(\Lambda_{\text{QCD}}/m_c)^2$ — this higher suppression compared to the conventional one of linear power is due to the fact that the binding potential of a hadronic molecule stems from the interaction of two color neutral objects. Thus, at least two magnetic gluons (each accompanied by a factor $1/m_c$) are necessary to induce a spin-dependent force in this case.

An observation of the $Y_\eta(4616)$ is expected to be possible at the B-factories in the channel $B \rightarrow \eta'_c K \pi \pi$ or in future experiments like PANDA *e.g.* in $\bar{p}p \rightarrow \bar{\Lambda}_c \Lambda_c$. An observation of the $Y_\eta(4616)$ with the properties predicted would be a strong confirmation also in favor of the assumed molecular structure of the $Y(4660)$.

4.5 Resonances versus background in meson-baryon scattering

The excitation and decay of baryon resonances in the energy range up to 3 GeV is presently investigated experimentally both with hadronic and electromagnetic probes. With growing energy, the extraction of resonance parameters via partial wave analyses gets increasingly difficult, so that other theoretical methods have to be developed. The Jülich meson-baryon coupled reaction channel approach is one of those new methods. It is based on effective Lagrangians and has recently been analytically continued so that the pole structure on the various Riemann sheets can be studied. The poles of the S-matrix characterize the baryon resonances in a model independent way. Fig. 51 shows the pole structure of the P_{33} amplitude on the second Riemann sheet.

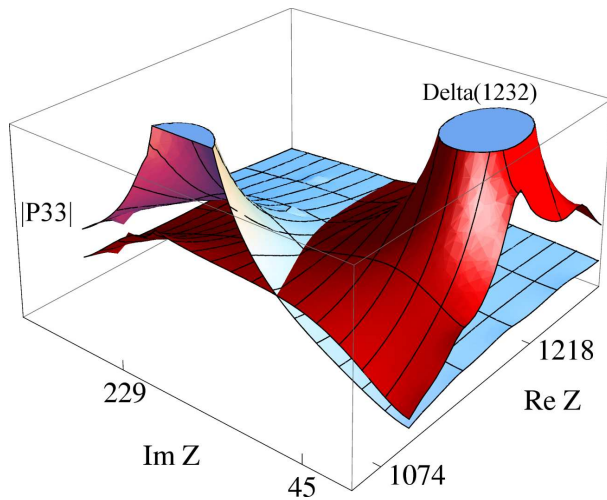


Fig. 51: The P_{33} amplitude on the second Riemann sheet.

The background amplitude generated by unitarizing the non-resonant processes (light blue surface) has a pole near $Z_0 = 1074 + 229i$ MeV, which may be interpreted as a dynamically generated baryon resonance. Including a bare resonance in the s-channel, however, the pole of the background amplitude is canceled. The full amplitude (red surface) has one pole close to the position of the physical Δ_{33} resonance and another one deep in the complex plane. The analysis illustrates that only the dressed poles can be used as an interface between theory and experiment, while attempts to deduce information about bare resonance parameters have to face serious model dependencies. The Jülich method has been employed to extract resonance parameters for baryons with mass less than 2 GeV and total spin up to $J = 3/2$, see

Table 3: Pole positions z_0 and moduli $|R|$ and phases θ of the residues to the πN decay channel for the Roper resonance and the $\Delta_{31}^*(1910)$ as determined by the Jülich coupled channel approach are compared with results of partial wave analyses.

	Re z_0 [MeV]	-2 Im z_0 [MeV]	$ R $ [MeV]	θ [deg] [$^\circ$]
$N^*(1440) P_{11}$	1387	147	48	-64
Arndt06	1359	162	38	-98
Hohler93	1385	164	40	
Cutkosky79	1375 ± 30	180 ± 40	52 ± 5	-100 ± 35
$\Delta^*(1910) P_{31}$	1840	221	12	-153
Arndt06	1771	479	45	+172
Hohler93	1874	283	38	
Cutkosky79	1880 ± 30	200 ± 40	20 ± 4	-90 ± 30

Table 3. While the partial wave analyses agree on the mass of a low mass resonance such as the Roper, there are considerable uncertainties concerning the width and the residues of high mass resonances, such as the $P_{31}(1910)$. The Jülich approach combines data of different decay channels and eventually will incorporate electromagnetically induced reactions.

4.6 The Primakoff effect on the proton

The width of neutral pion decaying into two photons, $\Gamma(\pi^0 \rightarrow 2\gamma)$, offers a stringent test of the anomaly and chiral structure of QCD. Recently, the PrimEx collaboration at Jefferson Lab has measured this decay by utilizing the Primakoff effect on heavy nuclei. To avoid the uncertainty related to the many-body effects that necessarily arise in the analysis of such processes, we have studied the feasibility of measuring the neutral pion width via the Primakoff effect on the proton. To achieve this, we have first performed a global analysis of the world data on the reactions $\gamma p \rightarrow \pi^0 p$ and $\gamma n \rightarrow \pi^0 n$ for photon energies from 3 to 18 GeV within a Regge approach. In this region resonance contributions are expected to be negligible so that the available experimental information on differential cross sections and single- and double-polarization observables at $-t \leq 2$ GeV² allows us to determine the reaction amplitude reliably. The Regge model was constructed by taking into account both pole and cut exchange t -channel helicity amplitudes and includes the ρ , ω and b_1 trajectories. The model parameters such as the helicity couplings were fixed by a fit to the available data in the considered photon energy (E_γ) and squared four-momentum transfer (t) range. An excellent overall description of the available data was achieved, indicating that for the energy and momentum transfer range in question single pion photoproduction is indeed dominated by nonresonant contributions. The model ampli-

tude was then used to predict observables for photon energies below 3 GeV. A detailed comparison with recent data from the CLAS (JLab) and CB-ELSA (Bonn) Collaborations in that energy region was presented. It turned out that the resulting differential cross sections for $\gamma p \rightarrow \pi^0 p$ were still in reasonable agreement with those new data down to $E_\gamma \simeq 2.45$ GeV for $-t \leq 2$ GeV², while the very forward data were reproduced even down to photon energies as low as 2 GeV. Since our Regge amplitude works so well for forward angles, even at very low energies, we utilized it to explore the prospects for determining the π^0 radiative decay width via the Primakoff effect from the reaction $\gamma p \rightarrow \pi^0 p$.

Those calculations indicate that corresponding measurements on a proton target could be indeed promising, see Fig. 52. But, evidently, the precision to which the decay width can be determined will depend crucially on the number of data points that one can collect at very small angles and on the accuracy and the angular resolution one can achieve.

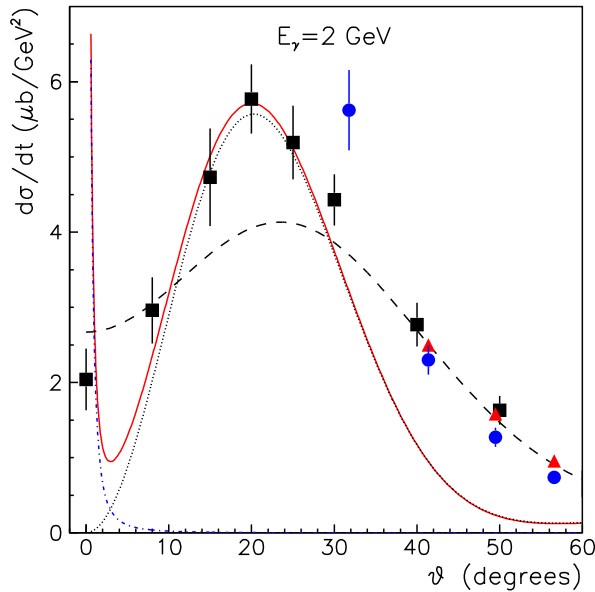


Fig. 52: Differential cross section for $\gamma p \rightarrow \pi^0 p$ as a function of the angle θ in the cm system shown for photon energy $E_\gamma = 2$ GeV. The dotted line shows the Regge calculations without one photon exchange, while the solid line is the results obtained with inclusion of one photon exchange. The dash-dotted line is the result for one photon exchange alone. The dashed line indicates the results based on the GWU PWA.

5 Preparation of the HESR

5.1 Beam Dynamics

A chromaticity correction scheme for the HESR consisting of sextupole magnets has been developed to reduce tune spread and thus to minimize the emittance growth caused by betatron resonances. The chromaticity correction scheme has been optimized through dynamic aperture calculations. The estimated field errors of the HESR dipole and quadrupole magnets have been included in the non-linear beam dynamics studies. Investigations concerning their optimization have been carried out. The ion optical settings of the HESR have been improved using dynamic aperture calculations and the technique of frequency map analysis. An example for this comprehensive beam simulation is shown in Fig. 53. The related diffusion coefficient was also used to predict long-term stability based on short-term particle tracking.

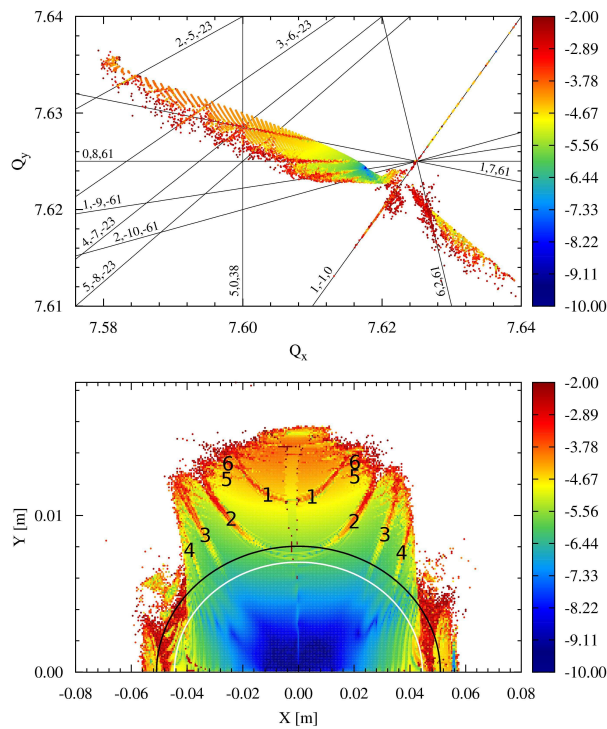


Fig. 53: Frequency map a) and corresponding dynamic aperture b) for $\Delta p/p = 0$. The color scale represents the diffusion coefficient. The two curves in b) depict the emittances at the geometrical acceptance limit (white) and at the dynamic aperture (black). The numbers in b) denote the resonances: 1) $Q_x + 7Q_y = 61$, 2) $8Q_y = 61$, 3) $Q_x - 9Q_y = -61$, 4) $2Q_x - 10Q_y = -61$, 5) $5Q_x - 8Q_y = -23$, 6) $4Q_x - 7Q_y = -23$.

5.2 Injection and Accumulation

Due to a recent decision by the FAIR committees for a modular realization of the FAIR project, RESR will be

build at a later stage. Only the C(A)R is going to be available for antiproton collection and cooling from the beginning. Therefore a new injection and accumulation scheme for HESR has to be applied. A first proposal is based on beam stacking of a 3 GeV antiproton beam from C(A)R in HESR utilizing a barrier bucket cavity and stochastic cooling. Beam simulations are presently carried out and system parameters specified to ensure the required efficiency in terms of accumulated number of antiprotons, beam quality, and accumulation time in the HESR.

5.3 Magnet Development

Magnet design of dipole, quadrupole, sextupole und correction dipole magnets has been finalized. 3D-Magnet calculations have been performed to minimize the multipole components of the various magnet types. After negotiations with tenders the magnet production is going to be started with a pre-series. A prototype sextupole and injection magnets will be build by the Romanian partner ICPE-CA Bucharest. Figure 54 shows the structure of a unit cell in the arcs.

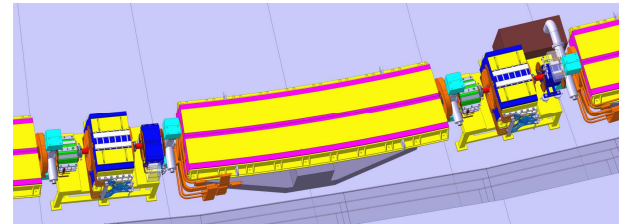


Fig. 54: Structure of a unit cell in the HESR arcs. The design drawing represents the exact positioning of the different magnets types together with the vacuum system components and beam diagnostics.

5.4 Vacuum System

During the last year a detailed concept for the vacuum system of the HESR was worked out. In total 140 pumping ports were placed both between the dipoles in the arcs and inside the straight sections. Including the PANDA and E-Cooler area 22 vacuum sections were defined. The length of each section ranges from 6 m to 45 m which corresponds to a maximum volume of 280 l while the total volume of the vacuum system amounts to 3.6 m³ without any further vacuum device. Figure 55 shows the detailed vacuum layout of the arc and a part of section 12, respectively.

Two test devices were under construction. The first test facility for testing the mechanical stability under ultra high vacuum conditions of the favoured EVAC-clamping flanges has already started with operation. The second test facility will be an original cut-out of the arc from one center of a dipole to the next neighboured one. There is the intention to measure the pressure profile inside the

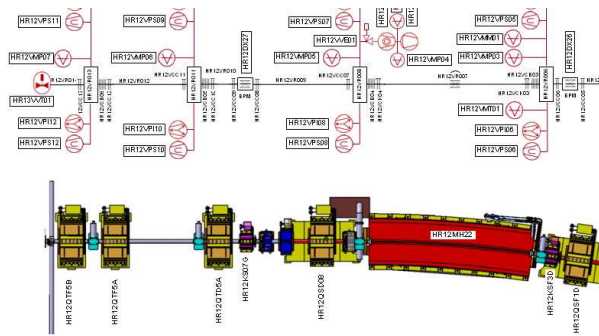


Fig. 55: Detail of the arc, complete vacuum layout of a part of section 12.

beam tube of the dipole. The necessary pump arrangement at the pumping body can be worked out as well as the pumping time and throughput of the system can be determined. Figure 56 shows the design of that test facility.

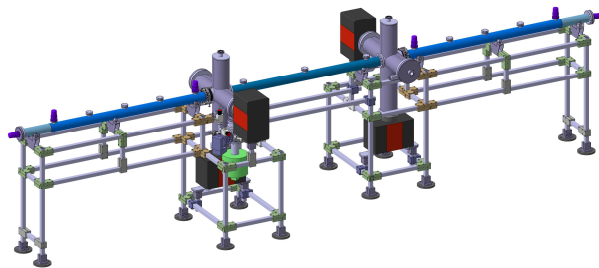


Fig. 56: Design of the test facility for measuring the pressure profile inside the beam pipe of the dipole.

Figure 57 shows the first test facility together with a first measurement result of a bending load on the flange connection. With a maximum force of 0.9 kN a displacement of 1.1 mm was measured. The pressure ranges from $4.0 \cdot 10^{-8}$ mbar to $7.0 \cdot 10^{-8}$ mbar.



Tests of EVAC Seals for HESR:
Influence of Bending the Tube

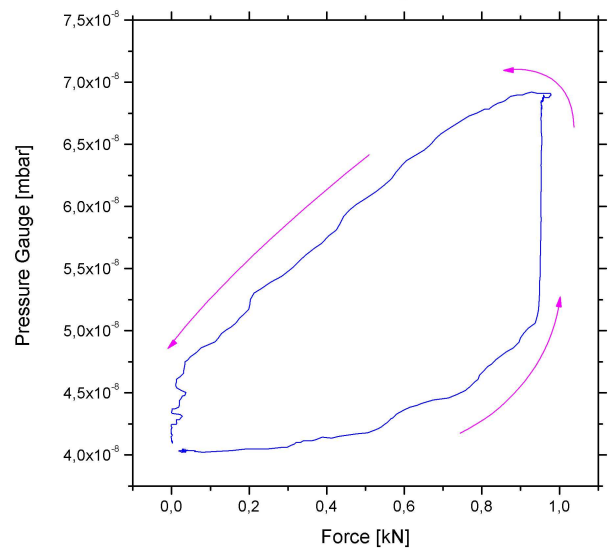


Fig. 57: Test facility for testing the EVAC-clamping flanges (top) with one result for a bending load (bottom).

6 The PANDA Experiment at FAIR

6.1 Introduction

With the discovery of many new states with unexpected features in the charmonium mass region by the B factories Belle and BaBar, large enthusiasm was coming into the field of charm physics. By design the B factories have their strength on states with certain quantum numbers matching to the e^+e^- beams they are using. But to explore the full range of the charmonium spectrum these machines are not well suited. Here an antiproton beam would be beneficial, which gives access to all quantum numbers. In addition an antiproton beam would allow to measure the width and the mass of all charmonium states with an unmatched precision.

One experiment which will use antiprotons is the **Anti-Proton Annihilation at Darmstadt** experiment (\bar{P} ANDA). It is part of the future Facility of Antiproton and Ion Research (FAIR) at Darmstadt.

The antiproton beam will be provided by the high energy storage ring (HESR) which is able to supply antiprotons with momenta between 1.5 GeV/c and 15 GeV/c and with a maximum luminosity in the order of $2 \cdot 10^{32} \text{ cm}^{-2} \text{ s}^{-1}$. Due to its stochastic and electron cooling capabilities it can achieve an unsurpassed beam momentum resolution of $\Delta p/p = 10^{-5} - 10^{-4}$ depending on the operation mode. With this excellent beam \bar{P} ANDA will be able to do precision measurements of certain charmonium states down to resolutions in the order of 100 keV being one order of magnitude better than the existing limits.

Besides the physics with charmed mesons \bar{P} ANDA will search for exotic hybrids and glueballs, study charmed and multi-strange baryons, investigate electromagnetic processes, probe single and double hypernuclei and the change of the properties of hadrons in nuclear matter. The physics program together with the simulation of selected reaction channels is discussed in the \bar{P} ANDA Physics Performance Report which was completed and published on the arXiv preprint server in 2009.

The experiment is build around an internal target where the antiproton beam interacts either with hydrogen atoms or other heavier nuclei. The detector is split into two parts: the central spectrometer which should provide an almost full coverage of the solid angle and a forward spectrometer focussed on the particles emitted in the forward direction (Fig. 58).

The central spectrometer uses a 2 T solenoidal magnetic field to measure the transversal momentum of charged particles. Directly around the interaction region a Micro-Vertex Detector (MVD) is foreseen which measures the track of charged particles with very high resolution to identify their decay vertex. It is followed by the central tracker, a large volume gaseous detector, being either a Straw-Tube Tracker (STT) or a Time-Projection Chamber (TPC) which are the main detectors for momentum measurements. The particle identification is done by a combination of a time-of-flight system, a DIRC Cherenkov detector and several layers of muon chambers

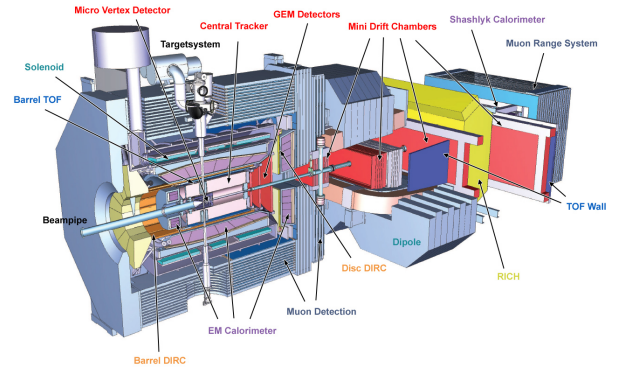


Fig. 58: Schematic overview of the \bar{P} ANDA detector

inside the iron yoke of the solenoid magnet. To further improve the PID capabilities of the \bar{P} ANDA detector for low momentum particles the dE/dx information of the central tracker and the MVD will be used. To measure the energy of the particles a high resolution PbWO electromagnetic calorimeter will be build.

6.2 Micro-Vertex Detector

The MVD sits right in the heart of the \bar{P} ANDA detector directly around the interaction point, see Fig. 59. The most challenging task it has is the identification of D -mesons by measuring their decay length with a precision better than $100 \mu\text{m}$. In addition, it helps the central detector to improve the momentum resolution to the order of $1\% \Delta p/p$.

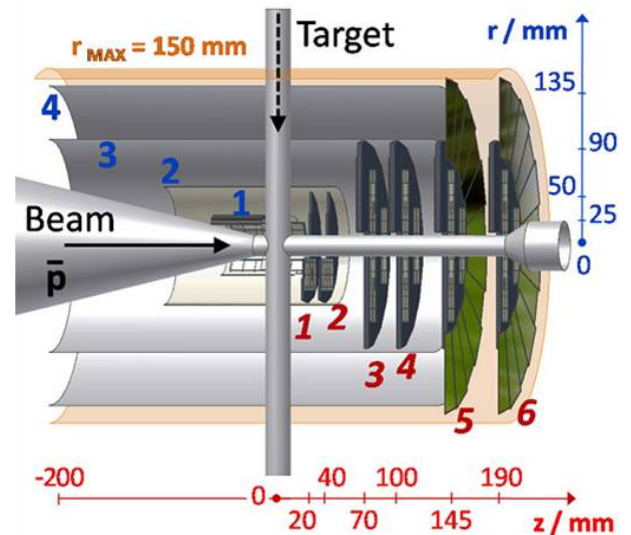


Fig. 59: Schematic overview of the \bar{P} ANDA Micro-Vertex Detector

It consist of silicon detectors which are arranged in four barrel layers and six disks in the forward region. In the inner part of the detector hybrid silicon pixel modules are used, which are more radiation hard and can handle higher data rates compared to the double sided sili-

con strip detectors which are used for the outer detection layers.

Large progress was made in the last year to optimize the design of the MVD to come to a realistic solution for the support structures and the cooling system to minimize the radiation length of the detector as far as possible. Furthermore the simulation software of the MVD was largely extended and detailed studies of the operation parameters and the performance of the MVD were done. One example for these studies are the calculations of the maximum radiation dose the MVD has to withstand during PANDA operation with different target materials.

6.2.1 Study of the expected radiation load on the PANDA MVD

Due to its proximity to the interaction region, the MVD will encounter a high radiation load. The total load during its desired operational time needs to be estimated in order to be able to design the detector in such a way that it can withstand the damaging effects. Extensive simulations have been performed using the pandaRoot simulation framework for both hydrogen and heavy nuclear targets at different antiproton beam momenta.

Since the damaging effects of particles traversing matter depend strongly on particle type and deposited energy, it is convenient to normalize the resulting effects to a base measure for better comparison. When discussing the damage done to silicon, the 1 MeV displacement equivalent silicon fluence (1 MeV DES) is used. Thus, the effects of the actual particle flux are normalized to the equivalent effects caused by the flux of neutrons with 1 MeV energy. Due to the large values, here the actual numbers are given as equivalent to the flux of 10^9 1 MeV DES per square millimeter and operational year (GDES), where one operational year corresponds to 10^7 s of continuous operation at a luminosity of $2 \cdot 10^{32} \text{ cm}^{-2} \text{ s}^{-1}$.

According to the simulations, the highest dose of around 300 GDES has to be expected in the first pixel barrel layer region at theta values around 90° for a Xenon target at 15 GeV/c beam momentum. For a proton target the most damaged regions are the inner radii of the forward discs. However, with around 100 GDES the absolute damage is significantly lower than in the case of a Xenon target (*cf.* Figs. 60 and 61).

In addition it is shown that only a relatively small detector area encounters the actual peak damage. As can be seen in the dose histogram depicted in Fig. 60, most of the MVD surface encounters a radiation load far below the peak value.

6.3 Luminosity Monitor

The basic conceptual design of the luminosity monitor is based on measuring the differential elastic AntiProton-Proton scattering rate. The detector will be located at about 10 m downstream of the target and will measure forward outgoing antiprotons which are emitted at an angle of 3–8 mrad with respect to the beam axis. The angle

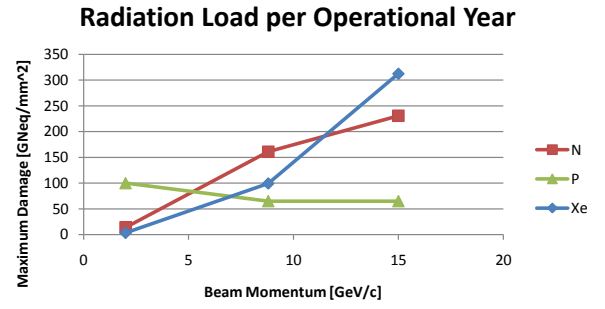


Fig. 60: Peak radiation load per operational year in 10^9 1 MeV displacement equivalent (silicon) fluence per square millimeter and operational year (GDES). One operational year corresponds to 10^7 s of continuous operation at a luminosity of $2 \cdot 10^{32} \text{ cm}^{-2} \text{ s}^{-1}$.

of the scattered antiproton will be reconstructed by measuring the track with 4 planes of silicon strip detectors. Each plane consists of 4 sensors arranged radially from the beam axis (up, down, left and right). The distance between two consecutive planes is 20 cm. Simulation study based on the conceptual design have been implemented with PANDARoot framework.

To meet the requirements of conceptual design two candidates of silicon strip detector have been proposed. One is double-sided silicon strip sensor with rectangular geometry ($2 \text{ cm} \times 5 \text{ cm} \times 300 \mu\text{m}$ with $50 \mu\text{m}$ pitch). The hits position of incident particle can be reconstructed by two dimension strips. Another is single-sided silicon strip sensor with trapezoidal geometry ($2 \text{ cm} \times 5.33 \text{ cm} \times 5 \text{ cm} \times 150 \mu\text{m}$ with $50 \mu\text{m}$ pitch). The silicon sensor is split into two symmetrical segments (left and right). The hits position of incident particle will be assumed at the center of the fired strip roughly. By fitting the measured hits the scattering angle of antiproton will be reconstructed. As shown in Fig. 62, the scattering angle resolution of 0.1 mrad and 0.15 mrad for two candidate silicon sensors with thickness of $150 \mu\text{m}$ and $300 \mu\text{m}$ at a beam momentum of 6.2 GeV/c can be reached, respectively. The simulation results indicate that multiple scattering will dominate the resolution of scattering angle of antiprotons emitted at interaction point. Simultaneously, the effects of strip direction, strip width, solenoid field and transverse divergence of HESR beam on scattering angle resolution have been investigated as well. With the claimed specification of transverse divergence (1 mm mrad) of HESR beam the pilot simulation shows that the scattering angle resolution will not be better than 0.3 mrad which has been observed with double-sided sensor at the beam momentum of 6.2 GeV/c. In order to verify the feasibility of an absolute precision of about 3% further study to evaluate the contribution of each effect on the precision of luminosity determination will be done and the detector design can be optimized accordingly.

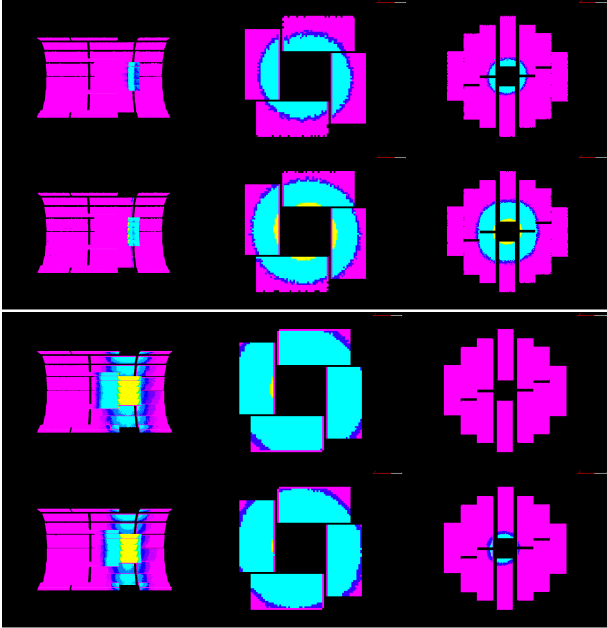


Fig. 61: Qualitative distribution of the radiation load on the pixel part of the MVD for a proton (upper panel) and a Xenon (lower panel) target. Upper rows are for 2 GeV/c beam momentum, lower row for 15 GeV/c beam momentum.

6.4 Straw-Tube Tracker

6.4.1 Construction of a full-scale prototype of the PANDA straw-tube tracker

The proposed Straw Tube Tracker (STT) as the central tracking detector for the PANDA experiment consists of two semi-barrels with an inner radius of 150 mm, outer radius of 420 mm and length of 1500 mm, placed around the intersection point of the horizontal beam pipe and vertical pipe for the pellet-target in the central PANDA spectrometer (see Fig. 63).

The purpose of the STT is to provide a precise measurement of the track coordinates with a resolution of about $150 \mu\text{m}$ ($\sigma_{r\phi}$) perpendicular to the beam axis and about a few mm (σ_z) along the beam axis. The momentum resolution for the measured helical trajectories inside the solenoidal magnetic field of 2 T has to be at the percent level requiring a low radiation length (X/X_0) of 1–2 % in the active detector volume. In addition, since the STT is surrounded by an electromagnetic calorimeter (EMC) and followed by a forward spectrometer setup it is essential to reduce the mechanical frame structure to the lowest limit to suppress secondary background production and distortions of the particle trajectories.

Therefore, the technique developed for the COSY-TOF straw tracker of planar, close-packed straw double-layers, which are self-supporting if pressurized, has been adopted for the PANDA-STT. The cylindrical detector volume is filled up by close-packed, planar double-layers arranged in a regular hexagonal shape (see Fig. 64).

All 4200 straw tubes have an inner diameter of 10 mm,

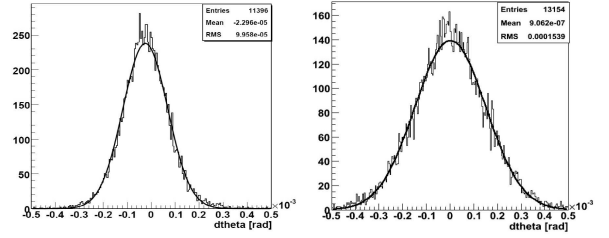


Fig. 62: The angle resolution of 0.1 mrad (left) and 0.15 mrad (right) for the single-sided silicon strip sensor with thickness of $150 \mu\text{m}$ and the double-sided silicon strip sensor with thickness $300 \mu\text{m}$ at a beam momentum of 6.2 GeV/c were plotted, respectively

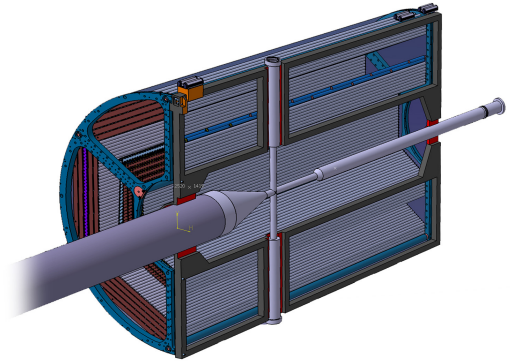


Fig. 63: Artists view of one of the two semi-barrels of the STT. Not all straw layers are drawn. CAD drawing by Dario Orecchini (INFN Frascati).

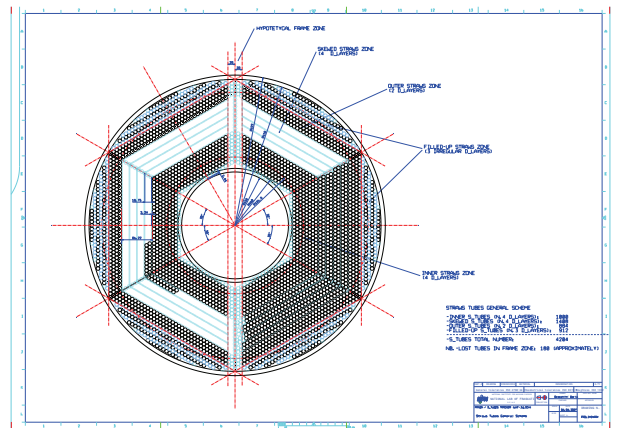


Fig. 64: Cross-section of the STT layout. Not all straw layers are visible (blue marked regions) for a better view of the details. CAD drawing by Dario Orecchini (INFN Frascati).

length of 1500 mm, and are made of $27 \mu\text{m}$ thin mylar film, which shows sufficient mechanical rigidity if the tubes are pressurized to about 1 bar. In radial direction

the STT contains 20 to 26 straw layers, starting with 4 double-layers parallel to the beam axis; then 4 double-layers with a relative, alternating stereo angle of $\pm 3^\circ$ to resolve z -coordinates; 2 further double-layers parallel to the beam axis; and then 6 single layers with a decreasing number of tubes to approach an outer cylindrical shape. During the year 2009 a first full-scale prototype has been assembled to study the mechanical properties and assembly techniques of the hexagonal straw layer stacks. About 2000 straw tubes have been assembled and glued together to double-layers. A simple mechanical frame structure consisting of two aluminium end flanges is used to hold the straw layers. The individual double-layers are positioned and attached to the flanges by only two pins at both ends. The (incomplete) setup is shown in Fig. 65 confirming that the pressurized straw layers are self-supporting and no or only weak support structures for the STT are needed. The scheme of gas supply and electric readout will be developed next. Finally, the mechanical precision of the setup will be measured by reconstructed tracks of cosmic rays or proton beam at COSY.

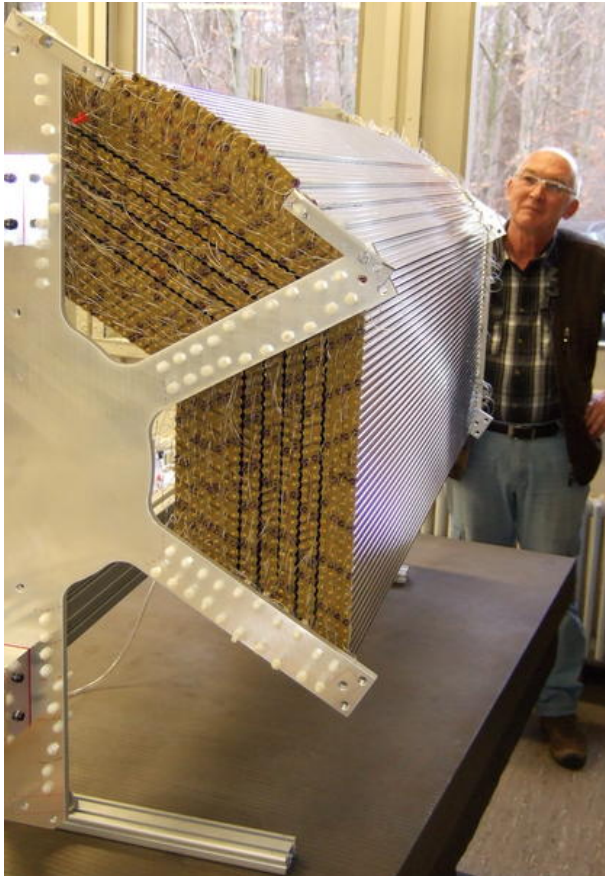


Fig. 65: Assembly of a full-scale semi-barrel prototype.

6.4.2 Measurements of the energy loss for particle identification with STT

Technical preparations and first investigations have been started towards particle discrimination with the PANDA

STT based on energy loss measurements. An additional aim of this work is to investigate options for electronics which are appropriate for this purpose and which are realistic candidates for implementation into the final Panda DAQ system.

An array of 128 Panda-type straw tubes has been installed in a laboratory setup together with state-of-the-art electronics. Initially very fast electronics and data-acquisition modules are used in order to collect analog information as detailed as possible and reach the limits defined by the physics of the detector. Currently a new 250 MHz Flash-ADC is being produced and interfaces are designed for coupling the high-density MSGCROC-ASIC to the straws. In the course of this work the mechanical and electrical coupling of front-end electronics to the straw chambers is being developed.

First raw data taken with β -particles from ^{90}Sr show a good linearity of the energy loss and a clean $1/\sqrt{E}$ behaviour of the resolution with increasing number of straw tubes contributing to a track. Ongoing work includes pulse-height calibration using monoenergetic particle sources and development of tracking software for proper treatment of the geometrical dependence of the energy loss.

A Councils

A.1 Hadron Physics Program Advisory Council

Prof. R. Beck	Universität Bonn	
Prof. J.-P. Blaizot	CEA Saclay, FR	
Prof. D.F. Geesaman	Argonne National Laboratory, U.S.A.	
Dr. P. Gianotti	Laboratori Nazionali di Frascati, I	
Prof. M. Harakeh	KVI Groningen, NL	
Prof. E. Jaeschke	Humboldt Universität Berlin	
Prof. K. Königsmann	Albert-Ludwigs-Universität Freiburg	
Prof. R. Kulesa	Jagellonian University Cracow, PL	
Prof. St. Paul	TU München	Chairperson
Prof. K. Peters	GSi Darmstadt	
Prof. U. Wiedner	Universität Bochum	
Prof. U.-J. Wiese	Universität Bern	

A.2 COSY Program Advisory Committee

Prof. M. Anselmino	L'Universita di Torino, IT	
Prof. D. Barber	DESY, DE	
Prof. J. Bijnens	Lund University, SE	
Prof. M. Garçon	CEA-Saclay, F	
Prof. N. Herrmann	Universität Heidelberg, DE	
Prof. N. Kaiser	TU München, DE	
Prof. B. Kämpfer	FZ Dresden-Rossendorf, DE	
Prof. H. Löhner	KVI Groningen, NL	
Prof. A. Magiera	Jagellonian University Cracow, PL	
Prof. W.T.H. van Oers	University of Manitoba, CA	Chairperson
Prof. A.K. Opper	George Washington University, USA	
Prof. U. Thoma	Universität Bonn, DE	

B Publications

1. Experiment

1. **Observation of an ABC effect in proton-proton collisions**
S. Dymov *et al.*
Phys. Rev. Lett. **102**, 192301 (2009) [arXiv:0902.0715 [nucl-ex]]
2. **Double-Pionic Fusion of Nuclear Systems and the ABC Effect — Approaching a Puzzle by Exclusive and Kinematically Complete Measurements**
M. Bashkanov *et al.*
Phys. Rev. Lett. **102**, 052301 (2009) [arXiv:0806.4942 [nucl-ex]]
3. **Polarizing a stored proton beam by spin flip?**
D. Oellers *et al.*
Phys. Lett. B **674**, 269 (2009) [arXiv:0902.1423 [nucl-ex]]
4. **Measurement of the $\eta \rightarrow 3\pi^0$ Distribution with the WASA Detector at COSY**
C. Adolph *et al.* [WASA-at-COSY Collaboration]
Phys. Lett. B **677**, 24 (2009) [arXiv:0811.2763 [nucl-ex]]
5. **Single-Pion Production in pp Collisions at 0.95 GeV/c (II)**
S. Abd El-Samad *et al.* [COSY-TOF Collaboration]
Eur. Phys. J. A **39**, 281 (2009) [arXiv:0807.1189 [nucl-ex]]
6. **The $dp \rightarrow ppn$ Reaction as a Method to Study Neutron-Proton Charge-Exchange Amplitudes**
D. Chiladze *et al.*
Eur. Phys. J. A **40**, 23 (2009)
7. **The High-Acceptance Dielectron Spectrometer HADES**
G. Agakishiev *et al.* [HADES Collaboration]
Eur. Phys. J. A **41**, 243 (2009) [arXiv:0902.3478 [nucl-ex]]
8. **Measurement of the isospin-filtering $dd \rightarrow {}^4\text{He}K^+K^-$ reaction at $Q = 39$ MeV**
X. Yuan *et al.*
Eur. Phys. J. A **42**, 1 (2009) [arXiv:0905.0979 [nucl-ex]]
9. **On the Production of $\pi^+\pi^+$ Pairs in pp Collisions at 0.8 GeV**
S. Abd El-Samad *et al.* [COSY-TOF Collaboration]
Eur. Phys. J. A **42**, 159 (2009) [arXiv:0906.3095 [nucl-ex]]
10. **Invariant mass distributions for the $pp \rightarrow pp\eta$ reaction at $Q=10$ MeV**
P. Moskal *et al.*
Eur. Phys. J. A **43**, 131 (2010) [arXiv:0912.1592 [nucl-ex]]
11. **Cross Section and Tensor Analysing Power of the $\vec{d}d \rightarrow \eta\alpha$ Reaction Near Threshold**
A. Budzanowski *et al.* [GEM Collaboration]
Nucl. Phys. A **821**, 193 (2009) [arXiv:0811.3372 [nucl-ex]]
12. **Exclusive measurement of two-pion production in the $dd \rightarrow {}^4\text{He}\pi\pi$ reaction**
S. Keleta *et al.*
Nucl. Phys. A **825**, 71 (2009) [arXiv:0904.2699 [nucl-ex]]
13. **Search for η -mesic nuclei in recoil-free transfer reaction**
A. Budzanowski *et al.* [COSY-GEM Collaboration]
Phys. Rev. C **79**, 012201 (2009) [arXiv:0812.4187 [nucl-ex]]
14. **Precision measurements of the $pp \rightarrow \pi^+pn$ and $pp \rightarrow \pi^+d$ reactions: importance of long-range and tensor force effects**
A. Budzanowski *et al.* [COSY-GEM Collaboration]
Phys. Rev. C **79**, 061001 (2009) [arXiv:0904.3417 [nucl-ex]]
15. **Near threshold production of the η meson via the quasi-free $pn \rightarrow pn\eta$ reaction**
P. Moskal *et al.*
Phys. Rev. C **79**, 015208 (2009) [arXiv:0807.0722 [hep-ex]]

16. **Production of the ω meson in the $pd \rightarrow {}^3\text{He}\omega$ reaction at 1450 MeV and 1360 MeV**
K. Schonning *et al.* [CELSIUS/WASA Collaboration]
Phys. Rev. C **79**, 044002 (2009) [arXiv:0902.3905 [nucl-ex]]
17. **Fission studies with 140 MeV α -Particles**
A. Buttkewitz, H. H. Duhm, F. Goldenbaum, H. Machner and W. Strauss
Phys. Rev. C **80**, 037603 (2009) [arXiv:0907.4042 [nucl-ex]]
18. **Photoproduction of η and η' Mesons off Protons**
V. Crede *et al.* [CBELSA/TAPS Collaboration]
Phys. Rev. C **80**, 055202 (2009) [arXiv:0909.1248 [nucl-ex]]
19. **Variation of nonequilibrium processes in $p+\text{Ni}$ system with beam energy**
A. Budzanowski *et al.* [Proton Induced Spallation Collaboration]
Phys. Rev. C **80**, 054604 (2009) [arXiv:0909.1436 [nucl-ex]]
20. **Precision study of the $dp \rightarrow {}^3\text{He}\eta$ reaction for excess energies between 20 and 60 MeV**
T. Rausmann *et al.*
Phys. Rev. C **80**, 017001 (2009) [arXiv:0905.4595 [nucl-ex]]
21. **Generalized Dalitz Plot analysis of the near threshold $pp \rightarrow ppK^+K^-$ reaction in view of the K^+K^- final state interaction**
M. Silarski *et al.* [COSY-11 collaboration]
Phys. Rev. C **80**, 045202 (2009) [arXiv:0909.3974 [hep-ph]]
22. **Precision measurements of the $pp \rightarrow \pi^+pn$ and $pp \rightarrow \pi^+d$ reactions: importance of long-range and tensor force effects**
A. Budzanowski *et al.* [COSY-GEM Collaboration]
Phys. Rev. C **79**, 061001 (2009) [arXiv:0904.3417 [nucl-ex]]
23. **Luminosity determination for the $dd \rightarrow \alpha K^+K^-$ experiment at ANKE/COSY**
X. H. Yuan, A. Dzyuba and M. Büscher [ANKE Collaboration]
Chin. Phys. C **33**, 20 (2009)
24. **Machine studies for the development of storage cells at the ANKE facility of COSY**
K. Grigoryev *et al.*
Nucl. Instrum. Meth. A **599**, 130 (2009)
25. **The central tracker of the PANDA detector**
A. Sokolov, J. Ritman, T. Stockmanns and P. Wintz [PANDA Collaboration]
Nucl. Instrum. Meth. A **598**, 75 (2009)
26. **Improving the performance of the cryogenic heat pipe-target system for the COSY-TOF experiment**
G. A. El-Awadi, S. Abdel-Samad, M. Abdel-Bary and J. Ritman
Vacuum **83**, 1321 (2009)
27. **A thin gold coated hydrogen heat pipe-cryogenic target for external experiments at COSY**
M. Abdel-Bary, S. Abdel-Samad, G. A. Elawadi, K. Kilian and J. Ritman
Cryogenics **49**, 192 (2009)

2. Theorie

28. **Modern Theory of Nuclear Forces**
E. Epelbaum, H. W. Hammer and U. G. Meissner
Rev. Mod. Phys. **81**, 1773 (2009) [arXiv:0811.1338 [nucl-th]]
29. **Implications of heavy quark spin symmetry on heavy meson hadronic molecules**
F. K. Guo, C. Hanhart and U. G. Meissner
Phys. Rev. Lett. **102**, 242004 (2009) [arXiv:0904.3338 [hep-ph]]
30. **On the extraction of the light quark mass ratio from the decays $\psi' \rightarrow J/\psi\pi^0(\eta)$**
F. K. Guo, C. Hanhart and U. G. Meissner
Phys. Rev. Lett. **103**, 082003 (2009) [arXiv:0907.0521 [hep-ph]]
31. **Investigation of the Exclusive ${}^3\text{He}(e,e'pn)p$ Reaction**
D. G. Middleton *et al.*,
Phys. Rev. Lett. **103**, 152501 (2009) [arXiv:0903.1215 [nucl-ex]]
32. **Isospin breaking in the pion-nucleon scattering lengths**
M. Hoferichter, B. Kubis and U. G. Meissner
Phys. Lett. B **678**, 65 (2009) [arXiv:0903.3890 [hep-ph]]
33. **Quark mass dependence of the pion vector form factor**
F. K. Guo, C. Hanhart, F. J. Llanes-Estrada and U. G. Meissner
Phys. Lett. B **678**, 90 (2009) [arXiv:0812.3270 [hep-ph]]
34. **Extraction of the strong neutron-proton mass difference from the charge symmetry breaking in $pn \rightarrow d\pi^0$**
A. Filin, V. Baru, E. Epelbaum, J. Haidenbauer, C. Hanhart, A. E. Kudryavtsev and U. G. Meissner
Phys. Lett. B **681**, 423 (2009) [arXiv:0907.4671 [nucl-th]]
35. **A method to measure the antikaon-nucleon scattering length in lattice QCD**
M. Lage, U. G. Meissner and A. Rusetsky
Phys. Lett. B **681**, 439 (2009) [arXiv:0905.0069 [hep-lat]]
36. **The role of the background in the extraction of resonance contributions from meson-baryon scattering**
M. Döring, C. Hanhart, F. Huang, S. Krewald and U. G. Meissner
Phys. Lett. B **681**, 26 (2009) [arXiv:0903.1781 [nucl-th]]
37. **Backward pion photoproduction**
A. Sibirtsev, J. Haidenbauer, F. Huang, S. Krewald and U. G. Meissner
Eur. Phys. J. A **40**, 65 (2009) [arXiv:0903.0535 [hep-ph]]
38. **Pion-nucleon charge-exchange amplitudes above 2 GeV**
F. Huang, A. Sibirtsev, S. Krewald, C. Hanhart, J. Haidenbauer and U. G. Meissner
Eur. Phys. J. A **40**, 77 (2009) [arXiv:0810.2680 [hep-ph]]
39. **Interactions between heavy mesons and Goldstone bosons from chiral dynamics**
F. K. Guo, C. Hanhart and U. G. Meissner
Eur. Phys. J. A **40**, 171 (2009) [arXiv:0901.1597 [hep-ph]]
40. **Ground state energy of dilute neutron matter at next-to-leading order in lattice chiral effective field theory**
E. Epelbaum, H. Krebs, D. Lee and U. G. Meissner
Eur. Phys. J. A **40**, 199 (2009) [arXiv:0812.3653 [nucl-th]]
41. **Neutral pion photoproduction at high energies**
A. Sibirtsev, J. Haidenbauer, S. Krewald, U. G. Meissner and A. W. Thomas
Eur. Phys. J. A **41**, 71 (2009) [arXiv:0902.1819 [hep-ph]]
42. **Lattice chiral effective field theory with three-body interactions at next-to-next-to-leading order**
E. Epelbaum, H. Krebs, D. Lee and U. G. Meissner
Eur. Phys. J. A **41**, 125 (2009) [arXiv:0903.1666 [nucl-th]]
43. **Regularization, renormalization and 'peratization' in effective field theory for two nucleons**
E. Epelbaum and J. Gegelia
Eur. Phys. J. A **41**, 341 (2009) [arXiv:0906.3822 [nucl-th]]

44. **Searching for signatures around 1920 MeV of a N^* state of three hadron nature**
A. Martinez Torres, K. P. Khemchandani, U. G. Meissner and E. Oset
Eur. Phys. J. A **41**, 361 (2009) [arXiv:0902.3633 [nucl-th]]
45. **The role of nucleon recoil in low-energy antikaon-deuteron scattering**
V. Baru, E. Epelbaum and A. Rusetsky
Eur. Phys. J. A **42**, 111 (2009) [arXiv:0905.4249 [nucl-th]]
46. **Electromagnetic corrections in $\eta \rightarrow 3\pi$ decays**
C. Ditsche, B. Kubis and U. G. Meissner
Eur. Phys. J. C **60**, 83 (2009) [arXiv:0812.0344 [hep-ph]]
47. **Final state interactions in the decays $J/\psi \rightarrow VPP$**
B. Liu, M. Buescher, F. K. Guo, C. Hanhart and U. G. Meissner
Eur. Phys. J. C **63**, 93 (2009) [arXiv:0901.1185 [hep-ph]]
48. **Coherent photon-photon interactions in very peripheral relativistic heavy ion collisions**
G. Baur
Eur. Phys. J. D **55**, 265 (2009) [arXiv:0810.1400 [nucl-th]]
49. **Ionization of highly charged relativistic ions by neutral atoms and ions**
G. Baur, I.L. Beigman, V.P. Shevelko, I.Yu. Tolstikhina and Th. Stoehlker,
Phys. Rev. A **80**, 012713 (2009)
50. **Renormalization of chiral two-pion exchange NN interactions with Delta-excitations: Central Phases and the Deuteron**
M. P. Valderrama and E. R. Arriola
Phys. Rev. C **79**, 044001 (2009) [arXiv:0809.3186 [nucl-th]]
51. **Description of the Giant Monopole Resonance in the Even-A $^{112-124}\text{Sn}$ Isotopes within the Microscopic Model Including Quasiparticle-Phonon Coupling**
A. Avdeenkov *et al.*
Phys. Rev. C **79**, 034309 (2009) [arXiv:0808.0478 [nucl-th]]
52. **The role of the $N^*(1535)$ in the $J/\psi \rightarrow \bar{p}\eta p$ and $J/\psi \rightarrow \bar{p}K^+\Lambda$ reactions**
L. S. Geng, E. Oset, B. S. Zou and M. Döring
Phys. Rev. C **79**, 025203 (2009) [arXiv:0807.2913 [hep-ph]]
53. **Gauge invariance in the presence of a cutoff**
A. N. Kvinikhidze, B. Blankleider, E. Epelbaum, C. Hanhart and M. P. Valderrama
Phys. Rev. C **80**, 044004 (2009) [arXiv:0904.4128 [nucl-th]]
54. **A Two Potential Formula and its Application to Proton-Proton Scattering**
M. Pavon Valderrama and E. Ruiz Arriola
Phys. Rev. C **80**, 024001 (2009) [arXiv:0904.1120 [nucl-th]]
55. **p-Wave pion production from nucleon-nucleon collisions**
V. Baru, E. Epelbaum, J. Haidenbauer, C. Hanhart, A. E. Kudryavtsev, V. Lensky and U. G. Meissner
Phys. Rev. C **80**, 044003 (2009) [arXiv:0907.3911 [nucl-th]]
56. **On-shell consistency of the Rarita-Schwinger field formulation**
H. Krebs, E. Epelbaum and U. G. Meissner
Phys. Rev. C **80**, 028201 (2009) [arXiv:0812.0132 [hep-th]]
57. **Two-pion exchange electromagnetic current in chiral effective field theory using the method of unitary transformation**
S. Kolling, E. Epelbaum, H. Krebs and U. G. Meissner
Phys. Rev. C **80**, 045502 (2009) [arXiv:0907.3437 [nucl-th]]
58. **Three-nucleon force effects in the $^1H(\vec{d}, \vec{p}p)n$ reaction at 135 MeV/nucleon**
K. Sekiguchi *et al.*,
Phys. Rev. C **79**, 054008 (2009)

59. **Forward antiproton-deuteron elastic scattering and total spin-dependent antiproton-deuteron cross sections at intermediate energies**
Yu. N. Uzikov and J. Haidenbauer,
Phys. Rev. C **79**, 024617 (2009) [arXiv:0810.3997 [nucl-th]]
60. **Aspects of meson-baryon scattering in three- and two-flavor chiral perturbation theory**
M. Mai, P. C. Bruns, B. Kubis and U. G. Meissner
Phys. Rev. D **80**, 094006 (2009) [arXiv:0905.2810 [hep-ph]]
61. **Analytic properties of the scattering amplitude and resonances parameters in a meson exchange model**
M. Döring, C. Hanhart, F. Huang, S. Krewald and U. G. Meissner
Nucl. Phys. A **829**, 170 (2009) [arXiv:0903.4337 [nucl-th]]
62. **Analyzing the Effects of Neutron Polarizabilities in Elastic Compton Scattering off ^3He**
D. Shukla, A. Nogga and D. R. Phillips,
Nucl. Phys. A **819**, 98 (2009) [arXiv:0812.0138 [nucl-th]]
63. **The mass of the Delta resonance in a finite volume: fourth-order calculation**
V. Bernard, D. Hoja, U. G. Meissner and A. Rusetsky
JHEP **0906**, 061 (2009) [arXiv:0902.2346 [hep-lat]]
64. **Depth of Interaction Enhanced Gamma-Ray Imaging**
C. W. Lerche
Nucl. Instruments and Methods in Phys. Res. A **600**, 624 (2009)
(see arXiv:physics/0611011 for Ph.D. thesis)
65. **Strategies for baryon resonance analysis**
M. Döring, C. Hanhart, F. Huang, S. Krewald and U. G. Meissner
Chin. Phys. C **33**, 1127 (2009)
66. **Total spin-dependent antiproton-deuteron elastic scatterings at low and intermediate energies**
J. Haidenbauer and Yu. N. Uzikov,
Hyperfine Interactions **194**, 283 (2009)

3. Accelerator (including conference proceedings)

67. **Experimental Test of a New Technique to Overcome Spin-Depolarizing Resonances**
V. S. Morozov et al.
Phys. Rev. Lett. **102**, 244801 (2009)
68. **Particle and x-ray generation by irradiation of gaseous and solid targets with a 100 TW laser pulse**
O. Willi et al.
Plasma Phys. and Control. Fusion **51**, 124049 (2009)
69. **A Study of the Proton Beam Lifetime in the COSY Storage Ring at low Momenta**
A. Garishvilli et al.
Int. J. Mod. Phys. E **18**, 492 (2009)
70. **Beam Dynamics of the High-Energy Storage Ring (HESR) for FAIR**
A. Lehrach, K. Bongardt, B. Lorentz, R. Maier, D. Prasuhn, H. Stockhorst, R. Tölle, D. M. Welsch
Int. J. Mod. Phys. E **18**, 420 (2009)
71. **Application of Cooling Methods to NICA Project**
E. Ahmanova *et al.*
Proc. COOL 2009; Lanzhou, China, August 31 – September 4, 2009
72. **Status of the 2 MeV Electron Cooler for COSY Jülich**
J. Dietrich, M. I. Bryzgunov, A. D. Goncharov, V. V. Parkhomchuk, V. B. Reva, D. N. Skorobogatov
Proc. COOL 2009; Lanzhou, China, August 31 – September 4, 2009
73. **Beam Profile Monitoring at COSY via Light Emitted by Residual Gas**
Ch. Böhme, L. Conradie, J. Dietrich, V. Kamerdzhev
Proc. 9th European Workshop on Beam Diagnostics and Instrumentation for Particle Accelerators, DIPAC 2009; Basel, Switzerland, May 24 – 27, 2009
74. **Beam Test of the FAIR IPM Prototype in COSY**
Ch. Böhme, J. Dietrich, V. Kamerdzhev, P. Forck, T. Giacomini, D. Liakin
Proc. 9th European Workshop on Beam Diagnostics and Instrumentation for Particle Accelerators, DIPAC 2009; Basel, Switzerland, May 24 – 27, 2009
75. **Non-destructive Beam Position Measurement in a Proton Therapy Beam Line**
D. T. Fourie, L. Anthony, A. H. Botha, J. L. Conradie, J. L. G. Delsink, P. F. Rohwer, P. A. van Schalkwyk, J. Dietrich
Proc. 9th European Workshop on Beam Diagnostics and Instrumentation for Particle Accelerators, DIPAC 2009; Basel, Switzerland, May 24 – 27, 2009
76. **Simulation Study of Simultaneous Use of Stochastic Cooling and Electron Cooling with Internal Target at COSY and HESR**
T. Katayama, T. Kikuchi, H. Stockhorst, J. Dietrich, D. Prasuhn, R. Maier
Proc. COOL 2009; Lanzhou, China, August 31 – September 4, 2009
77. **Cooling Experiments at COSY in Preparation for the HESR**
Prasuhn, D.; Dietrich, J.; Maier, R.; Stassen, R.; Stockhorst, H.
Proc. COOL 2009; Lanzhou, China, August 31 – September 4, 2009

C Talks and Colloquia

1. Büscher, M.
Symmetry Tests in Hadronic Systems in Hadronic Interactions at COSY-Jülich
4th Int. Symposium on Symmetries in Subatomic Physics (SSP2009)
Taipei, Taiwan: 02.06.2009
2. Büscher, M.
Meson Production Experiments at COSY-Jülich
5th Int. Conf. on Quarks and Nuclear Physics (QNP2009)
Beijing, China: 21.09.2009
3. Dietrich, J.
Status 2 MeV Electron Cooler for COSY
Winterseminar des Instituts für Angewandte Physik der J.W.Goethe-Universität
Riezlern: 08. – 14.03.2009
4. Dietrich, J.
Development of a High Energy Electron Cooler for Hadron Physics Experiments at COSY and HESR
BINP Novosibirsk, Russia: 18.03.2009
5. Dietrich, J.
Status of the 2 MeV Electron Cooler Development for COSY-Jülich
Particle Accelerator Conference (PAC)
Vancouver, Canada: 04. – 08.05.2009
6. Dietrich, J.
Development of a High Energy Electron Cooler for Hadron Physics Experiments at COSY and HESR
The Svedberg Laboratory, Uppsala University, Sweden: 14.05.2009
7. Dietrich, J.
COSY — Status and Future
iThemba LABS, Faure, South Africa: 03.06.2009
8. Dietrich, J.
Development of a High Energy Electron Cooler for Hadron Physics Experiments at COSY and HESR
Moscow, Russia: 21.06.2009
9. Dietrich, J.
Status of the 2 MeV Electron Cooler for COSY Jülich
27th HESR Consortium Meeting
Bucharest, Romania: 26.08.2009
10. Dietrich, J.
Status of the 2MeV Electron Cooler for COSY Jülich
COOL 2009
Lanzhou, China: 31.08. – 04.09.2009
11. Dietrich, J.
New Developments in the field of Accelerator Based Research
German-South African Research Lecture Series
Johannesburg, South Africa: 13.10.2009
12. Dietrich, J.
2 MeV Electron Cooler for COSY/HESR
28th HESR Consortium Meeting
Darmstadt, Germany: 08.12.2009
13. Döring, M.
Jülich analysis
EBAC Collaboration meeting
Newport News, Virginia, USA: 20. – 23.07.2009

14. Döring, M.
On the cross section ratio σ_n/σ_p in η photoproduction
PrimeNet Meeting
Bonn: 08. – 09.10.2009
15. Döring, M.
Resonance properties from a coupled channel meson exchange model
NSTAR 2009
Beijing, China: 19. – 22.04.2009
16. Döring, M.
Resonance properties from a coupled channel meson exchange model
The 5th International Pion-Nucleon PWA Workshop and Interpretation of Baryon Resonances
ECT* Trento, Italy: 01. – 05.06.2009
17. Döring, M.
S11 resonances in meson-baryon production
Narrow Nucleon Resonances Conference
Edinburgh, UK: 08. – 10.06.2009
18. Döring, M.
The reaction of $\pi\eta$ photoproduction in a unitary chiral model
Institutsseminar Universität Mainz
Mainz: 22.06.2009
19. Epelbaum, E.
Effective theory of nuclear forces
Sixth International Workshop on Chiral Dynamics
Bern, Switzerland: 06. – 10.07.2009
20. Epelbaum, E.
Modern theory of hadrons and nuclei
Symposium on Theoretischer Physik (Astro Particle Physics)
Basel, Switzerland: 25. – 26.05.2009
21. Epelbaum, E.
Modern theory of nuclear forces
Series of 3 invited lectures at the Nuclear physics school (Ecole Joliot-Curie)
Lacanau, France: 27.09. – 02.10.2009
22. Epelbaum, E.
Nuclear forces and chiral symmetry
4th International Symposium on Symmetries in Subatomic Physics (SSP2009)
Taipei, Taiwan: 02. – 05.06.2009
23. Epelbaum, E.
Nuclear forces from EFT
1st Bethe Center Workshop
Bad Honnef: 09. – 10.10.2009
24. Felden, O.
The COSY-Jülich Polarized H⁻ and D⁻ Ion Source
Polarized Sources, Targets and Polarimetry (PSTP 2009)
Ferrara, Italy: 07. – 11.09.2009
25. Gebel, R.
Status of the COSY-Jülich Injector Cyclotron
European Cyclotron Progress Meeting ECPM XXXVII
Groningen, The Netherlands: 28. – 31.10.2009
26. Goldenbaum, F.
Evaporation and pre-equilibrium emission in GeV p -induced spallation-fragmentation reactions
2nd International Conference on Nuclear Fragmentation; From basic Research to Applications (NUFRA2009)
Kemer, Turkey: 27.09. – 04.10.2009

27. Goldenbaum, F.
Hadron Spectroscopy at COSY
XIII International Conference on Hadron Spectroscopy
Tallahassee, Florida, USA: 29.11. – 04.12.2009
28. Guo, F.K.
 D_{s0}^* (2317) and charmed-meson — Goldstone-boson interactions from chiral dynamics
Seminar of IHEP
Beijing, China: 06.01.2009
29. Guo, F.K.
Heavy meson hadronic molecules
Workshop on Frontiers in Nuclear Physics
Bad Honnef: 18. – 20.06.2009
30. Guo, F.K.
Heavy quark spin symmetry and heavy flavor hadronic molecules
The 5th International Conference on Quarks and Nuclear Physics
Beijing, China: 21. – 26.09.2009
31. Guo, F.K.
Prominent candidates of hidden and open charm hadronic molecules
Workshop on Charmed Exotics
Bad Honnef: 10. – 12.08.2009
32. Guo, F.K.
S wave interactions between charmed mesons and Goldstone bosons from chiral dynamics
Excited QCD 2009
Zakopane, Poland: 08. – 14.02.2009
33. Haidenbauer, J.
Aspects of the hyperon-nucleon interaction
Symposium “Frontiers in Nuclear Physics”
Bad Honnef: 18. – 20.06.2009
34. Haidenbauer, J.
Baryon-baryon interaction from effective field theory
19th International IUPAP Conference on Few-Body Problems in Physics
Bonn: 31.08. – 05.09.2009
35. Haidenbauer, J.
Baryon-baryon interactions in effective field theory
10th International Conference on Hypernuclear and Strange Particle Physics (Hyp X)
Tokai, Ibaraki, Japan : 14. – 18.09.2009
36. Haidenbauer, J.
Hyperon-Nucleon Interaction: From meson exchange to effective field theory
Kolloquium, Institut für Theoretische Physik, Universität Graz
Graz, Austria: 19.05.2009
37. Haidenbauer, J.
Near threshold antiproton-proton enhancement in B and J/Ψ decays and the quest for baryonia
Workshop “Hadron Structure and Dynamics”
Bad Honnef: 13. – 14.08.2009
38. Haidenbauer, J.
The Jülich model of correlated $\pi\pi/KK$ exchange
Workshop on “Quark masses and hadron physics”
Universidad Complutense de Madrid
Madrid, Spain: 02. – 05.06.2009

39. Hanhart, C.
Exotic open and hidden charm states
Charm 2009
Leimen: 20. – 22.05.2009
40. Hanhart, C.
Extracting weak phases from Dalitz Plot CP studies
Workshop on Future Opportunities for open Charm Physics at PANDA
Mainz: 19. – 20.11.2009
41. Hanhart, C.
Light quark effects in the charm sector
PANDA-Kollaborations-Meeting
Jülich: 07. – 11.09.2009
42. Hanhart, C.
Meson loops in the charm sector
International Workshop on Hadron Spectroscopy
INT Seattle, USA: 14. – 20.11.2009
43. Hanhart, C.
QCD Exotics
International Workshop: MAMI and beyond
Mainz: 30.03. – 02.04.2009
44. Hanhart, C.
Quark mass dependence of resonance properties
Light quark masses and hadron physics
Madrid, Spain: 02. – 05.06.2009
45. Hodana, M.
Analysis of the $\eta \rightarrow e^+ e^- \gamma$ with WASA-at-COSY
PrimeNet Meeting
Bonn: 08. – 09.10.2009
46. Hodana, M.
Study of the $\eta \rightarrow e^+ e^- \gamma$ decay with WASA-at-COSY
DPG Frühjahrstagung
Bochum: 16. – 20.03.2009
47. Jankowiak, A.;
A Concept for a Polarized Electron-Nucleon Collider at the HESR of the FAIR Project
23rd Particle Accelerator Conference
Vancouver, Canada: 04. – 08.05.2009
48. Krewald, S.
Amplitudes at opening thresholds
Workshop Polarization Observables and Partial Wave Analysis
Bad Honnef: 01. – 03.03.2009
49. Krewald, S.
Baryon Resonance Analysis via Jülich coupled channel approach
International workshop on meson-baryon dynamics (in honor of Iraj Afnan), Thomas Jefferson National Laboratory
Newport News, Virginia, USA: 24.07.2009
50. Krewald, S.
Effective Field Theory Approach to Nuclear Matter
China Institute of Atomic Energy
Beijing, China: 24.04.2009
51. Krewald, S.
Low-density nuclear matter in effective field theory
19^{mathrmth} International IUPAP Conference on Few-Body Problems in Physics
Bonn: 31.08. – 05.09.2009

52. Krewald, S.
 Low-density nuclear matter in effective field theory
 XII International Seminar on Electromagnetic Interactions of Nuclei Photonuclear
 Laboratory of the Institute for Nuclear Research of Russian Academy of Sciences
 Moscow, Russia: 17. – 20.09.2009
53. Krewald, S.
 Strategies for baryon resonance analysis
 12^{mathrmth} International workshop on the Physics of Excited Nucleon (NSTAR2009)
 Beijing, China: 19. – 22.04.2009
54. Lehrach, A.
 Acceleration of polarised p and d in HESR/FAIR
 Common ENC/EIC workshop at GSI
 Darmstadt: 28. – 30.05.2009
55. Lehrach, A.
 Calculations of beam equilibrium and luminosities at ENC
 Common ENC/EIC workshop at GSI
 Darmstadt: 28. – 30.05.2009
56. Lehrach, A.
 The ENC@FAIR Accelerator Project, Workshop Electron-Ion Collider
 8th European Research Conference on Electromagnetic Interactions with Nucleons and Nuclei
 Milos Island: 27.09. – 02.10.2009
57. Lorentz, B.
 Lifetime Studies for Polarized and Unpolarized Protons in COSY
 23rd Particle Accelerator Conference
 Vancouver, Canada: 04. – 08.05.2009
58. Machner, H.
 Event reconstruction for a DIRC
 Workshop on fast Cherenkov detectors — Photon detection, DIRC design and DAQ
 Giessen: 11. – 13.05.2009
59. Machner, H.
 Hunting η -bound Nuclei
 The 5th International Conference on Quarks and Nuclear Physics (QNP09)
 Beijing, China: 21. – 26.09.2009
60. Machner, H.
 NY Interactions studied in final state interactions
 The 10th International Conference on Hypernuclear and Strange Particle Physics (Hyp-X)
 Tokai, Ibaraki, Japan: 14. – 18.09.2009
61. Machner, H.
 Search for η -mesic nuclei
 DPG Frühjahrstagung
 Bochum: 16. – 20.03.2009
62. Maier, R.
 Physik des Antiprotonenbeschleunigers HESR
 Bochumer Physikalisches Kolloquium
 Ruhr-Universität Bochum: 18.05.2009
63. Meißner, U.-G.
 Baryon-baryon interactions from effective field theory
 PANDA Kollaborations-Meeting
 Jülich: 07. – 11.09.2009

64. Meißner, U.-G.
EFT for nuclear physics
International Workshop on Effective Field Theories (EFT09)
Valencia, Spain: 01. – 06.02.2009
65. Meißner, U.-G.
Excited hadrons in a box
Colloquium in memory of Jan Stern, Institut Henri Poincaré
Paris, France: 02. – 03.10.2009
66. Meißner, U.-G.
Hadron Physics at the 1 GeV scale and its impact
International Workshop “MAMI and beyond”
Mainz: 30.03. – 02.04.2009
67. Meißner, U.-G.
Hadrons in a box
First Bethe Center Workshop
Bad Honnef: 09. – 10.10.2009
68. Meißner, U.-G.
Isospin violation, light quark masses and all that
5th International Conference on Quarks and Nuclear Physics (QNP 09)
Beijing, China: 21. – 26.09.2009
69. Meißner, U.-G.
Resonances in a finite volume
Workshop on Hadron Structure and Dynamics
Bad Honnef: 13. – 14.08.2009
70. Meißner, U.-G.
Theory of nuclear forces
Lecture week of the SFB/TR-16 “Subnuclear structure of matter”
Bonn: 03. – 07.08.2009
71. Meißner, U.-G.
Theory of nuclear forces
Invited lectures, Guangxi Normal University
Guilin, China: 15. – 30.09.2009
72. Mertens, M.C.
Application of a versatile digital readout system for the PANDA Micro Vertex Detector
DPG Frühjahrstagung
Bochum: 16. – 20.03.2009
73. Nogga, A.
Application of chiral and low-momentum nuclear forces
First International EMMI-EFES Workshop on Neutron-Rich Nuclei (EENEN 09)
GSI Darmstadt: 09. – 11.02.2009
74. Nogga, A.
On the action of four-nucleon forces in ^4He
International Workshop on Frontiers in Nuclear Physics
Bad Honnef: 18. – 20.06.2009
75. Nogga, A.
On the action of four-nucleon forces in ^4He
19th International IUPAP Conference on Few-Body Problems in Physics
Bonn: 31. – 05.09.2009
76. Pauly, Chr.
 η decays with WASA at COSY
Seminarvortrag
KVI Groningen, The Netherlands: 17.11.2009

77. Pauly, Chr.
 η Meson Decays with WASA-at-COSY
 The 3rd Workshop of the APS Topical Group in Hadron Physics
 Denver, CO, USA: 29.04. – 01.05.2009
78. Pauly, Chr.
 WASA-at-COSY
 CANU-Meeting
 Bad Honnef: 21. – 22.12.2009
79. Redmer, C.F.
 Analysis of $\eta \rightarrow \pi^+ \pi^- \gamma$ measured with WASA at COSY
 DPG Frühjahrstagung
 Bochum: 16. – 20.03.2009
80. Redmer, C.F.
 Analysis of $\eta \rightarrow \pi^+ \pi^- \gamma$ measured with WASA at COSY
 PrimeNet Meeting
 Bonn: 08. – 09.09.2009
81. Ritman, J.
 From COSY to HESR
 IUPAP Working Group (WG.9) on International Cooperation in Nuclear Physics (ICNP) Annual General Meeting
 Jülich: 30.08.2009
82. Ritman, J.
 Status von PANDA
 Jahrestreffen des Komitee für Hadronen- und Kernphysik
 Bad Honnef: 09.12.2009
83. Ritman, J.
 Wir sind Sternenstaub: Nukleosynthese nach dem Urknall
 Projektwoche fuer Schülerinnen und Schüler
 Bochum: 06.04.2009
84. Ritman, J.
 Wir sind Sternenstaub: Nukleosynthese nach dem Urknall
 Ringvorlesung: Kosmische Zusammenhänge: Vom Urknall bis zur Entstehung der Erde und des Lebens
 Bochum: 28.04.2009
85. Schadmand, S.
 Hadrons and Broken Symmetries with WASA at COSY
 International Symposium on Nuclear Physics
 BARC Mumbai, India: 08. – 12.12.2009
86. Schadmand, S.
 Hadrons and Broken Symmetries with WASA at COSY
 Indian Institute for Astrophysics, Bangalore, India: 15.12.2009
87. Schadmand, S.
 Hadrons in Nuclei: Experiments and Perspectives
 Physikalisches Kolloquium, Universität zu Köln
 Köln: 20.01.2009
88. Schadmand, S.
 Mutter Natur ist ein bißchen seltsam und nicht ganz symmetrisch
 Habilitandentag, Universität zu Köln
 Köln: 25.06.2009
89. Senichev, Yu.
 Theory and Applications of lattice with the negative momentum compaction factor
 23rd Particle Accelerator Conference
 Vancouver, Canada: 04. – 08.05.2009

90. Speth, J.
Complex Systems: From Nuclear Physics to Financial Markets
4th International Symposium on Symmetries in Subatomic Physics (SSP 2009)
Taipei, Taiwan: 02. – 05.06.2009
91. Stockhorst, H.
Compensation of mean energy loss due to an internal target by application of a barrier bucket and stochastic momentum cooling at COSY.
COOL 09
Lanzhou, China: 31.08. – 04.09.2009
92. Stockhorst, H.
Experiments at COSY with Internal Targets, Stochastic Cooling and RF
CERN-GSI Meeting on Internal Targets and Beam Cooling in Storage Rings GSI
Darmstadt: 29.10.2009
93. Stockmanns, T.
Open Charm Detection with the PANDA Detector at FAIR
Kernphysikalisches Kolloquium, HISKP Universität Bonn
Bonn: 16.07.2009
94. Stockmanns, T.
Open Charm Spectroscopy at PANDA
Workshop on Future Opportunities for Open Charm Physics at PANDA
Mainz: 19. – 20.11.2009
95. Stockmanns, T.
The PANDA Micro-Vertex-Detector
DPG Frühjahrstagung
Bochum: 16. – 20.03.2009
96. Wirzba, A.
Neutron-proton mass difference in nuclear matter and in finite nuclei and the Nolen-Schiffer anomaly
19th International IUPAP Conference on Few-Body Problems in Physics
Universität Bonn: 31. – 05.09.2009
97. Wirzba, A.
On rare η decays
PrimeNet Workshop
Universität Bonn: 08. – 09.10.2009
98. Xu, H.
Effect of the Solenoid Field on the Luminosity Monitor
XXX Panda Collaboration Meeting
Jülich: 07. – 09.09.2009
99. Xu, H.
Correction of the Effect of Solenoid Field with Geane Tools
XXXI Panda Collaboration Meeting
Darmstadt: 07. – 11.12.2009

D Diploma and Ph.D. Theses

1. Bachelor, Master, Diploma

1. S. Bour,
Lattice formulation of the hyperon-nucleon interaction,
Diplomarbeit, Universität Bonn
2. C. Eilhard,
Quark Mass dependence of the pion-nucleon coupling constant,
Diplomarbeit, Universität Bonn
3. A. Fayt,
Optische Untersuchung relativistischer Plasmen nach Beschuss von Gastargets mit einem Höchstleistungslaser,
Masterarbeit, Fachhochschule Köln
4. A. Filin,
Charge-symmetry breaking in $pn \rightarrow d\pi^0$,
Diploma thesis, ITEP Moskau, Russia
5. F. Golor,
Fermionische kalte Atome,
Diplomarbeit, Universität Bonn
6. M. Hoferichter,
Pion-nucleon scattering in covariant chiral perturbation theory,
Diplomarbeit, Universität Bonn
7. S. Kazmierowski,
Hyperon-nucleon scattering at next-to-leading order in chiral perturbation theory,
Diplomarbeit, Universität Bonn
8. S. Liebig,
 $\pi - ^3\text{He}$ scattering in chiral perturbation theory,
Diplomarbeit, Universität Bonn
9. G. Oswald,
Bau, Test und Inbetriebnahme einer Ionisations- und Proportionalzählkammer zum Nachweis laserbeschleunigter Ionen,
Diplomarbeit, Hochschule Merseburg (FH)
10. K. Ottnod,
The neutron electric dipole form factor from chiral perturbation theory,
Diplomarbeit, Universität Bonn
11. I. Romyantsev,
Feshbach Resonanz,
Diplomarbeit, Universität Bonn
12. M. Ruzzo,
Untersuchung relativistischer Plasmen nach Beschuss eines Gastargets mit einem Höchstleistungslaser,
Diplomarbeit, Fachhochschule Aachen
13. M. Seltmann,
Hochauflösende Interferometrie laserinduzierter Plasmen,
Diplomarbeit, Fachhochschule Aachen
14. E. Shikov,
Investigation of Σ^- production in the reaction $pn \rightarrow pK^+\Sigma^-$ using the ANKE spectrometer,
Diploma thesis, PNPI Gatchina, Russia
15. S. Urrutia,
Vier-Nukleon-Kräfte mit explizitem Delta unter Verwendung der Methode der unitären Transformation,
Diplomarbeit, Universität Bonn

16. P. Voigtländer,
Kalibration des COSY-TOF Straw Tube Tracker,
Diplomarbeit, Universität Bochum

2. Ph.D.

17. P. Bruns,
Multi-scale chiral dynamics,
Universität Bonn
18. Z. Chen,
Measurement of $pd \rightarrow {}^3AX$ reactions with WASA-at-COSY aiming at studies of the light scalar mesons $a_0/f_0(980)$,
IMP Lanzhou, China
19. E. Czerwinski,
Determination of the total width of the η' meson,
Jagiellonian University Cracow, Poland
20. A. Dzyuba,
Near threshold kaon pair production in nucleon-nucleon collisions,
PNPI, Gatchina, Russia
21. J. Klaja,
Isospin dependence of the η' meson production in nucleon-nucleon collisions,
Jagiellonian University, Cracow, Poland
22. P. Klaja,
Comparative studies of the interaction in the low energy $pp\eta$ and $pp\eta'$ systems,
Jagiellonian University, Cracow, Poland
23. Yu. Valdau,
Investigation of the $pp \rightarrow K^+n\Sigma^+$ reaction with the magnetic spectrometer ANKE-COSY,
Universität zu Köln

E Awards & Offers for Professorships

U.-G. Meißner: *Fellow of the American Physical Society* for leading the development of chiral perturbation theory with baryons, including many pioneering and successful predictions for the interactions of nucleons with photons, pions, and other nucleons.

E. Epelbaum: Received calls as Associate Professor from the University of Basel, Switzerland, and from the University of Bonn. Received call as Full Professor from the University of Bochum (accepted in January 2010).

F Funded Projects

Project	Responsible	Partner Institute	Funded by
Virtual Institute Spin and Strong QCD	U.-G. Meißner	GSI, Univ.'s Bern, Bonn, Ferrara, Cracow, Torino	HGF
Few Nucleon Systems in χ EFT	E. Epelbaum	Univ. Bonn	HGF
CARE	R. Tölle		EU/FP6
TA-COSY	D. Grzonka		EU/FP6
Hadron Physics Theory Netzwerk	U.-G. Meißner	Network	EU/FP6
Pellet Target	M. Büscher	ITEP, MPEI Moscow (Russia)	EU/FP6
EURONS/EXL	D. Grzonka		EU/FP6
EUROTRANS/NUDATRA	F. Goldenbaum		EU/FP6
DIRAC Secondary Beams	R. Tölle		EU/FP6
DIRAC Phase 1	R. Tölle		EU/FP6
DIRAC Secondary Beams PANDA-2	J. Ritman		EU/FP6
DIRAC Secondary Beams PANDA-4	J. Ritman		EU/FP6
Advanced Residual Gas Profile Monitor	J. Dietrich	GSI	EU/FP6
Design Study for Pick-up Electronic Development	J. Dietrich	GSI	EU/FP6
Project FAIR	R. Toelle	GSI	EU/FP7
HadronPhysics 2	D. Grzonka		EU/FP7
Meson-Baryon Scattering	M. Döring		DFG
Scalar Mesons	M. Büscher	ITEP, INR Moscow (Russia)	DFG
Pellet Target	M. Büscher	ITEP, MPEI Moscow (Russia)	DFG
Laser applications of a pellet target	M. Büscher	ITEP, MPEI Moscow (Russia), Univ. Düsseldorf	DFG
Polarized Nuclear Fusion	R. Engels	PNPI Gatchina (Russia)	DFG
Nucleon-Nucleon interactions	A. Kacharava	JINR Dubna (Russia)	DFG
PAX/COSY	F. Rathmann		DFG
K^- Production in Nuclei	M. Hartmann	ITEP Moscow (Russia)	DFG
Isospin Violation	M. Büscher	IMP Lanzhou (China)	DFG
Jets in Hard Processes	N.N. Nikolaev	Landau Inst., ITEP Moscow (Russia)	DFG
Properties of Unstable Nuclei	S. Krewald	Petersburg State Univ., IPPE Obninsk (Russia)	DFG
Signals of hadronic molecules	C. Hanhart	ITEP Moscow (Russia)	DFG
Response function of short-lived nuclear isotopes	S. Krewald		DFG
Fundamental Research with Hadrons	W. Oelert	Jagiellonian Univ. Cracow (Poland)	DFG

Project	Responsible	Partner Institute	Funded by
Neutron Properties from light nuclei	E. Epelbaum	Univ.'s Bochum, Bonn, Gießen	SFB/TR 16
Broken Symmetries	H. Machner	Univ. Helsinki (Finland)	DAAD
PPP Kanada	D. Grzonka	York Univ., Toronto (Canada)	DAAD
PANDA luminosity monitor	J. Ritman	Madagascar	HGF-DAAD
Rare Decays of η and η' Mesons	S. Schadmand	Indian Inst. of Technology Bombay	DAAD/DST India
Polarization observables in $\bar{p}d$ elastic scattering	J. Haidenbauer	JINR Dubna (Russia)	Heisenberg-Landau Program
Eta-Meson Physics	H. Machner	BARC Mumbai (India)	Int. Büro BMBF
Target Development for nuclear physics experiments at COSY and AEA cyclotron	J. Ritman	AEA Cairo (Egypt)	Int. Büro BMBF
Medical Applications of Accelerators	J. Dietrich	iThemba LABS (South Africa)	Int. Büro BMBF
A Pellet Target for PANDA	M. Büscher	ITEP, MPEI Moscow (Russia) Uppsala Univ. (Sweden), GSI	INTAS
Advanced Beam Dynamic for Storage Rings	A. Lehrach	GSI, TEMF (Darmstadt) TSL Uppsala (Sweden) ITEP Moscow, JINR Dubna (Russia) Univ. Kiev (Ukraine)	INTAS
Projectile Electron Losses in the Collisions of Fast and Relativistic Low Charged Ions	G. Baur	GSI, Stockholm, Tashkent, Moscow, Arkhangelsk	GSI-INTAS
Polarized Target	F. Rathmann	PNPI Gatchina (Russia)	ISTC
Baryon Resonance Analysis	U.-G. Meißner	JLAB (U.S.A.)	JLAB
Development of a high energy electron cooler	J. Dietrich	TU Dortmund; BINP Novosibirsk, JINR Dubna (Russia)	HGF
HGF/CSC Ph.D. fellowship	M. Büscher	IMP Lanzhou (China)	HGF/CSC
HGF/CSC Postdoc fellowship	M. Büscher	Xian Jiaotong Univ. (China)	HGF/CSC
Calculations of the Radiation Load to the PANDA MVD	J. Ritman	Israel	NRW-Israel

G COSY-FFE Projects

Project	Responsible	Institute
Entwicklung eines innovativen, kompakten Monitorsystems für einen elektromagnetischen Kristallkalorimeter und Entwicklung von Software-Werkzeugen zur Teilchenidentifikation	Prof. U. Wiedner	Univ. Bochum
Study of the rare decay $\eta \rightarrow e^+ e^- \pi^+ \pi^-$ in pp and pd reactions	Prof. U. Wiedner	Univ. Bochum
Entwicklung und Bau von Detektor-Komponenten für das WASA-at-COSY Experiment	Prof. K.-T. Brinkmann	Univ. Bonn
Investigation of ABC effect and Spin transfer coefficients at COSY	Prof. H.-W. Hammer	Univ. Bonn
Partialwellenanalyse von Daten aus Proton-induzierten Reaktionen	Prof. B. Metsch	Univ. Bonn
Inelastic baryon resonances from lattice QCD	Prof. A. Rusetsky	Univ. Bonn
Development of a Fast Orbit Feedback System for the HESR and Beam Tests at COSY	Prof. T. Weis	Univ. Dortmund
H-Strahl Laserdiagnose	Prof. T. Weis	Univ. Dortmund
COSY-TOF detector	Prof. H. Freiesleben	TU Dresden
Silicon Tracking Telescopes for ANKE and PAX	Prof. B. Kämpfer	FZ Dresden
Measurement of the degree of polarisation of laser accelerated protons	Prof. O. Willi	Univ. Düsseldorf
Vorbereitung und Durchführung von Experimenten an COSY-TOF und WASA	Prof. W. Eyrich	Univ. Erlangen-Nürnberg
Experiments with ANKE and PAX	Prof. E. Steffens	Univ. Erlangen-Nürnberg
FPGA-based trigger system for WASA	Prof. W. Kühn	Univ. Gießen
Mesonenproduktion in Nukleon-Nukleon- und Nukleon-Kern-Stößen an COSY	Prof. A. Khoukaz	Univ. Münster
Baryon resonance, g_A und die effektive Restrukturierung der chiralen Symmetrie	Prof. A. Schäfer	Univ. Regensburg
Installation und Inbetriebnahme des WASA-Detektors am COSY-Ring und Durchführung von Experimenten an WASA at COSY	Prof. H. Clement	Univ. Tübingen
Experimente an COSY-TOF	Prof. H. Clement	Univ. Tübingen

Project	Responsible	Institute
Lattice calculations of axial charges for baryons <i>np</i> system study with polarized beams and polarized Targets at ANKE	Prof. C. Gatttringer Prof. M. Nioradze	Univ. Graz (Austria) Tbilisi State Univ. (Georgia)
Spin dependence in <i>pd</i> interactions Analysis of WASA-at-COSY data Investigations of the CP symmetry with WASA Strangeness production with WASA-at-COSY Study of the decay $\eta' \rightarrow \eta\pi\pi$ with WASA Development of the PID method based on the dE/dx measurement for the Straw Tube Tracker	Prof. P. Dalpiaz Prof. A. Magiera Prof. P. Moskal Prof. B. Kamys Prof. Z. Rudy Prof. M. Jezabek	Univ. Ferrara (Italy) Jagellonian Univ. Cracow (Poland) Jagellonian Univ. Cracow (Poland) Jagellonian Univ. Cracow (Poland) Jagellonian Univ. Cracow (Poland) INP Cracow (Poland)
Study of the nature of the $\Lambda(1405)$ with WASA Silicon Tracking Telescope for ANKE Experiments with ANKE, WASA and PAX and FAIR Study of ω -meson production with WASA-at-COSY Development of a frozen-pellet target ϕ -meson production in <i>pn</i> and <i>pA</i> reactions Development of online software tools for COSY-TOF Development, commissioning and operation of components for the COSY experiments WASA and ANKE and spin-filtering studies at COSY as preparation of the PAX experiment in the framework of the FAIR project at GSI	Prof. W. Zipper Dr. V. Koptev Prof. V. Kulikov Prof. E. Stokovsky Dr. A. Gerasimov Prof. V. Kiselev Dr. V. Afanasyev Dr. A. Vasilyev	Univ. Silesia (Poland) PNPI Gatchina (Russia) JINR Dubna (Russia) JINR Dubna (Russia) ITEP Moscow (Russia) ITEP Moscow (Russia) MSU Moscow (Russia) PNPI Gatchina (Russia)
A pellet tracking system for PANDA and for WASA Cooperation COSY-WASA for $pp \rightarrow pp\eta$ and $pp \rightarrow pp\eta\pi^0$	Dr. H. Calen Prof. T. Johansson	Uppsala Univ. (Sweden) Uppsala Univ. (Sweden)
Trigger based on digitized QDC information for WASA Unified analysis of meson production in hadron- and photon-induced reactions	Prof. B. Höistad Prof. K. Nakayama	Uppsala Univ. (Sweden) Univ. of Georgia (U.S.A.)
SPIN@COSY: Spin-Manipulating Polarized Deuterons and Protons	Prof. A. Krisch	Univ. of Michigan (U.S.A.)

H Conferences (co-)organized by the IKP

H.1 19th International IUPAP Conference on Few-Body Problems in Physics

The Nineteenth International IUPAP Conference on Few-Body Problems in Physics (FB19) was held at the Rheinische Friedrich-Wilhelms Universität Bonn from August 31 to September 5, 2009. The purpose of this series is to bring together scientists who are interested in results and methods pertaining to few-body systems in particle, atomic, nuclear and molecular physics. Well over 250 participants from 30 countries around the world attended the conference. FB19 featured 25/27 invited plenary/lead parallel session and 128 contributed talks resulting in a total of 180 oral presentations. In addition, there were more than 40 poster presentations in a separate poster session.



Fig. 66: E. Oset answering questions after his talk during the FB19 conference.

Exciting new results from experiment and theory were presented at the conference. On the experimental side, these included new results on universal properties of few-body systems of ultracold atoms, precise new data on few-nucleon scattering observables and recent progress in hadron spectroscopy. A large number of theoretical talks addressed new developments in few- and many-body calculations including lattice simulations, effective field theories and the renormalization group, electroweak observables, exotic hadrons and nuclei, as well as astrophysical reactions.

The meeting clearly demonstrated that few-body physics is a vital and growing research area. This was especially highlighted by an overview talk of the exciting future physics program at FAIR with an eye on few-body aspects.

The conference was supported by the Helmholtz Institut für Strahlen- und Kernphysik and the Physikalisches Institut of the Rheinische Friedrich-Wilhelms Universität Bonn, the collaborative research center SFB-TR16 “Subnuclear Structure of Matter” from the Deutsche

Forschungsgemeinschaft, the Bundesministerium für Bildung und Forschung, the International Union of Pure and Applied Physics (IUPAP), the Forschungszentrum Jülich, the HGF virtual Institute on “Spin and Strong QCD”, the EU-FP7 project “Study of Strongly Interacting Matter” (HadronPhysics2) and the European Physical Journal A.

H.2 Workshop on Hadron Structure and Dynamics

The workshop “Hadron Structure and Dynamics” took place on August 13 and 14, 2009, in Bad Honnef. It focussed on the physics of hadron dynamics, such as final state interactions, production rates, and baryons with and without charm. The dynamics of mesons with flavors up, down, and strange was covered, which is important to understand the decay of mesons with open or hidden charm. E. Klempt (Bonn), B. Krusche (Basel), K. Brinkmann (Bonn) and E. Solodov (Novosibirsk) covered the field of Baryon and Hadron spectroscopy, presenting recent experimental results on nucleon excitations and the subsequent two-meson production. Two-pion production in nucleon-nucleon collisions was presented by M. Bashkanov (Tübingen), while M. Röder and A. Dzyuba reported on the recent progress made at COSY in determining the $p\Lambda$ scattering length and the status of Kaon pair production in Hadron-induced reactions.

Theory discussed the status of the σ meson (G. Colangelo, Bern), the interplay between lattice approaches and chiral effective field theory (U.-G. Meißner), Dyson-Schwinger calculations (C. Roberts, Argonne), and group theoretical approaches to exotics (Stancu, Liege). S. Eidelmann discussed the status of hadronic corrections in determining the anomalous magnetic moment of the muon.

The workshop clearly demonstrated the relevance of light-meson dynamics for future studies of open and hidden charm at FAIR. The interpretation of the enhancements of cross sections near threshold was discussed.

The organizers acknowledge financial support by VI-QCD.

H.3 Frontiers in Nuclear Physics

The joint meeting of the Virtual Institute on “Spin and strong QCD” and the Symposium “Frontiers in Nuclear Physics” in honor of Walter Glöckle was held on June 18–20, 2009 at the Physikzentrum Bad Honnef. Over many decades, the work of Walter Glöckle had a lasting impact on the theoretical and experimental investigations of few-nucleon systems, on the theory of nuclear forces, relativistic quantum mechanics and most recently, Coulomb effects in few-nucleon systems.

The meeting collected 35 participants and was organized with financial support from the the Virtual Institute on “Spin and Strong QCD”, the Network WP4 (QCD-net) of the HadronPhysics2 project of the seventh framework of the EU and the young investigator group “Few-

Nucleon Systems in Chiral Effective Field Theory” of the Helmholtz Association.

The presentations delivered at the Symposium focused on recent developments in few-body physics, precision calculation of the structure of light nuclei and reactions with few baryons and effective field theories and their application to describe the interaction between hadrons.

H.4 IUPAP Working Group on International Cooperation in Nuclear Physics

The annual meeting of the Working Group on International Cooperation in Nuclear Physics (WG.9: ICNP) of the International Union of Pure and Applied Physics was hosted by the IKP on August 30. The meeting was attended by 24 members and observers from 12 countries. The working group is an ad-hoc Committee on International Cooperation in Nuclear Physics (CICNP) and its main objectives are to

- promote international cooperation with the construction and exploitation of the large nuclear physics facilities — those which are intended for use by a worldwide nuclear physics community,
- organize meetings on a regular basis for the exchange of information on future plans for new nuclear physics facilities, and to
- stimulate the discussion of the future of nuclear physics and the need for high energy heavy-ion beam facilities, radioactive-ion beam facilities, multipurpose hadron beam facilities, and high energy electron beam facilities.

The detailed minutes of the Jülich meeting as well as related documents can be downloaded from <http://www.triumf.info/hosted/iupap/icnp/members/-minutes2009.html>. To give the participants of the IUPAP WG.9 an impression of the local facilities, a tour to COSY and its experiments was arranged. The committee stressed that COSY operations are essential to the hadron physics community.

H.5 PANDA Collaboration Meeting

The IKP hosted the 30th PANDA Collaboration Meeting from September 7–11, 2009. The meeting had 155 registered participants, 135 of which came from external institutions. The program was sub-divided into a part with two to four parallel sessions on Monday and Tuesday and a plenary part from Wednesday to Friday. The parallel part consisted of subgroup meetings mainly focussing on detector components, computing, and electronics, whereas status reports of general interest were given during the plenary sessions. The plenary part also included a session on physics issues relevant for the PANDA experiment. As external speaker F. de Fazio from INFN and University of Bari was invited to speak about “Insights in charm and charmonium



Fig. 67: Members of the IUPAP Working Group during the excursion to COSY.

spectroscopy”. Further physics talks were given by U.-G. Meissner on “Nucleon-nucleon and hyperon-hyperon interactions” and by C. Hanhart on “Light quark effects in charmed hadrons”.

H.6 ANKE/PAX Workshop on Spin Physics

The ANKE/PAX workshop on spin physics was jointly organized by the Joint Institute for Nuclear Research (JINR) and the IKP on June 22–26. About 50 participants — among them A. Sissakian and S.M. Schmidt as representatives of the laboratory managements — joint at the JINR in Dubna to discuss the physics program of COSY, the PAX project as well as other spin physics experiments with existing and future facilities.



Fig. 68: Participants of the ANKE/PAX workshop in front of JINR’s Laboratory of Nuclear Problems.

Further information about the workshop can be found under <http://nu73-198.jinr.ru/> and have been published as “Schriften des Forschungszentrums Jülich (Vol. 11, ISBN 978-3-89336-586-9, <http://www.zb.fz-juelich.de/publikationen/list.asp?jahr=2009>)

I Teaching Positions

Institute	Name	University
IKP-1	PD Dr. A. Gillitzer	Bonn
	PD Dr. F. Goldenbaum	Wuppertal
	Prof. Dr. H. Machner	Duisburg-Essen
	Prof. Dr. J. Ritman	Bochum
	PD Dr. S. Schadmand	Gießen
	Dr. T. Stockmanns	Bochum
IKP-2	PD Dr. M. Büscher	Köln
	PD Dr. D. Gotta	Köln
	PD Dr. F. Rathmann	Erlangen-Nürnberg
	Prof. Dr. H. Ströher	Köln
IKP-3/IAS-4	Prof. Dr. G. Baur (until March 31,2009)	Basel
	Prof. Dr. E. Epelbaum	Bonn
	Univ. Doz. Dr. J. Haidenbauer	Graz
	PD Dr. C. Hanhart	Bonn
	Prof. Dr. S. Krewald	Bonn
	Prof. Dr. U.-G. Meißner	Bonn
	Prof. Dr. N.N. Nikolaev	Moscow
	Dr. A. Nogga	Bonn
PD Dr. A. Wirzba	Bonn	
IKP-4	Prof. Dr. Dr. h.c. J. Dietrich	Dortmund
	PD Dr. A. Lehrach	Aachen, Bonn
	Prof. Dr. R. Maier	Bonn

J Beam Time at COSY

For 2009 in total 6720 hours of operation were scheduled. 4928 hours were scheduled for user beam time, 1008 hours were scheduled for dedicated beam dynamic studies and equipment tests for HESR, 784 hours were used for COSY machine development and experimental set-up, see Fig. 69. 193 hours were lost due to different technical breakdowns, mainly caused by faults in the RF-system of the cyclotron. For user beam times this results in an overall reliability of 98%. The distribution of user hours is listed in Table 4. The shutdown time was used to install additional 4 quadrupoles for the PAX low- β section. The COSY operation with the low- β insertion was commissioned in a PAX run in November 2009.

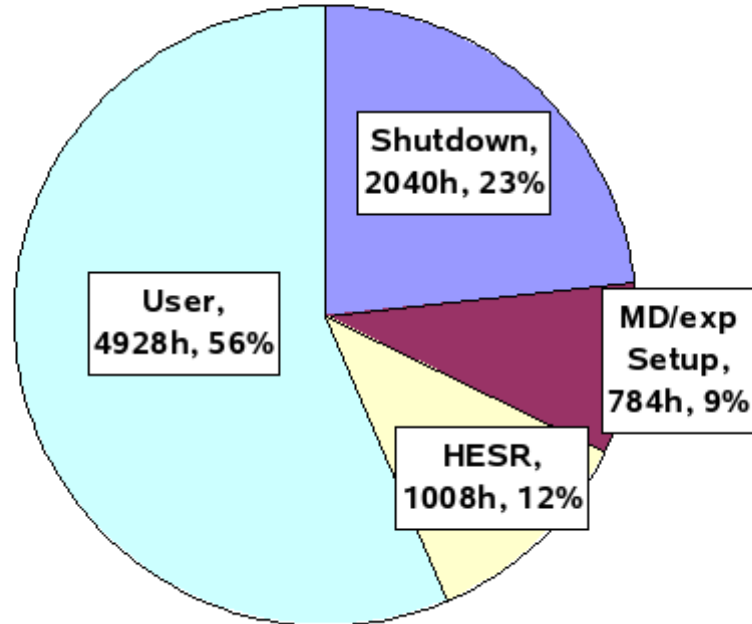


Fig. 69: COSY beam-time statistics. The scheduled beam time sums up to 6720 hours with a reliability of 98%.

Table 4: Overview over COSY user beam time in 2009.

Date	Experiment	Duration	Reaction, experiment #
2.02.09–08.02.09	PAX	1 week	accept.studies, 198
13.02.–15.03	ANKE	4 weeks	$pp \rightarrow ppK^-K^+$, 191
03.04.–12.04.	ANKE	1 week	$\bar{p}p \rightarrow (pp), \pi^0$, 158.2
13.04.–03.05.	ANKE	3 weeks	$\bar{p}n \rightarrow (pp), \pi^-$, 192
08.05.–24.05.	TOF	2 weeks	Hyperon Production at COSY-TOF, 141
29.05.–14.06	dEDM	2 weeks	\vec{d} beam, Polarimeter Development, 176.3
31.07.–30.08.	WASA	4 weeks	$pd \rightarrow {}^3\text{He} \eta$, 188.1
07.09.–04.10.	WASA	4 weeks	$pd \rightarrow {}^3\text{He} \eta$, 188.1
16.10.–15.11.	ANKE	4 weeks	$\vec{d}\vec{p} \rightarrow (pp)n$, 172.1
23.11.–06.12.	ANKE/PIT	2 weeks	$\vec{p}\&\vec{d}$, Commissioning PIT at ANKE, 201
Total '09		27 weeks	

K Personnel

K.1 Scientific Staff

L. Atar (IKP-1) (since 09 February, 2009)

Dr. V. Baru (IKP-3)

Prof. Dr. G. Baur (IKP-3) (until 31 January, 2009)

Dr. U. Bechstedt (IKP-4)

Dr. K. Bongardt (IKP-4)

DI N. Bongers (IKP-4)

DI R. Brings (IKP-4)

Y. Bsaison (IKP-3) (since 01 June, 2009)

PD Dr. M. Büscher (IKP-2)

M. Cleven (IKP-3) (since 01 August, 2009)

D. Coderre (IKP-3) (since 25 May, 2009)

DP E. Czerwinski (IKP-1) (until 30 September, 2009)

F.U. Dahmen (IKP-2) (since 01 November, 2009)

Prof. Dr.Dr.h.c. J. Dietrich (IKP-4)

DI N. Dolfus (IKP-TA)

Dr. M. Döring (IKP-3)

Dr. R. Engels (IKP-2)

Prof. Dr. E. Epelbaum (IKP-3)

DI F.-J. Etzkorn (IKP-4)

A. Fayt (IKP-2) (until 30 June, 2009)

Dr. P. Fedorets (IKP-2)

Dr. O. Felden (IKP-TA)

A. Filin (IKP-3) (until 30 June, 2009)

K. Frank (IKP-3) (since 01 February, 2009)

Dr. W. Gast (IKP-1)

Dr. R. Gebel (IKP-4)

PD Dr. A. Gillitzer (IKP-1)

PD Dr. F. Goldenbaum (IKP-1)

PD Dr. D. Gotta (IKP-2)

Dr. F. Grümmer (IAS-4)

Dr. D. Grzonka (IKP-1)

DI W. Günther (IKP-4)

Dr. F.-K. Guo (IKP-3)

Univ. Doz. Dr. J. Haidenbauer (IAS-4)

R. Halver (IKP-1)

J. Hampe (IKP-2) (since 01 June, 2009)

PD Dr. C. Hanhart (IAS-4)

Dr. M. Hartmann (IKP-2)

Dr. V. Hejny (IKP-2)

DI K. Henn (IKP-4)

DP M. Hodana (IKP-1) (until 31 October, 2009)

Dr. V. Jha (IKP-1) (since 01 September, 2009)

E. Jung (IKP-2) (since 16 November, 2009)

Dr. V. Kamerdjiev (IKP-4)

Dr. A. Kacharava (IKP-2)

S. Kazmierowski (IKP-3) (until 30 November, 2009)

L. Kröll (IKP-3) (since 01 September 2009)

DP St. Kölling (IKP-3)

Prof. Dr. S. Krewald (IAS-4)

DI K. Kruck (IKP-4)

DP W. Krzemien (IKP-1)

PD Dr. A. Lehrach (IKP-4)

DP S. Liebig (IKP-3)

Dr. B. Lorentz (IKP-4)

Prof. Dr. H. Machner (IKP-1)

Prof. Dr. R. Maier (IKP-4)

Prof. Dr. U.-G. Meißner (IKP-3)

Th. Mennicken (IKP-2) (since 01 October, 2009)

DP M. Mertens (IKP-1)

DP S. Mikirtychians (IKP-2)

DP D. Minossi (IKP-3)

Dr. M. Nekipelov (IKP-2)

Prof. Dr. N.N. Nikolaev (IKP-3)

Dr. A. Nogga (IAS-4)

Prof. Dr. W. Oelert (IKP-1)

DP D. Oellers (IKP-2)

Dr. H. Ohm (IKP-2)

DI N. Paul (IKP-1)

Dr. C. Pauly (IKP-1)

Dr. M. Pavon-Valderrama (IKP-3)

T. Pedri (IKP-3) (since 15 July, 2009)

D.-L. Pohl (IKP-1) (since 15 October, 2009)

Dr. D. Prasuhn (IKP-4)

DP N. Raab (IKP-4)

Dr. A. Raccanelli (IKP-4)	Dr. R. Stassen (IKP-4)
PD Dr. F. Rathmann (IKP-2)	Dr. H. Stockhorst (IKP-4)
DP Ch.F. Redmer (IKP-1)	Dr. T. Stockmanns (IKP-1)
DP M. Retzlaff (IKP-4)	Dr. Th. Strauch (IKP-2) (until 30 September, 2009)
DI A. Richert (IKP-4)	Prof. Dr. H. Ströher (IKP-2)
Prof. Dr. J. Ritman (IKP-1)	DP T. Tolba (IKP-1)
Dr. E. Roderburg (IKP-1)	Dr. R. Tölle (IKP-4)
DP M. Röder (IKP-1)	S. Urrutia-Millas (IKP-3) (since 01 January, 2009)
D. Rönchen (IKP-3) (since 01 June, 2009)	DI T. Vashegyi (IKP-4)
M. Ruzzo (IKP-2) (until 30 June, 2009)	DP P. Vlasov (IKP-1) (until 31 August, 2009)
DI J. Sarkadi (IKP-TA)	P. Voigtländer (IKP-1) (until 30 April, 2009)
DP P. Saviankou (IKP-3) (until 05 January, 2009)	Chr. Weidemann (IKP-2)
Dr. H. Schaal (IKP-1)	DP D. Welsch (IKP-4)
PD Dr. S. Schadmand (IKP-1)	Dr. P. Wintz (IKP-1)
Dr. R. Schleichert (IKP-2)	PD Dr. A. Wirzba (IAS-4)
DI G. Schug (IKP-4)	DI J.-D. Witt (IKP-4)
Dr. Th. Sefzick (IKP-TA)	Dr. M. Wolke (IKP-2) (until 31 January, 2009)
Prof. Dr. Y. Senichev (IKP-4)	Dr. H. Xu (IKP-1) (since 01 April, 2009)
DI M. Simon (IKP-4)	Dr. E. Zaplatin (IKP-4)
N. Sharmazanashvili (IKP-2) (since 13 February, 2009)	M. Zielinski (IKP-1) (until 08 January, 2009)

K.2 Technical and Administrative Staff

J. Ahlschläger (IKP-4)
J. Artz (IKP-TA)
C. Berchem (IKP-TA)
M. Böhnke (IKP-4)
J. Borsch (IKP-TA)
P. Brittner (IKP-4)
J. But (IKP-TA)
W. Classen (IKP-4)
M. Comuth-Werner (IKP-TA)
B. Dahmen (IKP-4)
C. Deliege (IKP-4)
W. Derissen (IKP-TA)
G. D'Orsaneo (IKP-2)
R. Dosedall (IKP-1)
R. Enge (IKP-4)
P. Erben (IKP-2)
B. Erkes (IKP-4)
K. Esser (IKP-TA)
H.-W. Firmenich (IKP-TA)
J. Göbbels (IKP-TA)
H. Hadamek (IKP-TA)
R. Hecker (IKP-4)
E. Heßler (IKP-TA)
M. Holona (IKP-TA)
H.-M. Jäger (IKP-1) (until 31 August 2009)
A. Kieven (IKP-4)
M. Kremer (IKP-TA)
G. Krol (IKP-4)
M. Küven (IKP-4)
K.-G. Langenberg (IKP-4)
H. Metz-Nellen (IKP-TA)
S. Müller (IKP-TA)
R. Nellen (IKP-TA)
H. Pütz (IKP-4)
G. Roes (IKP-TA)
N. Rotert (IKP-4)
D. Ruhrig (IKP-4)
T. Sagefka (IKP-4) (until 31 March 2009)
F. Scheiba (IKP-4)
H. Schiffer (IKP-TA)
J. Schmitz (IKP-4)
F. Schultheiß (IKP-TA)
H. Singer (IKP-4)
D. Spölggen (IKP-2)
G. Sterzenbach (IKP-1)
J. Strehl (IKP-TA)
J. Uehlemann (IKP-1)
P. Wieder (IKP-2)
P. Wurm (IKP-2) (since 01 November, 2009)
H. Zens (IKP-4)

IKP-1 = Experimental Hadron Structure
IKP-2 = Experimental Hadron Dynamics
IKP-3 = Theoretical Nuclear Physics
IKP-4 = Large-Scale Nuclear Physics Equipment
IKP-TA = Technical Services and Administration
IAS-4 = Theory of the Strong Interactions

L Substantiating Contributions (available on-line)

1. Experimental Hadron Physics

- 1.1 WASA-at-COSY $pd \rightarrow {}^3\text{He}\eta$ Beam Time 2009
- 1.2 $\eta \rightarrow 3\pi^0$ Decay with WASA-at-COSY
- 1.3 The $\eta \rightarrow \pi^+\pi^-\pi^0$ Decay with WASA-at-COSY
- 1.4 Towards measurement of ratio $BR(\eta \rightarrow 3\pi^0)/BR(\eta \rightarrow \pi^+\pi^-\pi^0)$
- 1.5 The Rare Decay $\eta \rightarrow \pi^0\gamma\gamma$ with WASA-at-COSY
- 1.6 Search for the C-violating η -meson decay $\eta \rightarrow \pi^0e^+e^-$ with WASA-at-COSY
- 1.7 Analysis of the rare decay $\eta \rightarrow e^+e^-\gamma$ with WASA-at-COSY
- 1.8 The $\eta \rightarrow e^+e^-\gamma$ Decay from pd Reactions with WASA-at-COSY
- 1.9 In search of $\eta \rightarrow e^+e^-e^+e^-$ with the WASA-at-COSY facility in the reaction $pd \rightarrow {}^3\text{He}\eta$ at 1 GeV
- 1.10 Experimental study of $pp\eta$ Dynamics with WASA-at-COSY
- 1.11 $pp \rightarrow pp3\pi^0$ Reaction Studies at 3.35 GeV/c Beam Momentum
- 1.12 Double π^0 Production in pp Collisions at $T_p = 1400$ MeV
- 1.13 The $\pi^0 \rightarrow e^+e^-$ Decay with WASA-at-COSY
- 1.14 Charge Symmetry Breaking in $dd \rightarrow {}^4\text{He}\pi^0$ with WASA-at-COSY
- 1.15 Luminosity determination for dd collisions at 1.2 GeV/c using $dd \rightarrow {}^3\text{He}n$
- 1.16 Studies of single photon production in dd interaction with WASA-at-COSY
- 1.17 Investigation of the $dd \rightarrow dpn$ Breakup Reaction with the WASA detector
- 1.18 Search for eta Mesic Helium using WASA-at-COSY
- 1.19 Investigation of scalar mesons $a_0/f_0(980)$ in the $pd \rightarrow {}^3\text{He}X$ reaction with WASA-at-COSY
- 1.20 Energy Resolution of the WASA-at-COSY Electromagnetic Calorimeter
- 1.21 The ABC-effect study at ANKE in the $pd \rightarrow pd\pi\pi$ reaction
- 1.22 Energy dependence of the $pp \rightarrow K^+n\Sigma^+$ reaction at ANKE
- 1.23 First investigation of the $pd \rightarrow p_{\text{sp}}pK^+\Sigma^-$ reaction at ANKE
- 1.24 ϕ -meson width in nuclear matter
- 1.25 Reaction $pp \rightarrow (pp)_s\pi^0$ at beam energies 1.7 and 2.4 GeV
- 1.26 Deuteron breakup $pd \rightarrow pp_s n$ with forward emission of a fast 1S_0 diproton
- 1.27 Analysing power measurement for the charge-exchange breakup reaction $\vec{d}p \rightarrow ppn$ at $T_d = 2.27$ GeV
- 1.28 Investigation of the ${}^3\text{He}\eta$ Final State in dp -Reactions at ANKE
- 1.29 Energy dependence of the $pp \rightarrow pp_s\gamma$ reaction cross section in the $\Delta(1232)$ isobar range
- 1.30 Double-Polarized Fusion
- 1.31 Measurement of the nuclear polarization in H_2 and D_2 molecules after recombination ...
- 1.32 Invariant mass distributions for the $pp \rightarrow pp\eta$ reaction at $Q = 10$ MeV
- 1.33 Determination of the total width of the η' meson with the COSY-11 detector
- 1.34 Measurement of the invariant mass distributions for the $pp \rightarrow pp$ reaction at $Q = 16.4$ MeV
- 1.35 Upper limit of the total cross section for the $pn \rightarrow pn\eta'$ reaction
- 1.36 Determination of the K^+K^- scattering length from the low-energy ppK^+K^- system produced at COSY-11
- 1.37 Comparative studies of the Fermi momentum distribution in ${}^3\text{He}$ nucleus for the search of the η -mesic helium
- 1.38 Event Display and Online Control Package for the upgraded COSY-TOF Experiment
- 1.39 Preliminary set of deuteron-proton breakup vector analyzing powers from GeWall experiments
- 1.40 Total production cross sections for $p+{}^{12}\text{C}$ reactions in the limiting fragmentation energy range

2. Developments for the Experimental Facilities

- 2.1 Measurements of the Response Characteristics of CsI(Na) Crystals
- 2.2 Trigger Developments for WASA-at-COSY
- 2.3 Development of a Pellet Tracking System for PANDA and WASA
- 2.4 RD for a DIRC detector for WASA-at-COSY
- 2.5 A Focussing Disc DIRC Concept for WASA-at-COSY

3. Accelerator Division

- 3.1 Commissioning of the Ionization Beam Profile Monitor at COSY
- 3.2 Fast Orbit Feedback systems for hadron and electron storage rings
- 3.3 Numerical Field Analysis of the Magnets for a proposed Ionisation Profile Monitor
- 3.4 Beam Profile Monitor using Residual Gas Scintillation.
- 3.5 Emittance measuring device EMA
- 3.6 Beam Instrumentation Test Facility
- 3.7 Magnets, Alignment and New Installations
- 3.8 Status of the COSY Injector Cyclotron and Ion Sources
- 3.9 Radiation Protection
- 3.10 Development of Beam Diagnostic Methods for Accelerator Based Medical Applications
- 3.11 A focussing system for laser-accelerated electrons

4. Preparations for FAIR

- 4.1 A new setup for measuring the energy loss of particles in the PANDA STT
- 4.2 First measurements of energy-loss using PANDA-type straw tubes
- 4.3 Constrained vertex and kinematic fitting tools in Pandaroot
- 4.4 Simulation Study on a Proposed Geometry of the Luminosity Monitor for the PANDA Experiment
- 4.5 Design studies for the layout of the PANDA Straw Tube Tracker
- 4.6 Effect of the Transverse Emittance of the HESR Beam on the Resolution of the PANDA Luminosity Monitor
- 4.7 Implementation of a Time-over-Threshold calculation for the Micro Vertex Detector in PandaRoot
- 4.8 A method for a precise measurement of the mass and width of the $D_{s0}^*(2317)$ meson
- 4.9 Simulation of the Reaction $pp \rightarrow \Lambda \bar{\Lambda}$ with the PANDA MVD
- 4.10 Towards a Pellet-Target Tracking System

5. Technical Developments

- 5.1 Electronics Laboratory